PROCEEDINGS

of

The International Conference on Electrodynamics of complex Materials for Advanced Technologies

PLASMETA'11

Navoi Samarkand State University, Samarkand, Uzbekistan

September 21, 2011 – September 26, 2011

Gur Emir, the mausoleum of Tamerlane The Great

The Conference PLASMETA is organized by:

Institute for Theoretical and Applied Electromagnetics (ITAE RAS), Russia

Navoi Samarkand State University, Samarkand, Uzbekistan

Laboratoire de Génie Electrique de Paris Supélec - Paris-Sud University, France

General co-chairs

Prof. S. Zouhdi

Prof. A. P. Vinogradov

Chairs

Dr. A.M. Merzlikin, Prof. E. Arzikulov, Dr. A. V. Dorofeenko

Advisory Board

The Conference supporters:

1. **Office of Naval Research Global (GRANT NUMBER: N62909-11-1-1082)**[1]

2. **Russian Academy of Sciences (Branch of energetics, machinery construction, mechanics and control processes)**

PROGRAM

21.09: Quantum plasmonics

Day chairman: A.M. Merzlikin

Time	Authors	Title
9.00	**Opening ceremony**	
9.30	**M. Stockman** Department of Physics and Astronomy Georgia State University	Quantum Nanoplasmonics and the Spaser
10.20	[1]**A. P. Vinogradov** [1]E.S. Andrianov, [1]A.A. Pukhov, [1]A.V. Dorofeenko, and [2]A.A. Lisyansky [1]Institute for Theoretical and Applied Electromagnetics, 13 Izhorskaya, Moscow 125412, RF [2]Department of Physics, Queens College of the City University of New York, Flushing, NY	Dynamics of Spaser in the external field
11.00	Coffee break	
11.30	**A. V. Dorofeenko,** [1]A. P. Vinogradov [1]E. S. Andrianov, [1]A.A. Pukhov, and [2]A.A. Lisyansky [1]Institute for Theoretical and Applied Electromagnetics, 13 Izhorskaya, Moscow 125412, RF [2]Department of Physics, Queens College of the City University of New York, Flushing, NY	Spasing in Metallic Groove
12.00	**E. S. Andrianov[1]** A. A. Pukhov[1], A. P. Vinogradov[1], A.V. Dorofeenko[1], and A.A. Lisyansky[2] [1]Institute for Theoretical and Applied Electromagnetics, 13 Izhorskaya, Moscow 125412, RF [2]Department of Physics, Queens College of the City University of New York, Flushing, NY	Eigenmodes of an 1D array of coupling spasers
12.30	Lunch	
14.30	**A.V. Krasavin**, **A. Zayats, W. Dickson, J.-S. Bouillard, G.A. Wurtz** Nano-optics and Near-field Spextroscopy Laboratory, Department of Physics, King's College London, Strand, London WC2R 2LS, United Kingdom	Nano-optics
15.20	**Andrey Fedyanin** Faculty of Physics, Moscow State University, Moscow	Femtosecond plasmonics in metamaterials
15.50	**Negmat Nizomov**[2] A.A.Ishchenko[1], J. Khamraev[2], A.U.Kholov[2]	Spectral-luminescent study of the interaction oxycoumarine dyes with BSA and DNA

	<u>N.Nizomov</u>[2], Sh.N.Nizamov[2], M.Barakaeva[2], E.N.Kurtaliev[2] [1]Institute of organic chemistry National academy of sciences of Ukraine, Murmanska Str. 5, Kyiv 02094, Ukraine [2]Samarkand State University, University blvd. 15, 140104 Samarkand, Uzbekistan	Spectroscopic study of the influence of solvent nature on the photostability of squaraine dyes
16.10	**J. T. Ruzimurodov** Samarkand State University, Department of Physics, 140104, University 15, Samarkand, Uzbekistan	Ferromagnetism in manganese ion implanted silicon samples
	Samarkand. Gur Emir Mausoleum (Tamerlan Mausoleum). Registan Square	

22.09: Homogenization of Metamaterials

Day chairman A.P. Vinogradov

9.00	**Graeme Milton,** **Johan Helsing** (Lund) and **Ross McPhedran** (Sydney) Department of Mathematics University of Utah	Spectral super-resolution in metamaterial composites
10.00	**David J. Bergman** Raymond and Beverly Sackler School of Physics and Astronomy, Faculty of Exact Sciences, Tel Aviv University, IL-69978 Tel Aviv, Israel	Magneto-transport in a composite medium
11.00	Coffee break	
11.30	**P. A. Belov**[1,2], **A. A. Orlov**[1], **A. V. Chebykin**[1], **Yu. S. Kivshar**[1,3] [1]National Research University of Information Technologies, Mechanics and Optics, St. Petersburg, Russia [2]Queen Mary University of London, London, UK [3]Australian National University, Canberra, Australia	Spatial dispersion in layered metamaterials
12.30	Lunch	
14.30	**Sergey Yu. Kosulnikov**[1] **A. Rahman**[2], **P. A. Belov**[1,2], **Yu. S. Kivshar**[1,3] [1]National Research University of Information Technologies, Mechanics and Optics, St. Petersburg, Russia [2]Queen Mary University of London, London, UK [3]Australian National University, Canberra, Australia	Subwavelength optical imaging with arrays of silver nanorods
14.50	**F.H. Tukhvatullin,** **A. Jumabaev, H. Hushvaktov, A. Absanov, B. Hudoyberdiev** Samarkand State University, Uzbekistan	Raman Spectra and Intermolecular Hydrogen Bonds in Solutions of Quinoline
15.10	**E. Arzikulov** **S. N. Srajev, Q. N. Srojev** Samarkand State University, Uzbekistan	About an Availability of Obtaining "Semiconductor Metamaterials" by Ion Implantation Method
	Samarkand. Shahi-Zinda, cathedral mosque Bibi-Khanym that was named after the oldest wife of Tamerlan, Siab bazaar.	

23.09: Materials of Modern optics

Day chairman M. F. Limonov

9.00	**A. B. Granovsky**[1] **A. Orlov[2], N. Perov[1], E.Gan'shina[1], A.P. Kazakov[1], L. Balagurov[2], A. Sapelkin[3], A. Rogalev[4], A. Smekhova[4]** [1]Faculty of Physics, Moscow State University, Moscow, 119991 Russia; [2]State Institute for Rare Metals, Moscow, 119017 Russia; [3]Queen Mary University of London, E1 4NS, London, UK; [4]European Synchrotron Radiation Facility, 38043, Grenoble, Cedex 9, France	Above Room Temperature Ferromagnetism in Si:Mn and $TiO_{2-\delta}$:Co
9.30	**A.B. Granovsky**[1,2,3], V. Prudnikov[1], A. Kazakov[1], A. Zhukov[2,3], V. Zhukova[3], J. Gonzalez[3], I. Dubenko[4] [1]Faculty of Physics, Moscow State University, Moscow, RF; [2] IKERBASQUE, the Basque Foundation for Science, 48011 Bilbao, Spain; [3]Basque Country University, 20080 San Sebastian, Spain; [4]Southern Illinois University Carbondale, IL, 62901, USA;	Magnetic Properties of a New Family of Quaternary Ni-Mn-In-Z Heusler Alloys
10.00	**D. Yu. Fedyanin** Moscow Institute of Physics and Technologies	Theory of SP amplification by stimulated emission of radiation in metal-semiconductor structures
10.30	**Arcady Zhukov**[2,3] **L. V. Panina[1,2], M. Ipatov[2], V. Zhukova[2], J. González[2]** [1]School of Computing and Mathematics, University of Plymouth, Plymouth, PL4 8AA, United Kingdom [2]Dpto. Física de Materiales, Fac. de Química, UPV/EHU, San Sebastián, Spain [3]IKERBASQUE, Basque Foundation for Science, 48011 Bilbao, Spain	Tunable metamaterials containing arrays of magnetically soft microwires
11.00	Coffee break	
11.30	**A.K. Arzhnikov** Physical-Technical Institute, Ural Division of RAS, Izhevsk, Russia	The spin-spiral magnetic order and phase separation in systems with itinerant electrons
12.00	**M. Lapine** **Ilya Shadrivov, David Powell, and Yuri Kivshar** Nonlinear Physics Centre, Research School of Physics and Engineering, Australian National University, Canberra ACT 0200, Australia	Nonlinear and tunable metamaterials: an overview
12.30	Lunch	
14.30	**A. Priou** University Paris Ouest Nanterre la Défense, Energy, Mechanics and Electromagnetic Lab.(LEME)50 rue de Sevres, 92410 Ville d'Avray, France	Tentative of Smart Skins Metamaterial Antennas embedded in the Structure of an Aircraft
15.00	**O.K. Kuvandikov E. U. Arzikulov** Samarkand State University, Samarkand, Uzbekistan	Magnetic Charge and Problems in Condensed Matter Physics
	Samarkand. Afrosiab, Ulugbeg Madrassah.	

24.09: Plasmonics

Day chairman M. Lapine

9.00	**V. V. Klimov** Lebedev Physical Institute, Russia	Nanoguiding of Light and Matter Waves by Negative Refraction Media: New Problem Definition and Applications
9.30	**C. R. Simovsky** **and D. C. Morits** Aalto University, Department of Radio Science and Engineering	Plasmonic metasurfaces for tandem thin-film solar cells
10.20	**A. Popov**[1] **M. I. Shalaev**[2], **S. A. Myslivets**[3], **and V. V. Slabko**[2] [1]University of Wisconsin-Stevens Point, Stevens Point, USA [2]Siberian Federal University, Krasnoyarsk, Russian Federation [3]Institute of Physics of Russian Academy of Sciences, Krasnoyarsk, Russian Federation Department of Physics & Astronomy University of Wisconsin-Stevens Point	Negative-index nonlinear optics: phonons vs plasmons
10.50	Coffee break	
11.20	**C. David[1],** **J. P. Conolly[2], A. Griol[2], C. Ramos[2], J. Hurtado[2], F. J. García de Abajo[1], G. Sánchez[2]** [1]Nanophotonics Group, Instituto de Óptica, CSIC, Serrano 121, 28006 Madrid, Spain [2]Nanophotonics Technology Center, Universidad Politécnica de Valencia, 46022 Valencia, Spain	Theory and Efficient Integration of Random Nanoparticle Layers in Photovoltaic Devices
11.40	**Maxim Shcherbakov**[1] **B. B. Tsema[2], Yu. B. Tsema[1], A. T. Le[1],** **A. A. Ezhov[1], and A. A. Fedyanin[1]** [1]Faculty of Physics, Lomonosov Moscow State University, Russia [2]Moscow State Institute of Radioengineering, Electronics and Automation, RussiaFaculty of Physics, Moscow State University, Moscow	Scanning near-field optical polarimetry of plasmonic metamateials
12.00	Lunch	
14.00	**Eldar Kurtaliev** Samarkand State University, Uzbekistan	Spectral-luminescent characteristics of styrylcyanine dye Sbt and its homodimers solutions
	Visit of national park Zeravshan	

25.09: Photonic Crystals

Day chairman P. Belov

9.00	**M. F. Limonov** **and M. V. Rybin** Ioffe Physical-Technical Institute, Russian Academy of Sciences, St. Petersburg, 194021, Russia	Fano resonance in photonic crystals: experiment and theory
9.50	**Yakov Strelniker**[1] D. J. Bergman[2], Y. Fleger[1], M. Rosenbluh[1], A. O. Voznesenskaya[3], A. P. Vinogradov[4], and A. M. Merzlikin[4] [1]Department of Physics, Bar-Ilan University, IL-52900 Ramat-Gan, Israel [2]Raymond and Beverly Sackler School of Physics and Astronomy, Faculty of Exact Sciences, Tel Aviv University, IL-69978 Tel Aviv, Israel [3]St. Petersburg State University of Information Technologies, Mechanics and Optics, 197101, St. Petersburg, Russia [4]Institute for Theoretical and Applied Electromagnetics,125412, Moscow, Izhorskaya 13, Russia	Manipulating the Light Transmission and Faraday Rotation through Periodic Metamaterials by Applying an External Field and by Changing the Nano-structures Shapes
10.20	**K. B. Samusev** **A. K. Samusev, I. S. Sinev, E. Yu. Trofimova, D. A. Kurdyukov** Ioffe Physical-Technical Institute, Russian Academy of Sciences, St. Petersburg, 194021, Russia	Light diffraction from opal-like photonic structures: transition from 2D to 3D regimes
10.50	Coffee	
11.20	**Alexander Ageyskiy**[1] **S. Yu. Kosulnikov[1], S. I. Maslovski[2], P. A. Belov[1,3], Yu. S. Kivshar[4]** [1]National Research University of Information Technologies, Mechanics and Optics (ITMO) [2]Instituto de Telecomunica¸c˜oes, Universidade de Coimbra [3]Queen Mary College, University of London [4]Nonlinear Physics Centre, Australian National University National Research University of Information Technologies, Mechanics and Optics, St. Petersburg, Russia	Quarter-wavelength wire lens for subwavelength imaging at terahertz frequencies
11.40	**Denis Vasilievich Fateev**[1,6] **V. V. Popov[1,5], T. Otsuji[2], Y. M. Meziani[3],** **D. Coquillat[4], W. Knap[4], S. A. Nikitov[15]** [1]Kotelnikov Institute of Radio Engineering and Electronics (Saratov Branch) of RAS, 410019 Saratov, Russia [2]Reseach Institute of Electrical Communication, Tohoku University, 2-1-1Katahira, Sendai 980-8577,	Terahertz detection in a gated planar plasmonic crystal with an asymmetric unit cell

	Japan [3]Dpto. de Fisica Aplicada, Universidad de Salamanca, Pza de la Merced s/n, 37008 Salamanca, Spain [4]Laboratoire Charles Coulomb UMR5221, CNRS&Université Montpellier 2, 34095 Montpellier, France [5]6Saratov State University named after N.G. Chernyshevsky, 410012 Saratov, Russia	
12.00	Lunch	
14.00	**Yann Danlée** **Christian Bailly, Isabelle Huynen** Universite catholique de Louvain, Belgium	Thin smart multilayer microwave absorber based on hybrid structure of polymer and carbonated nanoparticles
14.20	**Sergey G. Moiseev** Kotelnikov Institute of Radio Engineering and Electronics of Russian Academy of Sciences, Ulyanovsk Branch, Russia	Transmission and Reflection Spectra of Photonic Crystal with Plasmonic Defect
14.40	**Andrey Khyshov** **V. V. Ivanov, S. S. Ustavschikov, and M. A. Novikov** Institute for Physics of Microstructures RAS, Nizhny Novgorod, GSP-105, Russia	Experimental studies of light reflection from the boundary with a chiral medium
15.00	**Iarj Arghand Lafmajani** Semnan University, Iran	Design of Multiple Spiral Frequency Selective Double-Negative Metamaterial
15.20	**Mohammad Azad Davar** Semnan University, Iran	Fabrication and characterization e-beam evaporated film from doped SnO2 nanopowder for semiconductor gas sensor application
15.40	**Irina Khromova**[1] **R. Gonzalo**[1]**, I. Ederra**[1]**, J. Teniente**[1] **, K. Esselle**[2] [1]Public University of Navarra, Spain [2]Macquarie University, Australia Public University of Navarra, Spain	All-dielectric horn antennas based on woodpile structures
16.00	**Erkin N Shermatov** **Bahrom N. Shermatov** Samarkand State University, Uzbekistan	The role of the surface energy in the formation of unique properties of thin-film materials
17.00	Conference diner	

26.09: Diffusion and Anderson localization of light

Day chairman C. K. Simovsky

9.00	**M. Kaliteevski** Ioffe Physical-Technical Institute, Russian Academy of Sciences, St. Petersburg, 194021, Russia	Generation of non-diverging beams by negative refraction
9.50	**A. M. Merzlikin**[1], **A. I. Ignatov**[1], **A.P. Vinogradov**[1], **G. Samelsohn**[2], [1]Institute of Theoretical and Applied Electromagnetics RAS [2]Holon Institute of Technology, Holon 58102, Israel	Stochastization of light polarization in random system
10.20	**Wiqar Hussain Shah** King Faisal University, Hofuf, 31982 SAUDI ARABIA	Competing Interactions and Cluster Dynamics in Doped Rare-earth Manganites
10.40	**Maksim V. Sapozhnikov** Institute for Physics of Microstructures RAS, Nizhny Novgorod, GSP-105, Russia	Optical and magneto-optical resonances in nanostructured ferromagnetic films
11.00	Coffee	
11.30	**M.Yu.Barabanenkov**[2], **Yu. N. Barabanenkov**[1] **and S.A.Nikitov**[1] [1]V.A. Kotelnikov Institute of Radioengineering and Electronics, Russian Academy of Sciences, Mohovaya 11, 103907 Moscow, GSP-3, Russia [2]Institute of Microelectronics Technology, Russian Academy of Sciences,	Diamagnetism phenomenon in theory of wave multiple scattering on random discrete dielectric media
12.00	Lunch	
14.00	**B.U.Amonov** **H.O.Shakarov, Z.M.Shodiev, O.K. Kuvandikov** Samarkand State University, Dpt. of Physics, Samarkand, Uzbekistan	Study of Magnetic Properties Complex system (La0.8AgxMnO3) at High Temperatures
14.20	**Maysara Kamolidinovna Salakhitdinova** **M.M. Mirkamalov, A.N. Salakhitdinov,** **A.A. Yusupov** Samarkand State University, Uzbekistan	EPR spectroscopy of nanostructured units in iron-containing alkali-borate glasses obtained by the thermoradiation founding
	Shahrisabz. Aq-Saray Palace (Timur's Summer Palace). Hazrat-i Imam Complex. Kok Gumbaz Mosque.	

Poster session

21.09-26.09

C. G. Park[1] **and J. S. Kwak**[2] [1]Graduate School of Manufacturing and Automation, Pukyong National University, Republic of Korea [2]Department of Mechanical Engineering, Pukyong National University, Republic of Korea	An application of second-generation magnetic abrasive polishing
Dongyoon Kim[1] **and Young Whan Park**[2] [1]Department of Manufacturing and Automation, Pukyong National University, Busan, Korea [2]Department of Mechanical Engineering, Pukyong National University, Busan, Korea	Analysis for behavior of keyhole and plasma in aluminum laser welding using optical measurement of plasma generation
S. O. Kim[1] **and J. S. Kwak**[2] [1]Grauated School of Manufacturing and Automation, Pukyong National University, Republic of Korea [2]Department of Mechanical Engineering, Pukyong National University, Republic of Korea	A study on Magnetic Abrasive Polishing in Concave Type of Al6061
Ms. Mahdieh Dashtbani Moghari Semnan University, Iran	Location optimization of a simple and fast first-order PMD compensator using a polarizer
D.C. Choi[1]**, and T. W. Kim**[2] [1]Graduate School of Mechanical Engineering, Pukyong National University, South Korea [2]Department of Mechanical Engineering, Pukyong National University, South Korea	Scuffing wear monitoring using acoustic emission
H. Choi[1]**, D. H. Lee**[2] [1]Education Center for Vehicle Safety Component Technology, Pukyong National University, Korea [2]Department of Mechanical Engineering, Pukyong National University, Korea	Control of Braking Velocity on Vehicle using ABS Slip Ratio
J. González[1]**, V. Rodionova**[1,2,3]**, M. Ipatov**[1]**, M. Ilyn**[2]**, V. Zhukova**[1]**, N.Perov**[2]**, J.J. Del Val**[1]**, and A. Zhukov**[1] [1]Department of Materials Physics, Faculty of Chemistry, University of the Basque Country, Paseo Manuel de Lardizabal 3, 20018 San Sebastián, Spain [2]Faculty of Physics, Moscow State University, Leninskie Gory, Moscow, Russia [3]Institute for Theoretical and Applied Electromagnetics of Russian Academy of Sciences, Moscow, Russia 4TAMAG Ibérica S.L., Parque Tecnológico de Miramón, Paseo Mikeletegi 56, 1a Planta, 20009 San Sebastián, Spain	Magnetic properties of arrays of magnetostatically coupled glass-covered microwires for design new metamaterial family

Quantum Nanoplasmonics and the Spaser

Mark I. Stockman
Department of Physics and Astronomy, Georgia State University, Atlanta, GA 30302, USA
E-mail: mstockman@gsu.edu, web: http://www.phy-astr.gsu.edu

Nanoplasmonics deals with collective electron dynamics on the surface of metal nanostructures, which arises due to excitations called surface plasmons. The surface plasmons localize and concentrate optical energy in nanoscopic regions creating highly enhanced local optical fields. They undergo ultrafast dynamics with timescales as short as a few hundred attoseconds [1]. We will start with a brief overview of the state of nanoplasmonics and its many applications [2].

Until recently, all the effects, elements, and devices in nanoplasmonics have been passive: they use the external sources of optical energy and use this energy in different ways, always losing a fraction of it to heat and radiation. The first active effect and device to generate energy directly on the nanoscale has been spaser (surface plasmon amplification by stimulated emission of radiation) [3, 4]. Spaser and related nanolasers have been convincingly demonstrated recently in a number of experiments [5-9]. We will consider quantum theory of spaser as an ultrafast quantum generator and amplifier of nanoplasmonic fields [10]. We will also briefly consider application of theory of spaser to the problem of loss compensation by gain in metamaterials [11].

In perspective, the spasers will have applications as ultrafast nanoamplifiers (the same size as the field-effect transistors, they are at least two orders of magnitude faster), nanoscale sources of coherent and intense optical fields, and many others.

References

[1] M. I. Stockman *et al.*, Nat. Phot. **1**, 539 (2007).
[2] M. I. Stockman, Phys. Today **64**, 39 (2011).
[3] D. J. Bergman, and M. I. Stockman, Phys. Rev. Lett. **90**, 027402 (2003).
[4] M. I. Stockman, and D. J. Bergman, USA Patent No. 7,569,188 (August 4, 2009).
[5] M. A. Noginov *et al.*, Nature **460**, 1110 (2009).
[6] M. T. Hill *et al.*, Opt. Express **17**, 11107 (2009).
[7] R. F. Oulton *et al.*, Nature **461**, 629 (2009).
[8] R.-M. Ma *et al.*, Nat. Mater. **10**, 110 (2010).
[9] R. A. Flynn *et al.*, Opt. Express **19**, 8954 (2011).
[10] M. I. Stockman, Journal of Optics **12**, 024004 (2010).
[11] M. I. Stockman, Phys. Rev. Lett. **106**, 156802 (2011).

Dynamics of spaser in the external field

A.P. Vinogradov,[1] E.S. Andrianov,[1] A.A. Pukhov,[1] A.V. Dorofeenko,[1] and A.A. Lisyansky[2]
[1]Institute for Theoretical and Applied Electromagnetics, 13 Izhorskaya, Moscow 125412, RF
[2]Department of Physics, Queens College of the City University of New York, Flushing, NY

The interest in the optics of metamaterials – negative index materials – has grown explosively during the last decade (see Refs. [1 - 2] and references therein). One of the most perspective features of metamaterials is a possibility of creating of sub-wavelength lenses that can be used in supper-resolution imaging [3]. In the best case scenario, such lenses must be lossless because both loss and gain destroy the perfect image. Though such natural metamaterials have not been found, it was suggested using artificial composite materials with desirable properties. In optics, metal nanoparticles (NPs) have become the most popular components of such composites. Using surface plasmons (SPs) generated in metal NPs allowed for the host of innovative applications. The main limiting factor in using metal NPs is their high level of losses. This obstacle can be overcome by introducing a gain medium into the system [4-6]. Combination of the gain medium with NPs results in the formation of spasers first suggested by Bergman and Stockman [7]. It seems that exploiting spasers, opens up a groundbreaking way to dramatically reduce loss in composites made of metal NPs [7,8]. It is important that the spaser is a self-oscillating system and possesses an inherent frequency ω_a below referred to as an autonomous frequency [7, 8].

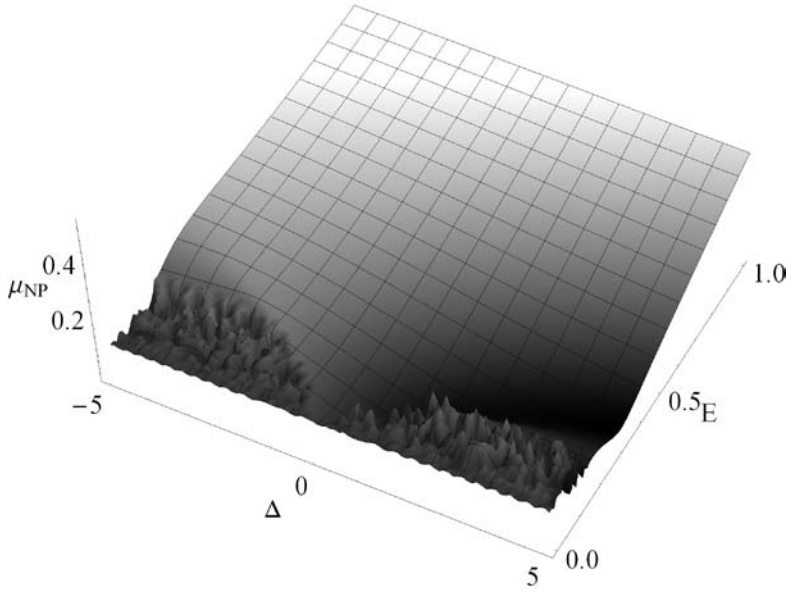

Fig. 1. The dependence of the plasmon dipole moment on the amplitude of the external field and the frequency detuning Δ. The speckle structure at low values of *E* corresponds to the chaotic behavior of the dipole moment.

We show that there is a domain (the Arnold tongue) of values of the amplitude E of the external wave and the frequency detuning $\Delta = \omega_a - \omega_E$ where the spaser synchronizes with the external wave. Outside the domain the spaser exhibits stochastic oscillations (Fig. 1). If $\Delta \neq 0$, then there is a threshold value of the external field intensity below which the spaser always exhibits stochastic oscillations.

We demonstrate that in the domain where a spaser can be synchronized with the external electromagnetic wave loss in metal nanoparticle can be compensated exactly(Fig. 2). We also show that the linear response of the spaser dipole moment to the external field is possible for exceedingly high fields comparing to the interatomic fields only.

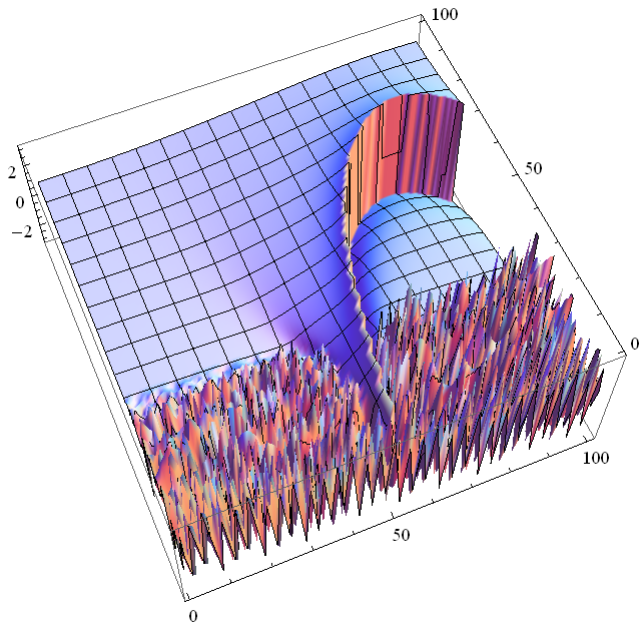

Fig. 2. The dependence of $\phi = \tan^{-1}(\mathrm{Im}\,\mu_{NP} / \mathrm{Re}\,\mu_{NP})$ on the amplitude of the external field E and detuning Δ. The smooth part of the surface corresponds to the Arnold tongue where the spaser is synchronized by the external field. On the rapture $\phi = \pi$.

References

[1] R. Marques, F. Martin, and M. Sorolla, *Metamaterials with negative parameters: theory, design and microwave applications* (Wiley, 2008).
[2] W. Cai and V. Shalaev, *Optical Metamaterials* (Springer, New York, 2010)
[3] J. Pendry

[4] S. A. Ramakrishna and J. B. Pendry, Phys. Rev. B **67**, 201101 (2003).
[5] A. K. Popov and V. M. Shalaev, Opt. Lett. **31**, 2169 (2006).

[6] A. K. Sarychev and G. Tartakovsky, Phys. Rev. B **75**, 085436 (2007).

[7] D. J. Bergman and M. I. Stockman, Phys. Rev. Lett. **90**, 027402 (2003)

[8] M. Premaratne and G.P. Agrawal, Light propagation in gain medium, Cambridge University Press, NY, 2011

Spasing in Metallic Groove

A. V. Dorofeenko,[1,*] **I.A. Nechepurenko,**[1] **A.P. Vinogradov,**[1] **A.A. Pukhov,**[1] **and A.A. Lisyansky**[2]

[1]Institute for Theoretical and Applied Electromagnetics RAS, Russia

[2]Department of Physics, Queens College of the City University of New York, USA

[*]corresponding author: alexandor7@gmail.com

Abstract- We suggest a new kind of spaser based on plasmons excited at a groove in a metal surface. The plasmons are amplified by quantum dots places at the groove bottom. It is shown that at the plasmon propagation along the groove the gain can exceed loss at realistic parameters of the system, which is enough for lasing in the circular groove. Employment of 1D plasmons instead of a nanoparticle plasmonic oscillations gives additional advantages to the spaser. First, the radiation is directional. Second, use of the proper geometry (form of the groove) can eliminate radiation into continuous spectrum (leaky modes).

Recently, a new branch of quantum optics – quantum nanoplasmonics – has arisen [1]. Advantageous plasmon properties such as small wavelength and a high energy concentration open new perspectives for constructing nano-devices such as waveguides, cavities, and antennas. In this regard, studies of plasmons propagating along 1D objects such as wires [2], wedges [3, 4], and channels [5, 6] are of great interest.

Losses in metals are the main obstacle to practical applications of plasmonics. It has been suggested that this problem can be overcome by compensating loss in a gain medium [7]. This relates nanoplasmonics to quantum optics [1, 2]. The first quantum nanoplasmonic device which was referred to as spaser (Surface Plasmon Amplification by Stimulated Emission of Radiation) was proposed in Ref. [1]. The spaser consists of a quantum dot (QD) located near a metal nanoparticle (NP). The plasmonic oscillations in the NP play the role of photons in a laser and the cavity effect is provided by the plasmon localization in the vicinity of the NP. Thus, a pumped QD nonradiatively transfers its excitation to surface plasmons localized at the NP. As a result, one observes an increase of intensity of the surface plasmon field. Thus, the spaser does not radiate an energy beam but generates a near field. The spaser has recently been realized [8].

In this paper, we study surface plasmons propagating along the bottom of a groove (channel) in the metal surface (see schematic in Fig. 1). The surface plasmons are coherently excited by a linear chain of QDs at the bottom of the channel.

Basing on the system of the Maxwell-Bloch equations, we show that the gain coefficient of a surface plasmon

$$\gamma = \Omega \frac{\tau_p |\mu|^2 N_0}{\hbar} \frac{|\mathbf{E}(0,0,z)|^2}{\Phi(z)} - \frac{\Omega}{4\pi} \frac{\int \varepsilon'' |\mathbf{E}(x,y,z)|^2 dxdy}{\Phi(z)} \quad (1)$$

can be made positive for realistic values of the system parameters.

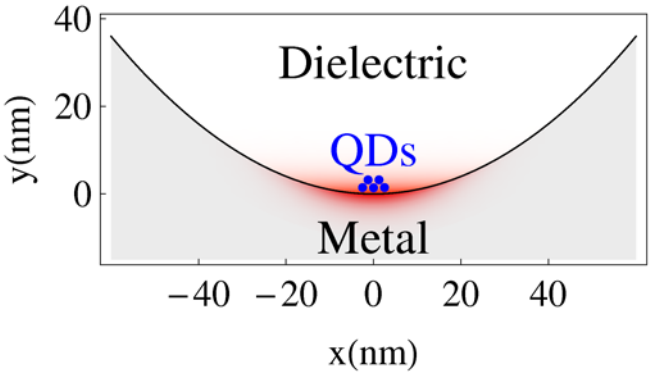

Fig. 1. Schematic of the system geometry. The shaded area around QDs shows the electric field intensity distribution. The QDs at the bottom of the channel in metal are shown by circles.

This means that the plasmon amplitude increases while it propagates, lasing appears in a ring channel. Alternatively, one can form an effective cavity in a linear channel. This requires a larger gain level. Thus, ring or linear channels can be employed in a new kind of spaser generating 1D plasmons. The radiation of flat surface plasmons can be suppressed by using the frequency range in which $\varepsilon_M(\omega)+\varepsilon_D>0$. For the vacuum channel in silver, this range is in the near UV. Replacing the vacuum by a high-permittivity dielectric and silver by a metal-dielectric composite, one can shift the working frequency of the suggested spaser into the visible range. Indeed, using either a dielectric matrix filled with silver inclusions or the silver foam with dielectric bubbles, the effective plasma frequency may be shifted into the visible range.

REFERENCES

1. Bergman, D. J. and M. I. Stockman, "Surface Plasmon Amplification by Stimulated Emission of Radiation: Quantum Generation of Coherent Surface Plasmons in Nanosystems," *Phys. Rev. Lett.*, Vol. 90, No. 2, 027402, 2003.
2. Pendry, J. B., J. B. Holden, D. J. Robbins, and W. J. Stewart, "Low frequency plasmons in thin-wire structures," *J. Phys.: Condens. Matter*, Vol. 10, 4785-4809, 1998.
3. L. C. Davis, "Electostatic edge modes of a dielectric wedge," *Phys. Rev. B*, Vol. 14, 5523–5525, 1976.
4. A. Eguiluz and A. A. Maradudin, "Electrostatic edge modes along a parabolic wedge," *Phys. Rev. B*, Vol. 14, 5526–5528, 1976.
5. I. V. Novikov and A. A. Maradudin, "Channel polaritons," *Phys. Rev. B*, Vol. 66, 035403, 2002.
6. D. K. Gramotnev and S. I. Bozhevolnyi, "Plasmonics beyond the diffraction limit," *Nat. Photon.*, Vol. 4, 83 - 91, 2010.
7. S. A. Maier, "Gain-assisted propagation of electromagnetic energy in subwavelength surface plasmon polariton gap waveguides," *Opt. Commun.*, Vol. 258, Iss. 2, 295-299, 2006.
8. N. I. Zheludev, S. L. Prosvirnin, N. Papasimakis, and V. A. Fedotov, "Lasing spaser," *Nat. Photon.*, Vol. 2, 351 - 354, 2008.

Eigenmodes of an 1D array of coupling spasers.

Pukhov A.A.,[1,2] Andrianov E.S.,[1,2] Dorofeenko A.V., [1,2] Vinogradov A.P.[1,2],

Lisyansky A. A[3]

[1] Moscow Institute of Physics and Technologies
[2] Institute of Theoretical and Applied Electromagnetics RAS
[3] Department of Physics, Queens College of the City University of New York, Flushing, NY 11367

Recently it has been suggested design of metamaterials, which contain both plasmonic and gain inclusion (quantum dots or dye molecules) [1,2].

A plasmonic nanoparticle (NP) and a gain inclusion consists a spaser [St 2003]. External pumping causes population inversion of quantum dot (QD) of the spaser. The transition of QD back into the ground state is accompanied with non-radiative excitation of surface plasmon (SP) localized on NP. Near field feedback results in stimulated radiation of QD. On pumping the spaser coherently amplifies the near field oscillations (plasmons). The competition of the Joule losses in NP with pumping of QD determines the amplitude of these autonomous oscillations.

The present communication is devoted to eigenstates of a system of spasers constituting the metamaterial with gain. The problem resembles the one of diode laser array with the difference that in spaser array the feedback is near field but optical and the dynamics of spaser and laser diode belong to different classes [3,4].

Due to near field nature of the feedback the energy transfer from spaser to spaser requires a shift between phases of dipole moment oscillations of two adjacent spasers [5,6]. Thus, the synchronization of spasers should result in travelling of some excitation over the spaser system.

We consider the simplest model, namely, a 1D array (a chain) of spasers. It is shown that the synchronization of the chain of spasers results in travelling over the system of a harmonic autovawes. These autovawes are perfectly harmonic waves but with fixed amplitude determined by pumping. We find out the dispersion equation for such autovawes. It turns out that spasers may exhibit synchronized oscillations at different frequencies. The frequency depends on the wavenumber of the corresponding harmonic autovawes.

We produce a linear analysis of the stability of such harmonic solitons. It is shown that there is only two stable autovawes with the same module of the wavenumber propagating in the opposite directions. Such an autovawe has the wavelength that is four times the distance between spasers, and its frequency equals the frequency of an autonomic spaser. Really, depending on the initial conditions survives only one of them. These results are confirmed by direct computer simulation.

1. M. A. Noginov, G. Zhu, M. Bahoura, J. Adegoke, C. E. Small, B. A. Ritzo, V. P. Drachev, and V. M. Shalaev, Opt. Lett. **31**, 3022 (2006).
2. A. K. Popov and V. M. Shalaev, Opt. Lett. **31**, 2169 (2006).
3. P. W. Milonni, J. H. Eberly, Laser Physics, Hoboken: John Wiley & Sons (2010)
4. J. Ohtsubo Semiconductor lasers Springer-Verlag Berlin Heidelberg (2008)
5. A.A. Kolokolov, G.V. Skrotskii, Sov. Phys. Usp. 35 (12) 1089–1093 (1992)
6. A.P. Vinogradov, A.V. Dorofeenko, Optics Communications 256, 333–336 (2005)

Nano-optics

A.V. Krasavin, W. Dickson, J.-S. Bouillard, G.A. Wurtz, A.V. Zayats

Nano-optics and Near-field Spextroscopy Laboratory, Department of Physics,
King's College London, Strand, London WC2R 2LS, United Kingdom

http://www.nano-optics.org.uk

We will discuss various plasmonic approaches for controlling photonic signals on sub-wavelength scales. Plasmonic crystals, plasmonic waveguiding components as well a new plasmonic platform based on metamaterials will be presented. Particular emphasis will be given to achieving active functionalities using various control stimuli such as electronic and magnetic fields and all-optically. Amplification of plasmonic signals and dispersion management will also be addressed. Active and tuneable plasmonic components are required for development of integrated photonic circuits, in high-density data storage as well as bio- and chemo-sensing lab-on-a-chip systems, to name a few.

LITERATURE

1. G. A. Wurtz and A. V. Zayats, "Nonlinear surface plasmon polaritonic crystals (review)," Laser and Photon. Rev., vol. 2, pp. 125-135, 2008.
2. W. Dickson, G. A. Wurtz, P. R. Evans, R. J. Pollard, and A. V. Zayats, "Electronically-controlled surface plasmon dispersion and optical transmission through hole arrays in metal films with liquid crystal," Nano Letters, vol. 8, pp. 281-286, 2008.
3. D. O'Connor, M. McCurry, B. Lafferty, and A. V. Zayats, "Plasmonic waveguide as an efficient transducer for high-density data storage," Appl. Phys. Lett., vol. 95, 171112, 2009.
4. Z. Chen, T. Holmgaard, S. I. Bozhevolnyi, L. Markey, A. Dereux, A. V. Krasavin, and A. V. Zayats, "Wavelength selection by dielectric-loaded plasmonic components," Appl. Phys. Lett., vol. 94, 051111, 2009.
5. A. V. Krasavin, A. V. Zayats, "Electro-optic switching element for dielectric-loaded SPP waveguides," Appl. Phys. Lett., vol. 97, 2010, 041107.
6. J.-S. Bouillard, S. Vilain, W. Dickson, and A. V. Zayats, "Hyperspectral imaging with scanning near-field optical microscopy: applications in plasmonics," Opt. Express, vol. 18, 2010, pp. 16513–16519.
7. A. V. Krasavin, A. V. Zayats, "Silicon-based plasmonic waveguides," Opt. Express, vol. 18, 2010, pp.11791-11799.
8. A.V. Kabashin, P. Evans, S. Pastkovsky, W. Hendren, G. A. Wurtz, R. Atkinson, R. Pollard, V. A. Podolskiy, A. V. Zayats, "Plasmonic nanorod metamaterial for biosensing," Nature Materials, vol. 8, pp. 867-871, 2009.
9. R. J. Pollard, A. Murphy, W. R. Hendren, P. R. Evans, R. Atkinson, G. A. Wurtz, V. A. Podolskiy, A. V. Zayats, "Optical nonlocalities and additional waves in epsilon-near-zero metamaterials," Phys. Rev. Lett., vol. 102, 127405, 2009.
10. G. A. Wurtz, R. Pollard, W. Hendren, G. P. Wiederrecht, D. J. Gosztola, V. A. Podolskiy, A. V. Zayats, "Designed ultrafast optical nonlinearity in a plasmonic nanorod metamaterial enhanced by nonlocality," Nature Nanotech., vol. 6, 2011, pp. 107-112.

Theory of surface plasmon amplification by stimulated emission of radiation in metal-semiconductor structures

D. Yu. Fedyanin
Laboratory of Nanooptics and Femtosecond Electronics, Department of General Physics, Moscow Institute of Physics and Technology (State University), 9, Institutsky lane, Dolgoprudny, 141700, Russian Federation
feddu@mail.ru

Abstract- I propose a novel scheme of surface plasmon polariton (SPP) amplification that is based on a minority carrier injection in a metal–semiconductor diode and present a rigorous theoretical study this scheme.

Operation frequency of modern microprocessors does not exceed a few gigahertz due to high heat generation and interconnect delays. SPPs at the interface between a metal and an insulator, are considered as very promising information carriers that can replace electrons in integrated circuits [1,2]. Owing to the exceedingly short wavelength and a very high spatial localization of the electromagnetic field near the interface, it becomes possible to get over the usual diffraction limit and design ultracompact interconnects with the transverse size of the order of 100 nm [1] that is comparable with electronic components. Nevertheless, the utilization of SPPs is limited by the power dissipation, since a significant amount of the SPP filed is concentrated in the metal that results in Joule losses and thus the propagating length of the SPP usually does not exceed 100 μm. To increase the propagation length, one has to utilize long-range SPPs that can show propagation length up to 1 cm. But long-range SPPs exhibit such small losses, since the portion of the SPP field inside the metal is very small while inside the surrounding insulators is, on the contrary, quit large and the penetration depth into the insulators substantially exceeds 1 μm. Thus, the only way to overcome Joule losses inside the metal is to compensate them. This can be done by using an active media placed near a metal surface.

In recent years, a number of paper devoted to the SPP amplification have been published and several methods have been proposed. Despite the advantages of these methods, the necessity of an external high power pump laser prevents us to use them in nanoscale circuits. Hence, one should replace the optical pump laser by a compact electrical pumping. Here, I propose an amplification technique that is based on the minority carrier injection in a Schottky barrier. This technique allows to design a compact and power efficient semiconductor surface plasmon amplifier based on a Schottky diode.

In spite of Schottky diodes are usually treated as majority carrier devices, the situation changes drastically when the metal work function metal work function Ψ_M exceeds $\chi_e+E_g/2$, where χ_e and E_g are the electron affinity and the band gap of the semiconductor, respectively. The concentration of holes near the metal-semiconductor contact becomes greater than the concentration of electrons and it is said that an inversion layer is formed. Under forward bias, holes are injected into the bulk of the

semiconductor and recombine with electrons that results in light emission.

To design an amplifier, one should satisfy the condition for net stimulated emission or gain [5,6]

$$F_e - F_h \geq \hbar\omega \geq E_g \tag{1}$$

where ω is the SPP frequency, F_e, F_h are quasi-Fermi levels for electron and holes, respectively. If we use a degenerate semiconductor, F_e-E_c is positive nearly everywhere inside the semiconductor under sufficient forward bias. Hence, we should only maximize E_v-F_h. It is obvious that, near the metal-semiconductor contact, F_h is very close to the metal Fermi level F_m=0 and we can decrease E_v-F_h by increasing the metal work function or decreasing the electron affinity of the semiconductor. Inside the semiconductor, E_v-F_h will decrease but in the region near the Schottky contact we can satisfy condition (1).

To analyze the amplifier, I solve simultaneously the photon rate and carrier transport equations

$$\begin{cases} \partial\varphi/\partial z = -E_z \\ \partial E_z/\partial z = 4\pi e/\varepsilon_{st} \times (p - n + N_d) \\ \partial n/\partial z = J_n/eD_n - \mu_n n E_z/D_n \\ \partial p/\partial z = -J_p/eD_p + \mu_p p E_z/D_p \\ \partial J_n/\partial z = eU \\ \partial J_p/\partial z = -eU \end{cases} \tag{2}$$

where symbols have their usual meaning [7]. And finally, I discuss the modal gain dependence on different parameters, such as the SPP power, SPP frequency and Schottky diode bias.

ACKNOWLEDGEMENTS

This work was supported in part by the Russian Foundation for Basic Research (grants no. 09-07-00285, 10-07-00618 and 11-07-00505), by the Ministry of Education and Science of the Russian Federation (grants no. P513 and P589) and by the grant MK-334.2011.9 of the President of the Russian Federation.

REFERENCES

1. E. Ozbay, "Plasmonics: Merging Photonics and Electronics at Nanoscale Dimensions," Science, Vol. 311, 189-193, 2006.
2. M. L. Brongersma, and V. M. Shalaev, "The Case for Plasmonics," Science, Vol. 328, 440-441, 2010.
3. D. Yu. Fedyanin, and A. V. Arsenin, "Surface plasmon polariton amplififcation in metal-semiconductor structures ," Opt. Express, submitted, 2011.
4. D. Yu. Fedyanin, and A. V. Arsenin, "Semiconductor Surface Plasmon Amplifier Based on a Schottky Barrier Diode," AIP Conf. Proc. Vol. 1291, 112-114, 2010.
5. N. K. Dutta, and Q. Wang, S*emiconductor Optical Amplifiers*, World Scientific, Singapore, 2006.
6. H. C. Casey, and M. B. Panish, *Heterostructure Lasers*, Part A, Academic, New York, 1978.
7. S. M. Sze, *Physics of Semiconductor Devices*, Wiley, New York, 1981.

Spectral-luminescent study of the interaction oxycoumarine dyes with BSA and DNA

A.A.Ishchenko[1], N.Nizomov[2*], J. Khamraev[2], A.U.Kholov[2]
[1]Institute of organic chemistry National academy of sciences of Ukraine,Murmanska Str. 5, Kyiv 02094, Ukraine,e-mail: alexish@i.com.ua
[2]Samarkand State University, University blvd. 15, 140104 Samarkand, Uzbekistan
e-mail: nnizamov@yandex.ru

Abstract. The spectral-fluorescent properties of water-soluble 7-hydroxicoumarine in the free state and binding to biological macromolecules: bovine serum albumin (BSA) and deoxyribonucleic acid (DNA), salmon were studied. The parameters of the binding: the binding constant (K) and the number of binding sites (N) c BSA dye and DNA.

Organic dyes used as fluorescent probes for analysis of nucleic acids and proteins for diagnostic purposes. Fluorescent probes have a number of features that make them useful for the study of proteins and membranes. First of all, the probe itself "chooses" binding site and can respond to changes not only in this fragment of the protein, but also in other places where there may be new binding sites to which the probe is redistributed. This differs from the probe is covalently linked to protein labels. Therefore, a natural interest in studying the interaction oxicoumarine dyes with biological objects by means of spectral-luminescent analysis. We have studied the spectral and fluorescence properties of water-soluble 7-hydroxicoumarine **1**, its methyl ester, **2**, and dye **3** in the free form and binding to biological macromolecules: bovine serum albumin (BSA) and deoxyribonucleic acid (DNA), salmon. Molecule compounds studied differ from each other by the presence of different substituents. In molecule **1**, there is OH group, whereas **2** differs from

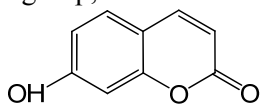

1

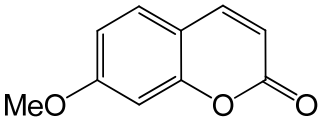

2

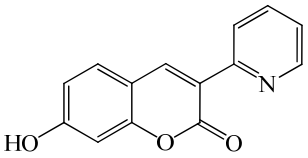

3

1 by the presence of a methyl group. Dye 3 differs from dye **1** and **2**, the presence of pyridine a six-membered heterocycle. It was interesting to see how the influence of such structural differences dyes on their interaction with biological objects. Established that the absorption and fluorescence spectra of compound **2** in the presence of BSA and DNA, remain constant compared with its solution in water. It was found that the addition of BSA to a solution of dye 1 leads to a bathochromic shift of the absorption spectra of ~ 5 nm and observed a new wavelength band with a maximum of λ_{max}=370 nm, the intensity of which increases with the amount of BSA in solution. The shape of the fluorescence spectrum remains virtually unchanged, and there is a small increase in emission intensity. Observed spectral changes are explained by the transition of the dye molecules **1** in anionic form. Similar phenomena are observed in the absorption and fluorescence spectra by adding DNA to an aqueous solution of dyes **1**and **3**. It shows that, as in the case of BSA, with a gradual increase in DNA in solution with the dye is observed bathochromic shift of the absorption spectra of ~ 17 nm, and a new wavelength band with a maximum of λ_{max}=400 nm, the intensity of which grows increase the amount of DNA in solution. According the parameters of the binding: the binding constant (K) and the number of binding sites (N) c BSA dye. Binding constant (K) for dye **1** in water of 5.3×10^5 M^{-1} and dye **2** 2.1×10^5 M^{-1}, and the number of binding sites (N) 1.4 and 0.43, respectively . As can be seen, the value of the binding constants and the number of binding sites of dye **1** in 2.5 times and 3.2 times, respectively, compared with dye **2**. To prove the effect of BSA and DNA fluorescence intensity was investigated the influence of concentration ratio of protein or DNA to the dye **1** and **2**. Established that the fluorescence intensity of dyes **1** and **2** increased to 40-80 dye molecules bind to a protein or DNA. Further increase in the number of dye leads to a decrease in intensity. Thus, when applying oxicoumarine as fluorescent probes and labels need to know the optimal ratio of dye molecules to molecules of protein or DNA. Binding of coumarin dye molecules mainly occurs by electrostatic interaction between the carbonyl oxygen, which has the greatest negative charge to bind to the positive parts of a protein. When the amount of dye (more than 80 dye molecules per protein molecule) is the aggregation of free dye molecules with dye molecules on the surface of the protein, which leads to a weakening of the fluorescence intensity. From these studies the most suitable dyes for

use as a fluorescent probe and marker proteins is dye **3**, which reaches saturation at a higher value of concentration ratio of dye to protein concentration. Therefore, the term dye **3** can be used as a fluorescent probe in biomedical practice to determine the pathological processes in the body.

Spectroscopic study of the influence of solvent nature on the photostability of squaraine dyes.

N.Nizomov*, Sh.N.Nizamov, M.Barakaeva, E.N.Kurtaliev
Samarkand State University, University blvd. 15, 140104 Samarkand, Uzbekistan
e-mail: nnizamov@yandex.ru

Abstract. The influence of solvent nature on spectral-luminescent and photochemical characteristics squaraine dyes were studyed. Established that the transition from the chloroform solution to the binary mixtures: chloroform+ethanol, chloroform+DMF and chloroform+dioxane absorption and fluorescence spectra of studied dyes a hypsochromic shift in the 12-27 nm. It is shown that as the irradiation of solutions there is a decline in the absorptivity and fluorescence capabilities, which is associated with photolysis of the solvent molecules and the subsequent destruction of dye molecules.

Dyes fluorescing in the red and near infrared (NIR) ranges, are best suited for use as fluorescent probes and labels in biomedical research . One of the most promising classes of compounds for this spectral region are polymethine dyes squaraine series (dyes 1-6) (Fig. 1). When using the dye solutions, along with the spectral-luminescent characteristics of a significant parameter in determining their working life, is photostable. Therefore, studying the spectral-luminescent characteristics and mechanisms of photochemical destruction squaraine dyes is of great scientific and practical importance.

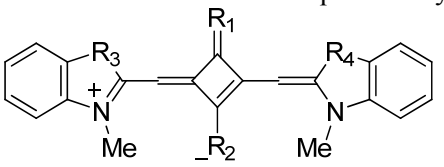

Figure 1. The general structural formula of the studied squaraine dyes. **1**-R_1=R_2=O, R_3=R_4=$(Me)_2$; **2**-R_1=O, R_2=S, R_3=R_4=$(Me)_2$; **3**-R_1=$(NC)_2$, R_2=O, R_3=R_4=$(Me)_2$; **4**-R_1=$(NC)_2$, R_2=O, R_3=R_4=$(Me)_2$; **5**-R_1=$(NC)_2$, R_2=O, R_3=$(Me)_2$ R_4=S; **6**-R_1=$C_4H_4N_2O_3$, R_2=O, R_3=R_4=$(Me)_2$.

The experiments show that the absorption and fluorescence spectra of dyes **1-5** in chloroform in the concentration range 10^{-6}-10^{-4} M remain constant, indicating that the dyes in these conditions are in solution in monomeric form. Based on experimental measurements data for aqueous solutions of the studied dyes, the main spectral-luminescent characteristics of dyes in free form were determined: extinction coefficient (ε), oscillator strength (f_e), radiative lifetime of the excited state (τ), the frequency of purely electronic transition ($\nu_{0\text{-}0}$) and Stokes shift (SS).It is found that when passing from chloroform solution to the binary mixture of chloroform+ethanol, chloroform+DMF and chloroform+dioxane absorption and fluorescence spectra of studied dyes a hypsochromic shift in the 5-27 nm, while spectral shape does not change noticeably. Phenomena observed in the absorption and fluorescence associated with changes in the solvation shells surrounding the dye molecules, which is due to universal and specific interactions of dye molecules with solvent molecules. It was established that as the irradiation fall absorbance and fluorescence capabilities of the solution, with significant changes in the shape of the absorption and fluorescence does not occur. The exposure time needed for bleaching solutions on the structure of the dye and the nature of the solvent and varies from 10 to 1800 seconds. It should be noted that the process of photobleaching increases as dilution. Photobleaching dyes are irreversible, that is, solutions are not stained and thus the absorption and fluorescence over time are not restored. This means

that the decay occurs in the photolysis of the dye molecule. Under the action of the same light irradiation ethanol, dioxane and DMF, and chloroform in different ways decomposes, which leads to varying degrees of bleaching of the same dye in different solvents. It is found that the most rapid photolysis studied dyes occurs in chloroform. Nature of the photobleaching in chloroform can be explained by the formation of phosgene and hydrogen chloride according to the scheme: $2CHCl_3 + O_2 \rightarrow 2OCCl_2 + 2HCl$. Next, hydrogen chloride reacts with the dye, which leads to a violation of the conjugation chain, which is observed bleaching of the dye solution. In the case of ethanol and DMF, the nature of the process of photobleaching can be explained by the fact that the first under the action f a photon is the photodegradation of solvent molecules by the following mechanism: in the case of ethanol: $C_2H_5OH + h\nu \longrightarrow C_2H_5(C_2H_4 + H) + \dot{O}H$ in the case of dimethylformamide $NCON(CH_3)_2 + h\nu \longrightarrow CH_3 + CH + CH_2O + \dot{N}H$. Subsequently, the formed radicals ($\dot{O}H, \dot{N}H$) interact with the active part of the dye molecules, while the conjugation chain of the dye molecules is disturbed, which leads to discoloration of the dye.

FERROMAGNETISM IN MANGANESE ION IMPLANTED SILICON SAMPLES.

J. T. Ruzimurodov
Samarkand State University, Department of Physics, 140104, University blvd. 15, Samarkand, Uzbekistan
E-mail: ruzimurodov_j@samdu.uz

In this work is discussed experimental results of magnetic property and mechanism origin of the ferromagnetism in high compensated, manganese ion implanted silicon samples.

The experimental results and theoretical explanation prover existence of ferromagnetism caused by magnetic nanoclusters of manganese are presented.

Using AFM is proved experimentally, formation high spin magnetic nanoclusters consisting from impurity atoms of manganese with the sizes 20-25 nm at annealing of the certain conditions. Presence of a hysteresis of the curve magnetization in manganese ion implanted samples Si<B, Mn> at room temperature shows presence ferromagnetism.

Ferromagnetism manganese ion implanted silicone samples relating to intercluster superexchange between manganese ions through boron ions. In addition exist some indirect exchange intercluster interactions through conduction band or crystal defects.

Analysis last publications connected in this problem shows, that the opinion about origin ferromagnetism in silicon were divided, same authors ferromagnetism in manganese ion implanted silicon samples closely connects by properties of impurity and others only by presence of defects of a lattice, in which the basic role is played only electrons trapping center and that, neglecting the contribution of properties of impurity. Magnetization measurements of silicone samples doped by manganese high temperature diffusion method in which the concentration of defects is essential low shows presence of a hysteresis and ferromagnetism at low temperatures and that, denying the dominant contribution of defects in ferromagnetism of silicon doped by manganese.

Spectral super-resolution in metamaterial composites

G. Milton
Department of Mathematics University of Utah

We investigate the optical properties of periodic composites containing inclusions having a frequency dependent negative electrical permittivity, with a very small imaginary part,in a normal material matrix. We consider the case where these inclusions have sharp corners, and following Hetherington and Thorpe, use analytic results to argue that it is then possible to deduce the shape of the corner (its included angle) by measurements of the absorptance of such composites when the scale size of the inclusions and period cell is much finer than the wavelength. These analytic arguments are supported by highly accurate numerical results for the effective permittivity function of such composites as a function of the permittivity ratio of inclusions to matrix. The results show that this function has a continuous spectral component with limits independent of the area fraction of inclusions, and with the same limits for both square and staggered square arrays. In other words, the composite absorbs significant energy over a range of frequencies with limits controlled by the corner angle. In this range energy flows towards each corner where it ends up being absorbed in an infinitesimal neighborhood of the corner. For staggered arrays where the squares are almost touching, the absorption spectrum is an extremely sensitive probe of the inclusion separation distance and acts like a Vernier scale. This is joint work with Johan Helsing (Lund) and Ross McPhedran (Sydney).

Strong-field magneto-transport in a composite medium: Why is it interesting and why is it so simple?

David J. Bergman
Raymond and Beverly Sackler School of Physics and Astronomy
Faculty of Exact Sciences, Tel Aviv University, IL-69978 Tel Aviv, Israel
bergman@post.tau.ac.il

Abstract—

In an isotropic or cubic point-symmetry composite made of electrical conductors with scalar conductivities σ_i that satisfy $\sigma_1 \leq \sigma_i \leq \sigma_2$, the macroscopic conductivity is also a scalar σ_e which always satisfies $\sigma_1 \leq \sigma_e \leq \sigma_2$. Therefore, although calculating σ_e might be difficult there is no "new physics". New physics appears when $\sigma_1 = 0$ or when $\sigma_2 = \infty$. The geometric percolation threshold is then a "critical point" in the macroscopic response. However, when an external magnetic field $\mathbf{B}$ is present, which is strong enough so that the Hall resistivities are greater than the Ohmic resistivities in at least some of the constituents, surprising new physical phenomena appear. These include a macroscopic response in periodic microstructures that is strongly anisotropic even when the microstructure has a very high point symmetry (i.e., cubic or square or triagular or hexagonal). Also appearing are a number of new critical points. These are found in disordered microstructures even when all the constituents are characterized by comparable (though different) resistivity tensors,

Perhaps even more surprising is the fact that, when the Hall-to-transverse-Ohmic-resistivity ratio is large, the local electric field and current density become much simpler than even in the total absence of any magnetic field. This simplification enables some elements of the macroscopic resistivity tensor $\hat{\rho}_e$ to be calculated in closed form to leading order in the reciprocal of that ratio. Another surprise is that, in some cases, the macroscopic Ohmic resistivity of such a composite medium keeps increasing as the square of that ratio, and therefore as the squared magnetic field $\mathbf{B}^2$, without any saturation, even when the constituent Ohmic resistivities are all saturated. This is a kind of "giant magneto-resistance" whose origin is entirely classical: The entire calculation is based on classical conductivity equations, without having to invoke any kind of quantum phenomena or effects.

A large Hall-to-transverse-Ohmic-resistivity ratio is easiest to achieve in a doped semiconductor. This opens up the possibility of developing new strong-$\mathbf{B}$ devices based upon this new type of giant classical magneto-resistance.

In the talk I will describe numerical computations as well as exact asymptotic calculations and effective medium approximations that were used to obtain some of these results. I will also describe some new, unpublished calculational results about systems where a strong, non-saturating $\mathbf{B}^2$ behavior of the Ohmic resistivity is found.

Spatial dispersion in layered metamaterials

P. A. Belov[1,2], **A. A. Orlov**[1], **A. V. Chebykin**[1],, **Yu. S. Kivshar**[1,3]

[1]National Research University of Information Technologies, Mechanics and Optics, St. Petersburg, Russia
[2]Queen Mary University of London, London, UK
[3]Australian National University, Canberra, Australia
belov@phoi.ifmo.ru

Abstract— We have accomplished rigorous dispersion analysis and showed clearly impact of nonlocality on properties of multilayered metal-dielectric metamaterial. The main discovered effect is an appearance of additional extraordinary waves in the metamaterial which leads to the splitting of the TM-polarized beam at the air-MDN interface.

Optical metamaterials formed by periodic layered metal-dielectric nanostructures (MDNs) provide great possibilities for near-field manipulations. This property is employed in numerous applications including subwavelength imaging [1, 2, 3], nanolithography [4], optical nanocircuitry [5], and even invisibility cloaks [6].

The effective medium model (EMM) is a conventional approach to description of MDNs. EMM describes the metamaterial under consideration as an uniaxial anisotropic medium with permittivity tensor of the form:

$$\varepsilon_{\text{eff}} = \begin{pmatrix} \varepsilon_\perp & 0 & 0 \\ 0 & \varepsilon_\parallel & 0 \\ 0 & 0 & \varepsilon_\parallel \end{pmatrix}, \quad \begin{aligned} \varepsilon_\parallel &= \frac{\varepsilon_1 d_1 + \varepsilon_2 d_2}{d_1 + d_2}, \\ \varepsilon_\perp &= \left(\frac{\varepsilon_1^{-1} d_1 + \varepsilon_2^{-1} d_2}{d_1 + d_2} \right)^{-1}, \end{aligned} \tag{1}$$

where $\varepsilon_1, \varepsilon_2$ and d_1, d_2 are dielectric permittivities and thicknesses of the layers, respectively.

The principal elements of the permittivity tensor can have nearly arbitrary values. For example, if $\varepsilon_\parallel$ and $\varepsilon_\perp$ have different signs then the MDN is a typical realization of indefinite medium [7]. Such medium features negative refraction effect since its isofrequency contours have hyperbolic form.

In this work we considered spatial dispersion in three MDNs formed by layers of metal and dielectric with various thickness ratios (3:2, 1:1, and 2:3), but fixed total period. Configurations and parameters of the structures are illustrated schematically in the insets of Fig. 1. The dispersion diagrams $\omega(k_y)$ for the three MDNs under consideration shown in Fig. 1 were computed using two approaches: the effective medium model (approximate approach) and the well-known classical dispersion relation for 1D photonic crystals (exact description).

Different ratios of layers thicknesses were chosen in order to demonstrate different behaviors of dispersion curves. In all cases the dispersion curves consists of two branches with joint surface plasmon polariton (SPP) resonance as asymptote if $k_y \to \infty$ for actual MDN and of one branch with $\epsilon_\perp = \infty$ resonance for effective medium model. The presence of two branches of dispersion

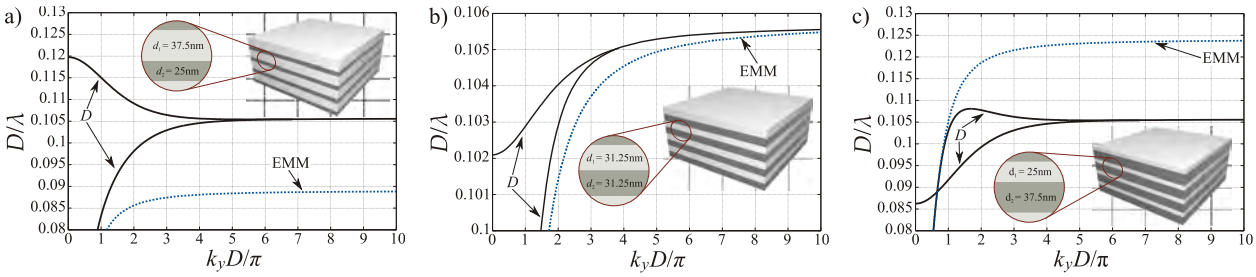

Figure 1: The dispersion diagrams and geometry of the MDNs composed of alternating HfO_2 and Ag layers. The permittivity of HfO_2 is assumed to be equal to $\varepsilon_1 = 4.6$. The permittivity of silver is given by Drude model: $\varepsilon_2 = 1 - \omega_p^2/\omega^2 = 1 - \lambda^2/\lambda_p^2$, where $\lambda_p = 2\pi c/\omega_p$=250 nm. The ratio of layers thicknesses is varied as follows: a) $d_1 = 1.5d_2$, b) $d_1 = d_2$, and c) $d_2 = 1.5d_1$.

curve (in contrary to just one brunch predicted by effective medium model) is a consequence of strong spatial dispersion in the structure.

In the first case (Fig. 1.a), the SPP resonance appears above the frequency where epsilon very large behavior is expected and the dispersion diagram features forward and backward wave branches with different frequency bands. In the second case (Fig. 1.b), the frequencies are chosen to be equal and both branches correspond to forward waves, but the waves exist at the same frequency band in contrary to the previous case. In the third case (Fig. 1.c), the branches cross each other at certain point and one of the branches has a maximum leading to existence of backward and forward waves simultaneously at the same range of frequencies. The effective medium model in all cases predicts only one forward propagating wave at all frequencies. The presence of two propagating waves is a consequence of nonlocality and strong spatial dispersion which are caused by SPPs at the interfaces of the layers.

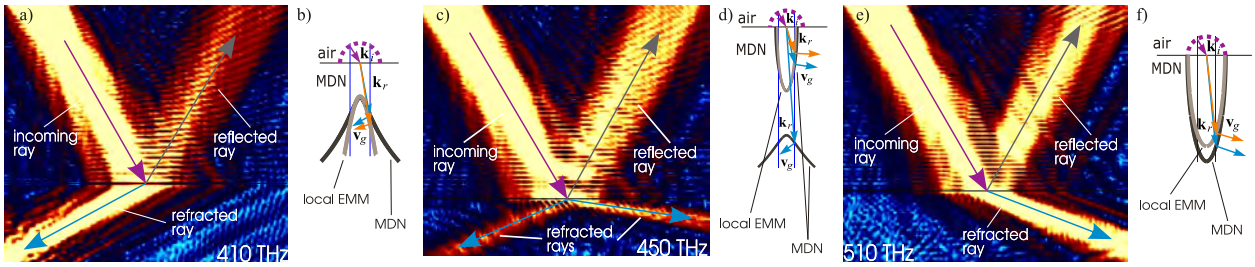

Figure 2: Results of ray refraction simulations with corresponding refraction diagrams based on isofrequency contours both for local effective medium model and actual MDN.

Next, we have performed numerical experiments of ray refraction at the air-MDN interface at different frequencies (see Fig. 2). At 410 THz only one negatively refracted ray is observed (see Fig. 2.a,b) and effective medium model is applicable in such a situation. Appearance of an ellipse at the isofrequency contour at 450 THz shown in Fig. 2.d as compared to Fig. 2.b leads to birefringence phenomena in the MDN. The negatively refracted ray is still there while in addition to it a positively refracted ray corresponding to the ellipse appears. In this case the local effective medium model is not able to predict the presence of the two rays and describes only one of them. At the higher frequency (510 THz) only one positively refracted ray is observed and this fact is well described by effective medium model.

In conclusion, we compared dispersion characteristics of actual periodic structure with ones predicted by effective medium model and revealed significant differences between them. In particular, two dispersion branches of extraordinary waves are observed instead of one predicted by effective medium model. Our numerical simulations revealed the splitting of the TM-polarized wave at the interface between air and metal-dielectric-nanostructure into two refracted waves inside of the structure instead of one extraordinary wave predicted by effective medium model. All obtained results demonstrate presence of strong spatial dispersion in the structure and provide a proof that the metal-dielectric nanostructure is actually a nonlocal material. These conclusions are in a good agreement with results of precedent works where the guiding modes of metal-dielectric multilayered structures [8] and the surface waves at interfaces of metal-dielectric nanostructures [9] were investigated. All discovered effects can be described by means of nonlocal effective medium which we've derived for MDNs using a homogenization technique suggested by Silveirinha in [10].

REFERENCES

1. S. A. Ramakrishna and J. B. Pendry, Phys. Rev. B **67**, 201101 (2003).
2. P. Belov and Y. Hao, Phys. Rev. B **73**, 113110 (2006).
3. Z. Liu, H. Lee, Y. Xiong, C. Sun, and X. Zhang, Science **315**, 1686 (2007).
4. Xiong, Y., Liu, Z., and Zhang, X., Appl. Phys. Lett. **93**, 111116 (2008).
5. N. Engheta, Science **317**, 16981702 (2007).
6. W. Cai, U. K. Chettiar, A. V. Kildishev, and V. M. Shalaev, Opt. Express **16**, 5444 (2008).
7. D. Smith and D. Schurig, Phys. Rev. Lett. **90**, 077405 (2003).
8. J. Elser, V. A. Podolksiy, I. Salakhutdinov, I. Avrutsky, Appl. Phys. Lett. **90**, 191109 (2007).
9. S. M. Vukovic, I. V. Shadrivov, and Y. S. Kivshar, Appl. Phys. Lett. **95**, 041902 (2009).
10. M. G. Silveirinha, Phys. Rev. B **75**, 115104 (2007)

Subwavelength optical imaging with arrays of silver nanorods

S. Yu. Kosulnikov[1], **A. Rahman**[2], **P. A. Belov**[1,2], **Yu. S. Kivshar**[1,3]

[1]National Research University of Information Technologies, Mechanics and Optics, St. Petersburg, Russia
[2]Queen Mary University of London, London, UK
[3]Australian National University, Canberra, Australia
serg.kosulnikov@phoi.ifmo.ru

Abstract— Tailoring the parameters of silver nanorods array for subwavelength imaging of arbitrary coherent sources has been discussed recently in [Phys. Rev. B **82**, 113408 (2010)]. In this paper we examine the performance of the proposed superlens. In particular, we evaluate the operational bandwidth of the device. The impact of source-offset is also investigated and this provides an idea about the level of tolerance offered by the superlens with regard to source location. The performance of device is analyzed numerically both through analysis of transmission and reflection coefficients and by full-wave simulation for a particular sample source arrangement.

A superlens formed by an array of silver (Ag) nanorods was suggested in [1]. An improved multi-segment version of this nanolens was proposed in [2] and promises to offer colour imaging and magnification capabilities. The typical scanning speed of a conventional scanning near-field optical microscope (SNOM) employing a single probe is 10 microns per second which makes the process of near-field scan very slow due to the fact that an automatic mechanical control system is needed to control the tip-sample distance. In contrast to this conventional method the above mentioned superlenes offer the advantage of simultaneous imaging of the whole area of interest thus reducing the time of scanning significantly.

Theoretical and experimental studies of subwavelength imaging with metallic rods have been previously conducted in microwave [4], terahertz [5] and [**?**] domains. As discussed in [7] by the authors, the proper imaging by such a structure requires the length of rod L to obey Fabry-Pérot resonance condition $L = n\lambda_g/2$, where λ_g is the guided wavelength and n is an integer number. In this paper we study the functional characteristics of a superlens formed by an array of silver nanorods in the visible domain.

The fundamental problem with the nanolens proposed in [1] is that the parameters of rods suggested by the authors produce anomalous results: the field distribution produced by an incoherent source is transported perfectly, but the nanolens fails to reproduce the distribution of an arbitrary coherent sources, and therefore, the further investigation is required to explain and to eliminate the problem in order to provide stable and convincing operation of such a device with arbitrary sources. A detailed step-by-step procedure how to calculate the nanorod parameters for proper operation at a particular frequency is given in [3] where it was suggested that a rod-length of 80 nm (in contrast to 50 nm as in [1]) enables operation of the superlens with a rod diameter and period of 20 and 40 nm respectively, at 614 THz frequency. The idea of this paper is to throw some light on the performance of the modified device through analysis of its operational bandwidth and sensitivity to transverse location of a source.

The nanorod array with triangular lattice pattern which was numerically modeled using full-wave electromagnetic simulator CST^{TM} Microwave Studio. We have used the Drude model for permittivity of Ag defined as $\varepsilon_m(\omega) = \varepsilon_\infty$ - $\omega_p^2/(\omega^2 + \mathrm{i}\Gamma\omega)$ with $\varepsilon_\infty = 4.9638$, $\omega_p = 1.4497{\cdot}10^{16}$ rad/s and $\Gamma = 8.33689{\cdot}10^{13}$/s [1] which gives us the permittivity value of -9.121 + i0.304 at wavelength of 488 nm. The calculations have been done for rods with 80 nm length, 20 nm diameter and 40 nm period of array. The imaging capability of the lens is tested with the help of six in-phase point sources positioned on the axes of rods in a hexagonal arrangement. Each point source is a small dipole polarized along the rod axis (X-axis) and placed 10 nm away from the array interface (front-interface). The source and the image plane field distributions plotted at different frequencies under this circumstance are shown in Figs.1. It is evident from the figure that the lens exhibits good imaging performance in the 554 - 614 THz range as the source-field-distributions are reproduced well at the image plane in this range. This allows us to conclude that the operational bandwidth of the device is around 10% which is quite good compared to that of other similar imaging devices. Outside this operational regime the device cannot replicate the source-field-distributions at the

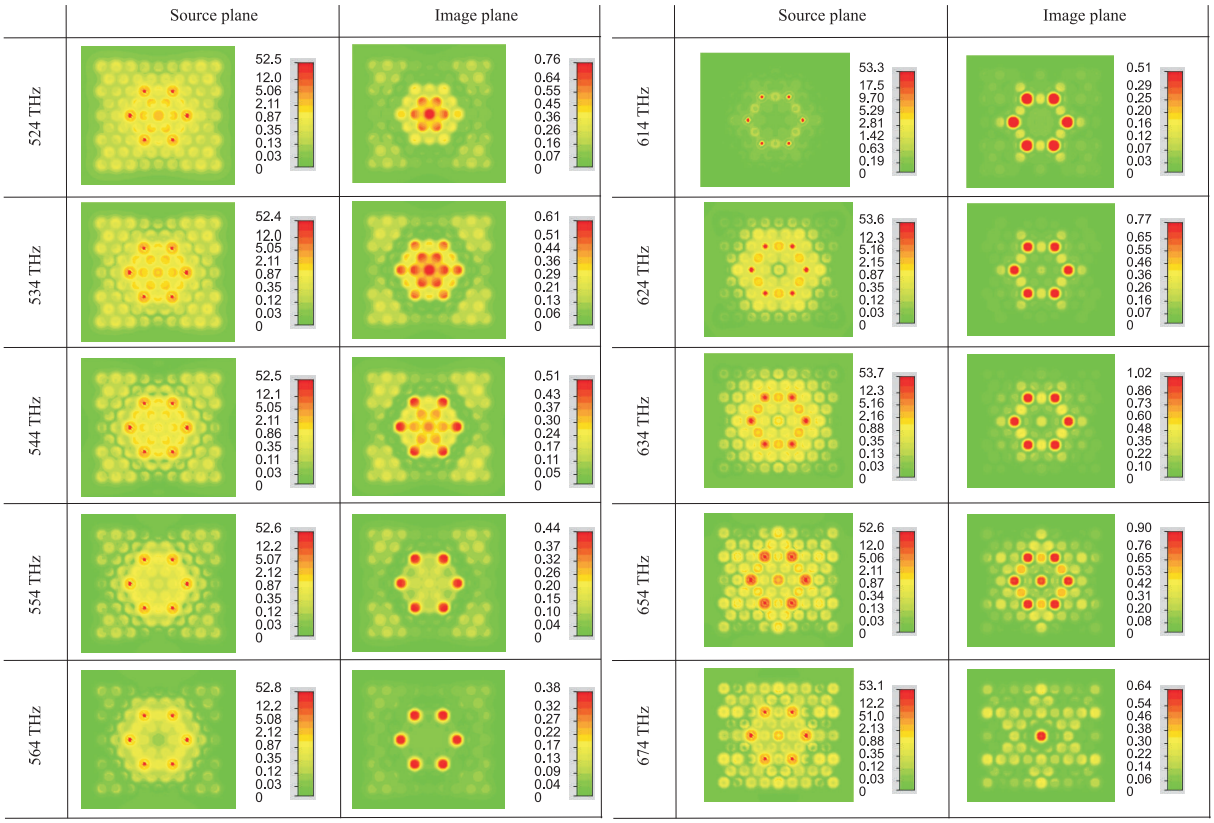

Figure 1: Electric field distributions at the source and the image plane at various frequencies.

image plane and consequently produces a misleading vision of the source. Below the lower limit of the operational band the lens gives us a wrong impression of seven point sources since a maxima at the centre of the hexagon is also discerned. On the other hand, above the higher limit of the operational band the lens gives a false vision of single point source.

We have also calculated the transmission and reflection coefficients of an infinite array in order to have more insight into the transmission characteristics of the lens. A resonance-free transmission coefficient magnitude and constant phase is mandatory to reproduce the source field distributions correctly. The desired transmission characteristics are achievable through proper selection of rod parameters e.g., rod-length, diameter, rod spacing and lattice arrangement. Such tailoring of transmission characteristics is found to be more convenient through modification of rod's intrinsic parameters such as rod length and diameter.

REFERENCES

1. A. Ono, J. Kato and S. Kawata, "Subwavelength optical imaging through a metallic nanorod array", *Phys. Rev. Lett.*, vol. 95, pp. 267407 (1-4), 2005.
2. S. Kawata, A. Ono and P. Verma, "Subwavelength colour imaging with a metallic nanolens", *Nature Photonics*, vol. 2, pp. 438-442 (2008).
3. A. Rahman, P. A. Belov and Y. Hao, "Tailoring silver nanorod arrays for subwavelength imaging of arbitrary coherent sources", *Phys. Rev. B* **82**, 113408 (2010).
4. P. A. Belov, Y. Zhao, S. Tse, P. Ikonen, M. G. Silveirinha, C. R. Simovski, S. Tretyakov, Y. Hao and C. G. Parini, "Transmission of images with subwavelength resolution to distances of several wavelengths in the microwave range", *Phys. Rev. B* **77**, 193108 (2008).
5. G. Shvets, S. Trendafilov, J. B. Pendry and A. Sarychev, "Guiding, Focusing, and Sensing on the Subwavelength Scale Using Metallic Wire Arrays", *Phys. Rev. Lett.* **99**, 053903 (2007).
6. M. Silveirinha, P. A. Belov and C. R. Simovski, "Ultimate limit of resolution of subwavelength imaging devices formed by metallic rods", *Optics Letters* **33**, 1726-1728 (2008).
7. A. Rahman, P. A. Belov, M. G. Silveirinha, C. R. Simovski, Y. Hao and C. G. Parini, "Role of Fabry-Perot resonance and shielding in subwavelength imaging performance of multiwire endoscopes", *Appl. Phys. Lett.* **94**, 031104 (2009).

Raman Spectra and Intermolecular Hydrogen Bonds in Solutions of Quinoline

F.H.Tukhvatullin, A.Jumabaev, H.Hushvaktov, A.Absanov, B.Hudoyberdiev
Samarkand State University, 15, University blvd., 140104, Samarkand, Uzbekistan. E-mail: ahmad@samdu.uz

Abstract

With the help of the diffraction spectrometer DFS-52 the Raman spectra in quinoline - isopropyl alcohol solution were studied. Обнаружены признаки образования межмолекулярной водородной связи между разнородными молекулами. The signs of formation of intermolecular hydrogen bonding between unlike molecules were revealed.

Key words: Hydrogen bond, parallel and perpendicular polarized component, Raman spectra, energy profit of dimerization.

The half-width of bands 1014,3 and 1033,8 sm^{-1} of Raman spectrum of quinoline at its dilution in neutral solvents (benzene, CCl_4) narrowed in 1,3-1,5 times at high dilution. The effect is associated with increased time of vibrational relaxation.

Another picture of the behavior of 1033.8 cm^{-1} band we observe for solution of quinoline with propan-2-ol. Figure 1 shows the spectra of 1033.8 cm^{-1} band of quinoline in solution with propan-2-ol. The concentration dependence of the band shape shows that the newly appeared high-frequency band corresponds to quinoline - propan-2-ol aggregates. Judging by the results of this study the doublet character of 820 cm^{-1} band of the alcohol occurs in solutions of alcohol with quinoline. This can be judged by the concentration dependence of 820 cm^{-1} band. In the process of dilution of the alcohol, the band firstly is widened from 6.4 cm^{-1} in pure alcohol up to 9 cm^{-1} in solution with 0.1 m.f. of alcohol concentration. At lesser concentrations one should expect narrowing of the line.

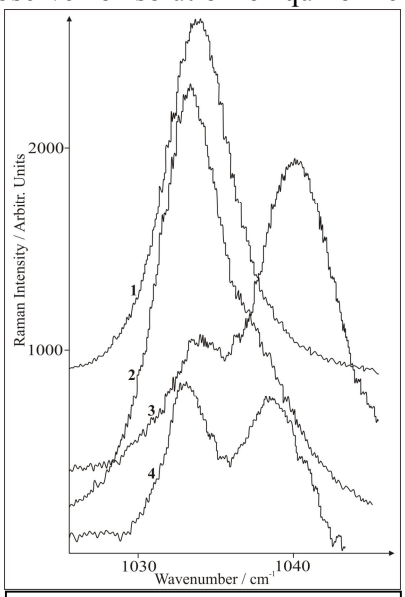

Figure 1. 1034 cm^{-1} bands in pure liquid quinoline (1); in solution with propan-2-ol; 2, 3 concentration of quinoline, respectively, 0.8 m.f. and 0.15 m.f., and ternary mixture quinolin - propan-2-ol - benzene (concentration of components, respectively, 0.02 m.f., 0.20 m.f. and 0.78 m.f.)

For 520 cm^{-1} band in pure liquid quinoline parallel polarized component at 20 ^{0}C is asymmetric in the high-frequency region. The shape of perpendicular polarized component is complicated. A non-coincidence of peak frequencies of parallel and perpendicular polarized components is observed (~2cm^{-1}). Quantum-chemical calculations showed that in the region of 520 cm^{-1} we really should have for a monomer molecule two closely spaced lines with wave-numbers 530 and 527 cm^{-1} (scaling factor 0,97) with depolarization ratio 0,61 and 0,26. We should also note that 520 cm^{-1} bands of quinoline in the mixture with chloroform became resolvable, too (Figure 2). Even at 0.2 m.f. of chloroform 520 cm^{-1} band becomes non-monotonic in the high-frequency side. As the concentration of quinoline this non-monotonic feature becomes clearer, and at 0.4 m.f. of quinoline in the solution the non-monotonic features appear in $I_{\perp}(\nu)$ component. Note that the ratio of the intensity of bands is not noticeable with further dilution. At 0.2 m.f. of quinoline two lines with wave-numbers 518.2 cm^{-1} and 521.4 cm^{-1} are clearly manifested in the spectrum.

In solutions with propan-2-ol band 1033.8 cm^{-1} (figure 1) becomes of doublet character. Resolution of bands becomes better by dilution of the binary solution of quinoline-alcohol with large amount of neutral solvent (benzene). Wave number of bands in the triple mixture are 1033,0 cm^{-1} and 1039,0 cm^{-1}. Doublet nature of the band in the binary and triple mixtures is associated with the presence in a liquid mixture of monomer molecules and aggregates of quinoline-propan-2-ol (high-frequency line). Formation of aggregates also is seen in the band

820 cm^{-1} of propan-2-ol. A similar picture is for the band 667 cm^{-1} of chloroform in a mixture with quinoline. Figure 3 shows the calculated structure of monomers of quinoline and isopropyl alcohol, and propan-2-ol – quinoline aggregate. It is evident that there is the hydrogen bond between the molecules involving the hydrogen of OH group of alcohol and the nitrogen atom of quinoline. The length of the hydrogen bond is 1.958 Å. We also note that quite intensive interaction takes place between the oxygen atom O^{19} of alcohol and one of hydrogen atom of quinoline H^{13} (atom numbers are the same as in the figure). Distance O^{19}-H^{13} is 2.627 Å. The overall energy profit during the formation of such aggregate is 22.0 kJ/mole. The figure shows that the formation of the aggregate is accompanied by changes in the lengths of some bonds and charge redistribution between the atoms for both molecules. In full accordance with experiment the calculated frequency of 1037 cm^{-1} band (experimental value is 1033.8 cm^{-1}) of monomer shifts to higher frequencies in the process of formation of H-aggregate (~7 cm^{-1}).

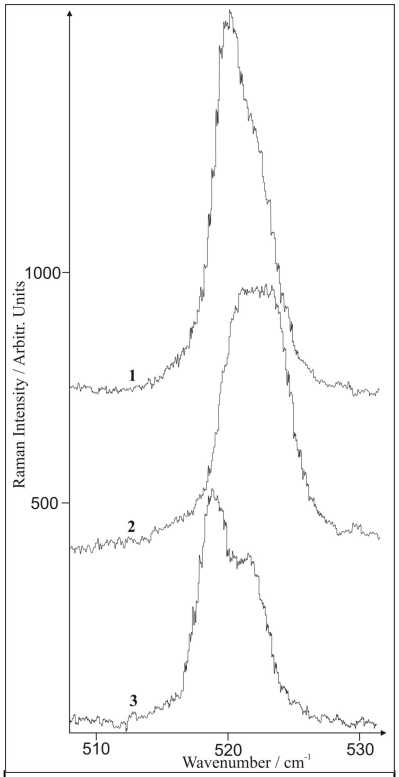

Figure 2. 520 cm^{-1} bands of spectra of Raman scattering in quinoline: 1-parallel-polarized component, 2 – perpendicular-polarized component, 3 - solution of quinoline (0.2 m.f.) with chloroform (0.8 m.f.). Here and below the intencities are not reduced to a unified scale.

1). Non-coincidence of peak frequencies of bands in spectra of Raman scattering of different polarization is connected with the complexity of these bands - the presence within the band of two lines, which are slightly different with respect to peak frequency and possess different magnitude of the depolarization ratio.

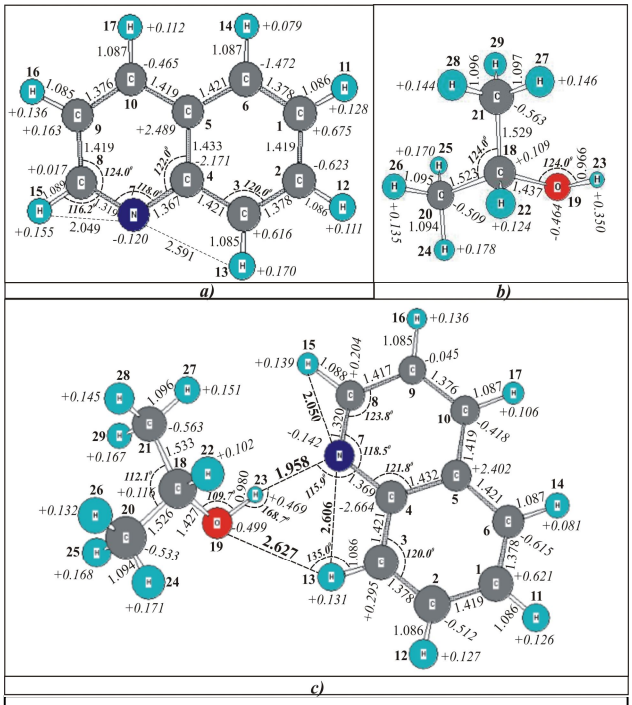

Figure 3. Structure of monomeric molecules of quinoline (a) and propan-2-ol (b), as well as quinoline – propan-2-ol aggregate (c) (distance is in Å, charges are un the units of electron's charge).

2). Just as in other nitrogen-containing compounds, the formation of intermolecular hydrogen bond between the molecules of quinoline leads to appearance of the bands of aggregates in the high-frequency part of vibrations involving the nitrogen atom, that is connected with the strengthening of bonds of π–electrons in the closed ring of quinoline molecule.

3). The strong decrease in the width of the bands in neutral solvents is connected with the destruction of aggregates in liquid media and with increase of the lifetime of molecules in a given vibrational state.

About an Availability of Obtain "Semiconductor Metamaterials" by Ion Implantation Method

E. U. Arzikulov*, S. N. Srajev, Q. N. Srojev

Samarqand State University, 140104, university blvd. 15, Samarqand, Uzbekistan
*corresponding author: e-mail: eshquvat@mail.ru

Abstract

In this paper is discussed about an opportunity use dislocation loops in semiconductors for obtain "semiconductor metamaterials".

It is known, that crystal structures practically of all elementary and compound semiconductors to contain a various sort of dislocations. The size, type and concentration such dislocations depend on a number of the factors and they can be operated various ways. Besides it is known, that dislocations strongly influences optical, electrical and other properties of semiconductors, together with metals. Operating a type, the concentration and sizes dislocation loops can in a wide interval be operated practically all parameters of semiconductors.

Some impurity (for example, nickel and copper in silicon) in semiconductors were in interstitial position of a crystal lattice at high-temperature annealing are capable to be incorporation on lines dislocation loops. As a matter of fact these loops is metal, as impurity is metals and consequently they can serve resonators for absorption of electromagnetic radiation. Operating concentration of entered impurity and also concentration dislocations it is possible to obtain on the basis of compensated (on an example silicon, gallium arsenide) and semi-insulating materials (on an example semi-insulating gallium arsenide and cadmium sulphide) with negative ε and μ.

On seen, the best method of input of impurity in volume of the semiconductor is ion implantation, as at ion bombardment in semiconductors arises in addition to existing, various defects. Besides by ion implantation we can to introduce such quantity of impurity which on some orders more than their equilibrium concentration, even is possible to enter at high temperatures. Operating ions energy, implantation dose and annealing temperature it is possible to select an optimum condition for obtaining "semiconductor metamaterials".

Magnetic Properties of a New Family of Quaternary Ni-Mn-In-Z Heusler Alloys

A. Granovsky[1,2,3], V. Prudnikov[1], A. Kazakov[1], A. Zhukov[2,3], V. Zhukova[3], J. Gonzalez[3], I. Dubenko[4]

[1]Faculty of Physics, Moscow State University, Moscow, 119991 Russia; [2] IKERBASQUE, the Basque Foundation for Science, 48011 Bilbao, Spain; [3] Basque Country University, 20080 San Sebastian, Spain; [4] Southern Illinois University Carbondale, IL, 62901, USA; [3] Basque Country University, 20080 San Sebastian, Spain

granov@magn.ru

The strong interest to Heusler alloys is mainly due to the two unique properties: half-metallic behaviour and martensitic phase transition. The first feature leads to the 100% spin polarization of the electronic states at the Fermi level and makes these systems extremely attractive for spintronics. The second feature leads to magnetic shape memory effect, magnetic superelasticity, large magnetocaloric effect, exchange bias, metamagnetism, giant magnetoresistance, giant Hall effect, kinetic arrest [1,2]. Therefore Heusler alloys offer an excellent opportunity to investigate a rich collection of novel, interconnected physical properties that related to the various aspects of magnetic and structural phase transformations. Besides, Heusler alloys can be considered as multifunctional smart materials promising for spintronics, magnetic refrigeration, and magnetic sensors. In this report, we present experimental results on structural, magnetic, magnetotransport properties, magnetocaloric effect in Ni-Mn-In-Z alloys focusing on the specific behavior of Hall effect and magnetocaloric effect in the vicinity of martensitic transformation.

The $Ni_{50}Mn_{35}In_{15}$, $Ni_{48}Co_2Mn_{35}In_{15}$, $Ni_{50}Mn_{35}In_{14}Ge_1$, $Ni_{50}Mn_{35}In_{14}Al_1$ samples were fabricated using the conventional arc-melting method. The magnetization M(T,H) was measured using VSM (Lake Shore 7400 System) and SQUID (Quantum Design) magnetometers in the temperature interval 4-400K and magnetic field up to 50 kOe. Magnetotransport measurements were carried out by the standard four-probe method using a fully automated system in a temperature interval 77-400K at magnetic fields in the range 0.005-15 kOe. Direct measurements of magnetocaloric effect, namely the adiabatic change of temperature (ΔT) under an applied magnetic field up to 18 kOe, were carried out using MagEq MMS 801 set up.

It was obtained that a martensitic transformation is accompanied by a change in the sign of the constant of the normal Hall effect, which means a strong change in the electronic spectrum in the martensitic transformation, while the anomalous Hall effect (AHE) constant is positive in both the austenite and martensite phases. In both phases, there are no correlations between the AHE constant and the square of the resistivity, which are characteristic of the side jump mechanism in the AHE theory. In the near vicinity of the martensitic transformation, the field dependences of the Hall resistance are complex and nonmonotonic, indicating a change in the relative concentrations of the austenite and martensite phases in strong fields. ΔT is negative at the martensitic transition and is about –(1.5 –1.9)K in 18 kOe, and ΔT is up to +2K at the Curie temperature of austenitic phase.

This research was supported by the Russian Foundation for Basic Researches, by the Basque Foundation for Science, by the Office of Basic Energy Sciences, Material Sciences Division of the U. S. Department of Energy.

[1] Ferromagnetic Shape Memory Alloys II, Ed. V.A. Chernenko, J.M. Barandiaran, Trans. Tech. Publ. Ltd, Switzerland, 210 p., 2009.

[2] I. Dubenko, A. Pathak, S. Stadler et al. Phys.Rev.B **80**, 092408 (2009).

Above Room Temperature Ferromagnetism in Si:Mn and $TiO_{2-\delta}$:Co

A. Granovsky[1], A. Orlov[2], N. Perov[1], E.Gan'shina[1], L. Balagurov[2], A. Sapelkin[3], A. Rogalev[4], A. Smekhova[4]

[1]Faculty of Physics, Moscow State University, Moscow, 119991 Russia; [2] State Institute for Rare Metals, Moscow, 119017 Russia; [3] Queen Mary University of London, E1 4NS, London, UK; [4] European Synchrotron Radiation Facility, 38043, Grenoble, Cedex 9, France

granov@magn.ru

We present recent experimental results on the structural, electrical and magnetic properties of Mn-implanted Si. and Co-doped TiO_2 magnetic oxides.

Si wafers, both *n*- and *p*-type, with high and low resistivity, were used as the starting materials for implantation with Mn ions at the fluencies up to 5 x 10^{16} cm^{-2}. After implantation and vacuum annealing at 850^0C, the materials were investigated with SIMS, SRP, TEM, XRD, XAS, XMCD, VSM, SQUID and magneto-optical techniques. The saturation magnetization was found to show the lack of any regular dependence on the Si conductivity type, type of impurity and the short post- implantation annealing. According to XMCD Mn impurity in Si does not bear any appreciable magnetic moment at room temperature. The obtained results indicate that above room temperature ferromagnetism in Mn-implanted Si originates not from Mn impurity but rather from structural defects in Si .

The $TiO_{2-\delta}$: Co thin films were deposited on $LaAlO_3$ (001) substrates by magnetron sputtering in the argon–oxygen atmosphere at oxygen partial pressure of 2.10^{-6}-2.10^{-4} Torr. It was obtained that Transversal Kerr Effect (TKE) spectra in ferromagnetic samples are extremely sensitive to the Co volume fraction, the crystalline structure, and technology parameters. The observed well-pronounced peaks in TKE spectra for anatase Co-doped $TiO_{2-\delta}$ films at low Co (<1%) volume fraction are not representative for bulk Co or Co clusters in $TiO_{2-\delta}$ matrix that indicates on intrinsic ferromagnetism in these samples. With increase of Co volume fraction up to 5-8% the fine structure of TKE spectra disappears and the magneto-optical response in reflection mode becomes larger than that for thick Co films. Moreover, the TKE increases further in the case of the films fabricated onto $SrTiO_3$ substrates. We observed also above room temperature ferromagnetism in V-doped $TiO_{2-\delta}$ with magnetic moment per V impurity larger but magneto-optical response smaller than those in the case of Co-doped $TiO_{2-\delta}$.

We discuss possible mechanisms of ferromagnetic order at room temperature in magnetic oxides based on $TiO_{2-\delta}$ and in ferromagnetic semiconductors based on Si, as well as perspectives of applications of these novel materials in spintronics and magnetophotonics.

This research was supported by the Russian Foundation for Basic Researches.

Femtosecond plasmonics in metamaterials

M.R. Shcherbakov, P.P. Vabishchevich, V.V. Komarova, V.O. Bessonov, T.V. Dolgova, and A.A. Fedyanin*

[1] Faculty of Physics, M.V. Lomonosov Moscow State University, Russia

*corresponding author: fedyanin@nanolab.phys.msu.ru

Abstract-Femtosecond-scale polarization state conversion is experimentally found in optical response of a plasmonic nanograting metamaterial by means of time-resolved polarimetry. Simultaneous measurements of the Stokes parameters as a function of time with an averaging time-gate of 130 fs reveal a remarkable alteration of polarization state inside a single fs-pulse reflected from a plasmonic crystal. The effect is attributed to excitation of time-delayed polarization-sensitive surface plasmons with a highly birefringent Fano-type spectral profile.

Polarization is a property of electromagnetic waves which describes the time-averaged trajectory of the electric field vector at a given point of space. It is a commonplace that the timescale over which the polarization is averaged is usually much greater than the period of a single electromagnetic field oscillation. However, recent works demonstrated that the polarization state could be switched on the sub-picosecond scale by means of elementary excitations in quantum-sized media at subzero temperatures [1]. A convenient system for observation of sub-picosecond-lifetime elementary ex- citations at room temperatures is a modulated surface of a noble metal film where surface plasmon-polaritons (SPPs) are excited. Proved by numerous ultrafast experiments involving femtosecond laser pulse sources the mean lifetime of a resonantly excited SPP is found to be varying from tens to hundreds of femtoseconds which is mainly defined by radiative losses of the SPPs. In this contribution we use resonantly excited surface plasmons to control the state of polarization (SoP) inside a single sub-picosecond telecom laser pulse reflected from a plasmonic nanograting with enormous spectrally dependent optical anisotropy [2]. Plasmon-induced birefringence and dichroism with a Fano-type spectral shape cause a pronounced shift of the polarization state inside a single femtosecond telecom laser pulse at the maximal rate of 13 ps−1 in the Stokes vector space. Time-dependent non-zero depolarization is found which indicates the sub-130fs polarization change inside the pulse. We support the experimental data with an analytic model which predicts the four-fold enhancement of polarization conversion which makes plasmonic crystals a perspective media for ultra- fast polarization control. Temporal modification of femtosecond pulses upon the resonant excitation of surface plasmon–polaritons is also studied in one-dimensional metallic nanogratings by femtosecond cross-correlation spectroscopy when the laser pulse duration is comparable with the SSP relaxation time [3]. Modification reveals itself in the pulse duration changes and the pulse shift relative to the unperturbed pulse and manifests itself in the maximum shift and the width changes of the second-order cross-correlation function. Spectral behavior of the pulse shape changes is governed by the femtosecond SSP relaxation dynamics described by the Fano-type resonance. Both a decrease and an increase in the reflected pulse duration are found. Leading and delaying of the pulse reflected from the sample relative to the unperturbed pulse are found to be up to 24 ± 2 fs and 43 ± 2 fs, respectively, for the pulse width 200 fs and SSP time decay about 90 fs. The schematic of the setup for femtosecond Stokes parameters measurements is provided in Fig. 1. The input SoP is prepared by a quarter-wave plate and a Glan-Taylor prism. The beam reflected from the sample is transformed by a half-wave plate (HWP) and a photoelastic modulator (PEM), and analyzed by a Glan-Taylor prism. The analyzed

pulse contains the temporal distribution of a particular Stokes' vector coordinate at different harmonics of the PEM operating frequency. Cross-correlation functions (CFs) measured this way provide the 130fs-averaged temporal distribution of the Stokes parameters. This technique allows one to measure the evolution of all the Stokes vector components of the beam reflected from the sample in only two delay line scans.

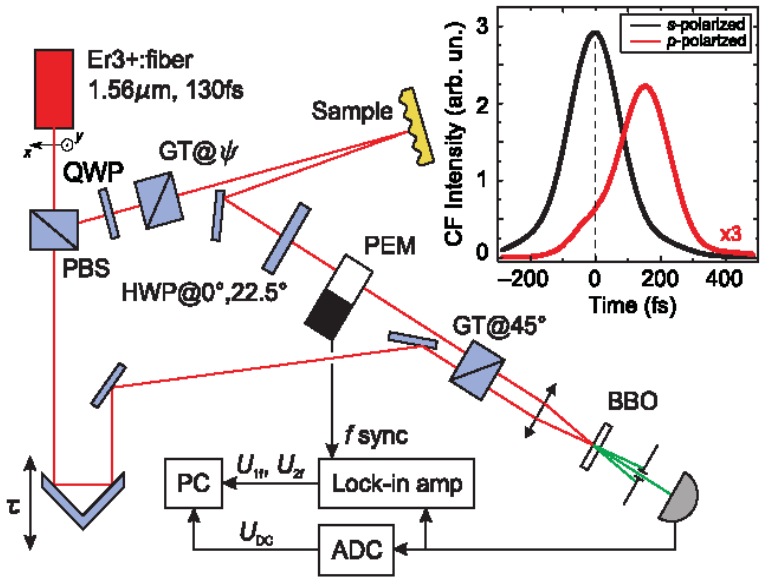

Fig.1. Schematic of the setup for time- resolved Stokes parameters measurement. PBS – polarizing beam splitter, QWP – quarter-wave plate at 45 deg◦ with respect to the Oy axis, GT@ψ – Glan-Taylor polarizer oriented at an angle ψ with respect to the Oy axis, HWP – half-wave plate, PEM – photoelastic modulator, GT@45◦ – Glan-Taylor analyzer. The inset shows the correlation functions measured with s-polarized and p-polarized pulses.

REFERENCES

1. A. E. Paul, J. A. Bolger, A. L. Smirl, and J. G. Pellegrino, "Time-resolved measurements of the polarization state of four-wave mixing signals from GaAs multiple quantum wells," *J. Opt. Soc. Am. B* 13, 1016, 1996.
2. M. R. Shcherbakov, P. P. Vabishchevich, V. V. Komarova, T. V. Dolgova, A. A. Fedyanin, "Ultrafast polarization conversion with plasmonic crystals," arXiv:1105.4730v1 [physics.optics].
3. P. P. Vabishchevich, V. O. Bessonov, F. Yu. Sychev, M. R. Shcherbakov, T. V. Dolgova, and A. A. Fedyanin, "Femtosecond Relaxation Dynamics of Surface Plasmon–Polaritons in the Vicinity of Fano-Type Resonance," *JETP Lett*. 92, 575, 2010.

Tuneable metamaterials containing arrays of magnetically soft microwires

L. V. Panina[1,2], M. Ipatov[2], V. Zhukova[2], J. González[2] and A. Zhukov2,3
[1]School of Computing and Mathematics, University of Plymouth, Plymouth, PL4 8AA, United Kingdom [2]
[2]Dpto. Física de Materiales, Fac. de Química, UPV/EHU, San Sebastián, Spain
[3]IKERBASQUE, Basque Foundation for Science, 48011 Bilbao, Spain
[*]corresponding author: arkadi.joukov@ehu.es

Abstract- We report novel results on the magnetic field effect on the dielectric response in composites of continuous and short-cut parallel magnetic wires arrays in the frequency region of 0.9-17 GHz utilising free-space measurement method and analysis in terms of the effective permittivity depending on the wire surface impedance. Both the real and imaginary parts of ε_{ef} show strong variations with increasing the field owing to the field dependence of the wire impedance which controls the losses in the dielectric response. Long-wire composite has a plasmonic type dispersion of ε_{ef} with negative values of its real part below the plasma frequency which is in the GHz range for wire spacing of about 1 cm and wire diameter of few microns. The presence of the external magnetic field suppresses low-frequency plasmons increasing the value of the real part of the permittivity. In the case of cut-wire composites, it is confirmed that their effective permittivity has a resonance-type dispersion due to the dipole resonance in wires at half wavelength condition. The application of the field broadens the resonance and shifts it towards the higher frequencies.

Composites containing long parallel wires can be characterised by plasma-like dispersion of ε_{ef} [1] with a negative value of the real part of the permittivity below the characteristic plasma frequency, f_p. A number of experimental studies confirmed a negative permittivity in the GHz region for wire media. Surface impedance ζ_{zz} may change under applied magnetic field, H_{ex}, as a result of the MI effect [2]. Then, the permittivity spectra will depend on H_{ex}.

We studied composites containing amorphous magnetically soft Co-rich microwires exhibiting large MI effect (up to 300% at 500 MHz) by free space methods. Large MI effect makes them very promising for engineering artificial dielectrics with tuneable microwave properties. The S-parameters were measured at 0.9-17 GHz in the presence of external field ranging up to 3000A/m. The effective permittivity spectra were deduced from S-parameters with the help of Reflection/Transmission Epsilon Fast Model.

Both the real and imaginary parts of ε_{ef} show strong variations with increasing H_{ex} owing to the MI effect which controls the losses in the dielectric response. Long-wire composite has a plasmonic type dispersion of ε_{ef} with negative values of its real part below the plasma frequency (GHz range) for wire spacing of about 1 cm and wire diameter of few microns (Fig.1). The presence of H_{ex} suppresses low-frequency plasmons increasing the value of the real part of the permittivity [3]. For cut-wire composites we confirmed a resonance type of ε_{ef} dispersion due to the dipole resonance in wires at half wavelength condition. Application of H_{ex} broadens the resonance and shifts it towards the higher frequencies (Fig.2).

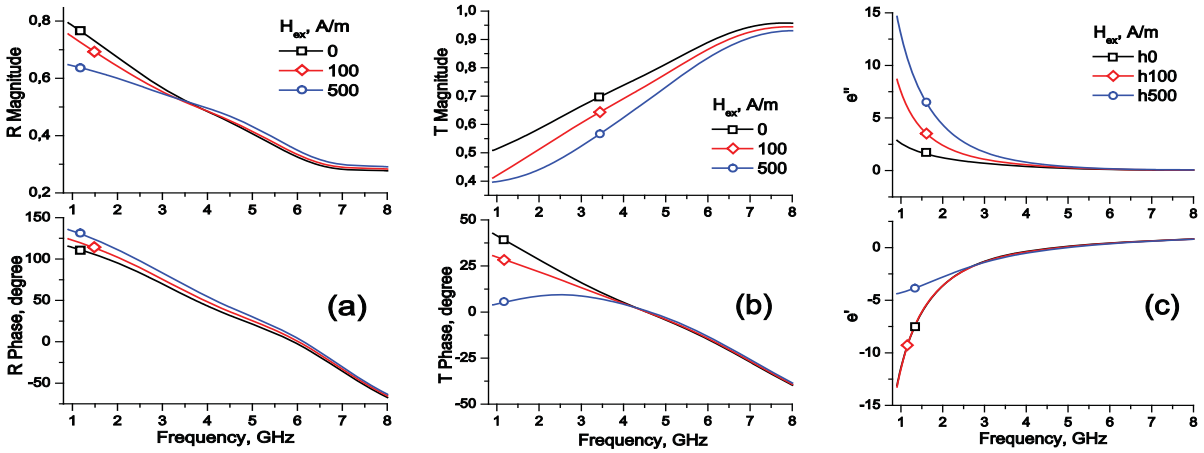

Figure 1. Spectra of R, T and ε_{ef} for composites with long wires with H_{ex} as a parameter (H_{ex}=0,100, 500A/m).

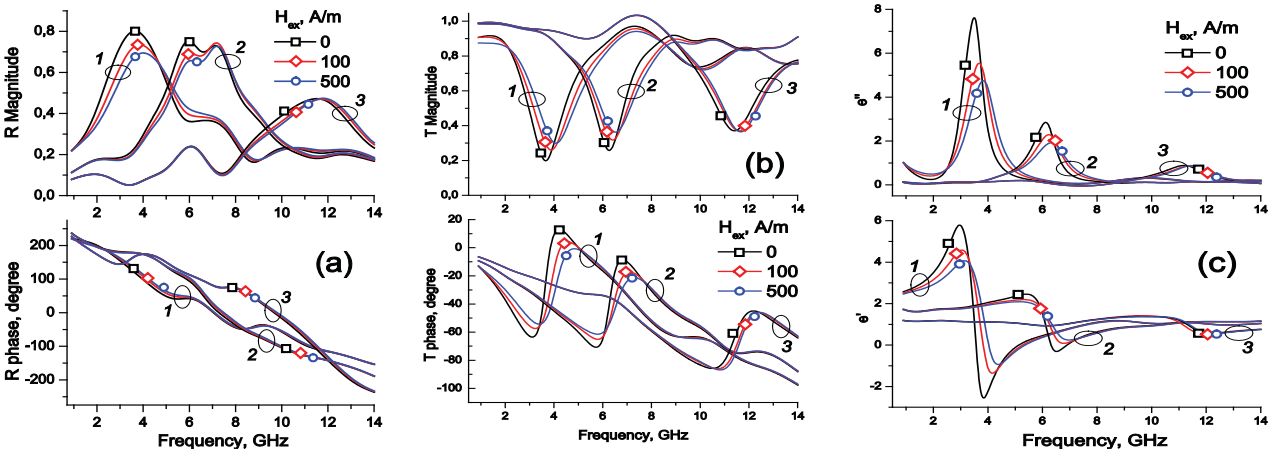

Fig. 2. Spectra of R, T and ε_{ef} of composites with cut wires of length 40 , 20 and 10 mm with the field as a parameter.

Therefore, both types of wire composites exhibit strong ε_{ef} (H_{ex}) dependence and suitable for applications.

ACKNOWLEDGEMENTS This work is supported by EU ERA-NET under project "SoMaMicSens" (MANUNET-2010-Basque-3), by EU under FP7 "EM-safety" project and by Spanish Ministry of Science and Innovation MICINN under project MAT2010-18914.

REFERENCES

1. Pendry, J. B., A. J. Holden, W. J. Stewart, and I. Youngs, "Extremely Low Frequency Plasmons in Metallic Mesostructures," *Phys. Rev. Lett.*, Vol. 76, No. 25, 4773-4776, 1996.
2. Makhnovskiy D. P., L. V. Panina, "Field dependent permittivity of composite materials containing ferromagnetic wires," *J. Appl. Phys*. **93** 4120, 2003.
3. Panina L.V., Ipatov M., Zhukova V., Zhukov A. and Gonzalez J., " Microwave metamaterials with ferromagnetic microwires", Applied Physics A: Materials Science and Processing (2011), DOI: 10.1007/s00339-010-6198-7

Negative-index nonlinear optics: phonons vs plasmons

A. K. Popov[1], **M. I. Shalaev**[2], **S. A. Myslivets**[3], **and V. V. Slabko**[2]

[1]University of Wisconsin-Stevens Point, Stevens Point, USA
[2]Siberian Federal University, Krasnoyarsk, Russian Federation
[3]Institute of Physics of Russian Academy of Sciences, Krasnoyarsk, Russian Federation
apopov@uwsp.edu

Abstract— The possibility to exploit ordinary crystals instead of plasmonic negative-index nonlinear-optical metamaterials is shown in order to observe similar extraordinary nonlinear-optical frequency-conversion propagation processes. Their exotic properties stem from backwardness of the optical phonons with negative dispersion in such crystals. Comparative review of unparallel properties of coherent energy exchange between ordinary and backward electromagnetic waves in negative-index materials and between ordinary electromagnetic waves coupled through backward vibrational wave is given. Unique photonic devices with the properties similar to those predicted for negative-index metamaterials are proposed.

Optical negative-index (NI) metamaterials (NIMs) form a novel class of electromagnetic media that promises revolutionary breakthroughs in photonics. The possibilities of such breakthroughs originate from backwardness, the extraordinary property that electromagnetic waves acquire in NIMs. Unlike ordinary positive-index materials, the energy flow, $\mathbf{S}$, and the wave-vector, $\mathbf{k}$, become counter-directed in NIMs, which determines their unique linear and nonlinear optical (NLO) propagation properties. Usually, NIMs are nanostructured metal-insulator composites with a special design of their building blocks at the nanoscale. Metal component imposes strong absorption of optical radiation in NIMs, which presents a major obstacle towards their numerous prospective exciting applications. Extraordinary features of coherent NLO energy conversion processes in NIMs that stem from wave-mixing of ordinary and backward electromagnetic waves and the possibilities to apply them for compensating the outlined losses have been shown in [1, 2]. Most remarkable feature is distributed feedback behavior which allows for sharp resonance increase of the conversion efficiency. Essentially different properties of three-wave mixing (TWM) and second harmonic generation have been shown in [3, 4].

Herein, we propose and investigate a different scheme of TWM of ordinary and backward waves (BW). It builds on stimulated Raman scattering (SRS) where two ordinary electromagnetic waves excite backward elastic vibrational wave in a crystal, which results in TWM. The possibility of such BWs was predicted by L. I. Mandelstam in 1945 [5], who also had pointed out that negative refraction was a general property of the BWs. This work is to show the possibility to substitute sophisticatedly fabricated nanostructured negative index metal-dielectric composites by the extensively used and studied ordinary crystals in order to simulate unparallel properties of coherent NLO energy exchange between the ordinary and backward waves.

Basic idea that underlies the proposed concept is as follows. The dispersion curve $\omega(k)$ of phonons in the crystals containing more than one atom per unit cell has two branches: acoustic and optical. For the optical branch, the dispersion is negative in the range from zero to the boundary of the first Brillouin's zone (Fig. 1). Hence, the group velocity of optical phonons, $\mathbf{v}_v^{gr}$, is antiparallel with respect to its wave-vector, $\mathbf{k}_v^{ph}$, and phase velocity, $\mathbf{v}_v^{ph}$. This is because $v_{gr} = \partial\omega(k)/\partial k < 0$. Optical vibrations can be excited by the light waves through two-photon (Raman) scattering. The latter gives the ground to consider crystal as the analog of the medium with negative refractive index at the phonon frequency and to examine the processes of parametric interaction of three waves. Two of which are ordinary electromagnetic waves. The third one is the backward wave of elastic vibrations with the directions of the energy flow and of the wave-vector opposite to each other.

We show extraordinary nonlinear propagation and output properties of the Stokes electromagnetic wave in one of two different coupling geometries, both utilizing backward elastic waves. Specific features essentially different for continuous-wave and short-pulse regimes are investigated. The possibility to localize coherent energy conversion and to fit it in to the crystal of given thickness is

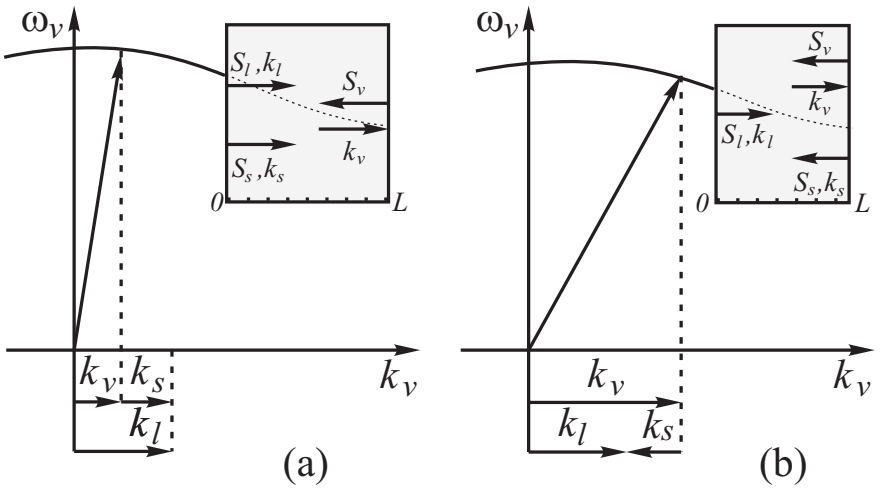

Figure 1: Negative dispersion of optical phonons and two phase matching options: (a) – co-propagating, (b) – contra-propagating fundamental, control, and Stokes, signal, waves. Insets: relative directions of the energy flows and the wave-vectors.

shown. Such unusual properties are in a striking contrast with those attributed to their counterparts in the standard schemes that build on the coupling of co-propagating photons and phonons [6]. They are also different from the properties of the phase-matched mixing of optical and acoustic waves for the case where the latter has energy flux and wave vector directed against those of one of the optical waves [7]. The revealed properties can be utilized for creation of optical switches, filters, amplifiers and cavity-free optical parametric oscillators based on ordinary Raman crystals without the requirement of periodically poling at the nanoscale [8] (and references therein). The results of numerical simulations and estimates for both continuous wave and short pulse regimes will be presented. Some details can be found in ref. [9].

ACKNOWLEDGMENT

This work was supported by the Russian Federal Program on Science, Education and Innovation under Grant No 2010-121-102-018, by the Presidium of the Russian Academy of Sciences under Grant No 27.1, by the Siberian Division of the Russian Academy of Sciences under Integration Project No 5 and by the US National Science Foundation under Grant ECCS-1028353.

REFERENCES

1. Popov, A. K. and V. M. Shalaev, "Compensating losses in negative-index metamaterials by optical parametric amplification," *Opt. Lett.*, Vol. 31, 2169-2171 (2006).
2. Popov, A. K., "Nonlinear optics of backward waves and extraordinary features of plasmonic nonlinear-optical microdevices," *Eur. Phys. J. D* Vol. 58, 263-274 (2010).
3. Popov, A. K., V. V. Slabko, and V. M. Shalaev, "Second harmonic generation in left-handed metamaterials," *Laser Phys. Lett*, Vol. 3, 293-297 (2006).
4. Popov, A. K. and V. M. Shalaev, "Negative-index metamaterials: second-harmonic generation, Manley Rowe relations and parametric amplification," *Applied Physics B: Lasers and Optics* Vol. 84, 131–137, 2006.
5. Mandelstam, L. I., "Group velocity in a crystall lattice," *ZhETF* Vol. 15, 475–478 (1945).
6. Shen, Y. R. and N. Bloembergen, "Theory of stimulated brillouin and raman scattering," Phys. Rev. Vol. 137, A1787–A1805, 1965.
7. Bobroff, D. L., "Coupled-modes analysis of the phonon-photon parametric backward-wave oscillator," J. Appl. Phys. Vol. 36, 1760–1769, 1965.
8. Khurgin, J. B., "Mirrorless magic," *Nat. Photonics* Vol. 1, 446–448, 2007.
9. Slabko, V. V., S. A. Myslivets, M. I. Shalaev, and A. K. Popov, "Negative group velocity and three-wave mixing in dielectric crystals," *arXiv*: 1104.0891 v1.

Nonlinear and tunable metamaterials: an overview

Mikhail Lapine, Ilya Shadrivov, David Powell, and Yuri Kivshar

Nonlinear Physics Centre, Research School of Physics and Engineering,
Australian National University, Canberra ACT 0200, Australia

The study of metamaterials became a research frontier in electrodynamics, solid-state physics, and material science that is drawing wide interest in applied fields ranging from microwave engineering to photonics. In particular, the possibility of nonlinear phenomena in metamaterials [1,2] was fruitfully explored, having established a new research area and giving rise to fruitful ideas on tunable and active metamaterials [3].

The initial idea to realise strong nonlinear response in metamaterials was based on either a nonlinear host medium [1] or nonlinear elements constituting the metamaterial [2]. Both the approaches resulted in the nonlinear response on the level of a single element, which was further enhanced through collective response of a metamaterial, providing tools for a variety of nonlinear effects such as harmonic generation, parametric amplification, frequency conversion, solitons, tunability, and other processes and phenomena [3,4].

Up to that stage, the structure of metamaterial remained fixed in such studies. At the same time, we have reported recently [5] that structural changes in metamaterials offer an excellent means to control its properties, remarkably affecting the resonance position and thus providing enhanced tunability of transmission, reflection and absorption. These structural effects are driven by the peculiarities of near-field interactions, determined by mutual arrangement and coupling between the elements [6].

Finally, we take a next step forward and consider *a novel type of nonlinearity* in metamaterials, which is achieved through the "conformational" changes in metamaterial, analogous to those employed for structural tunability. This results in a variety of self-action mechanisms, which can be very efficient.

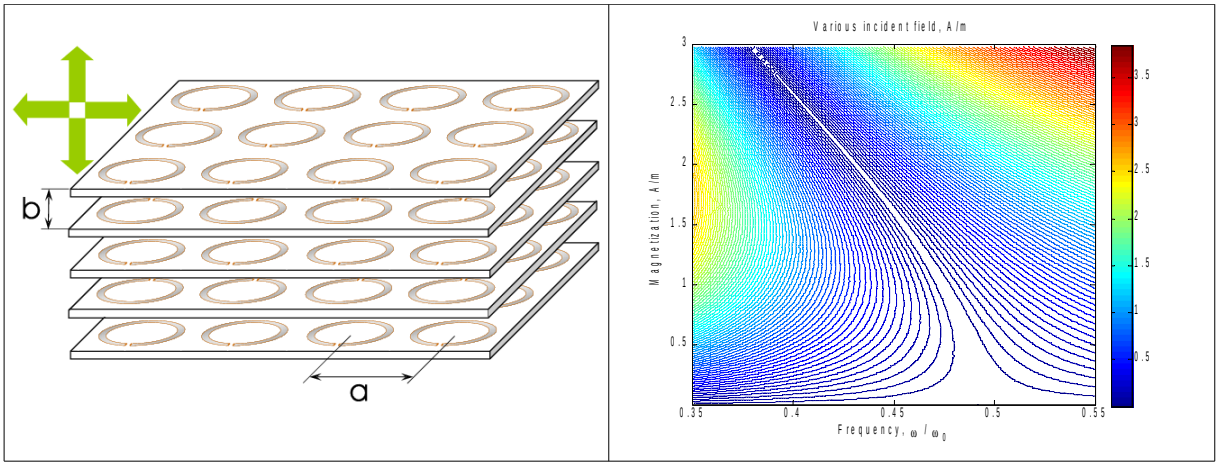

Fig. 1 (a) General schematic of a metamaterial which can undergo structural changes. Parallel boards of resonator arrays form a three-dimensional lattice with *variable* constants *a* and *b*. (b) Nonlinear dependence of the effective average magnetization induced in such metamaterial at various incident field intensity, plotted against normalized frequency.

To give a practical example, we consider an artificial magnetic metamaterial assembled with subwavelength resonators arranged in an anisotropic lattice featuring an extra degree of freedom (Fig.1a), and analyse nonlinear phenomena resulting from the self-induced structural changes. We reveal that magnetization dependence on the incident field intensity and frequency is remarkably nonlinear (Fig.1b), giving rise to bistability, parametric processes and many other useful nonlinear phenomena [7].

References

[1] A.A. Zharov, I.V. Shadrivov, and Yu.S. Kivshar, *Phys. Rev. Lett.* **91**, 037401, (2003).
[2] M. Lapine, M. Gorkunov, and K.H. Ringhofer, *Phys. Rev. E* **67**, 065601 (2003).
[3] A.D. Boardman, V.V. Grimalsky, Yu.S. Kivshar, S.V. Koshevaya, M. Lapine, N.M. Litchinitser, V.N. Malnev, M. Noginov, Yu.G. Rapoport, and V.M. Shalaev, *Laser Photonics Rev.* 1–21 (2010) / DOI 10.1002/lpor.201000012.
[4] M. Lapine and M. Gorkunov, Nonlinear Metamaterials, in: *Metamaterials Handbook, edited by F. Capolino* (CRC Press, 2009).
[5] M. Lapine, D. Powell, M. Gorkunov, I. Shadrivov, R. Marqués, and Yu. Kivshar, *Appl. Phys. Lett*. **95**, 084105 (2009).
[6] D. Powell, M. Lapine, M. Gorkunov, I. Shadrivov, and Yu. Kivshar, *Phys. Rev. B* **82**, 155128 (2010).
[7] M. Lapine, I.V. Shadrivov, and Yu.S. Kivshar, „Magnetoelastic nonlinear metamaterials" (submitted, 2011).

The spin-spiral magnetic order and phase separation in systems with itinerant electrons

A.K. Arzhnikov

Physical-Technical Institute, Ural Division of RAS, Izhevsk, Russia

. We investigate the systems with itinerant electrons. We treat a commensurate collinear magnetic order as well as incommensurate spin spiral magnetic states and collinear incommensurate magnetic states. Our study shows that all of the listed phases appear to be the ground state at certain parameters of the model. The magnetic phase diagram was plotted. For interpretation of the behavior of the magnetic properties of the superconductive curates we considered the two–dimensional single-band Hubbard model. We treat a spin spiral states as well as phase separation at a finite temperature. We have performed numerical calculations comparing thermodynamical potential of different magnetic phases at different n and T, We argue that temperature dramatically influence the collinear and spiral magnetic phases, parameters of the spin spiral states and phase separation.

Tentative of Smart Skins Metamaterial Antennas embedded in the Structure of an Aircraft: MSIE French project from Aeronautic Cluster ASTECH

Alain Priou
University Paris Ouest Nanterre la Défense, Energy, Mechanics and Electromagnetic Lab.(LEME)
50 rue de Sevres, 92410 Ville d'Avray, France
*alain.priou@u-paris10.fr

The Smart Materials and Structures for Electromagnetics project (MSIE) funded by the French Ministry of Finance and DGA will deal with the new possibility offered by metamaterial and structures using metamaterials to arrive with efficient and very small antennas embedded directly on the composite structure of an aircraft. During the presentation we will show some results obtained for low profile and low frequency antennas, for double frequency and multiple function antennas, for new metamaterial barriers placed in between antenna arrays and for having more information on deformable antenna situated on the wings of an aircraft.

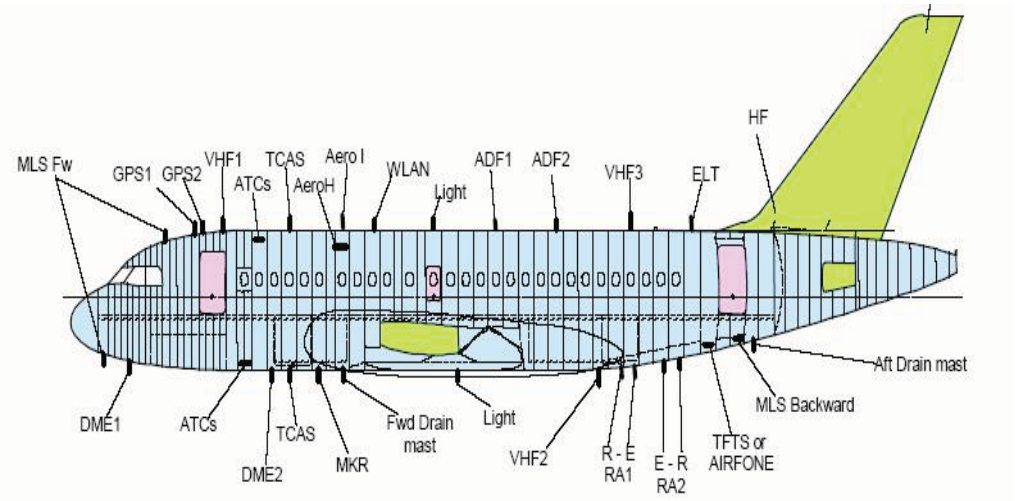

As shown on this figure, we can see that a civilian aircraft is composed of many antennas located on the structure for communication, navigation, radar activity. Some of these antennas are going outside the aircraft structures that contributes greatly to increase the drag and increase the gasoline consumption. There is tentative for the last 15 years to reduce the number of antennas, to reduce the number of site for antennas and try to embed completely all the antennas in the structure.. That can be done if we can design smart skins structures integrated in the structure. The high impedance surface and the metamaterial structures are very good candidates for materials and structures to obtain new integrated antennas.

In the Smart Materials and Structures for Electromagnetic(MSIE project), nine partners are working under the leadership of INEO Defense and LEME lab, University Paris Ouest. The industries are Dassault-Aviation,

EADS, INEO Defense and SATIMO working very close to the academic and research laboratories for developing prototypes and evaluate the possibilities of these new materials. For the research lab, we have University Paris Ouest with the Mechanics and Electromagnetic Group, LGEP from SUPELEC, Paris Tech Mines and Paris Tech Arts and Metiers for health monitoring of composites with embedded sensors in the aircraft structures.

Several workpackages are organized for developing the research in between partners:

-WP1 low profile and compact antennas in lower frequency band under 1 GHz,

-WP2 Double frequencies and multiple function antennas from 1 GHz to 2 or 3 GHz

- WP3 Metamaterials barriers for insertion between antenna arrays

- WP4 Modelization of Metamaterials and Measuring Techniques

- WP5 Deformable and conformable antennas and effect on metamaterial antenna arrays

-WP6 Health monitoring with embedded sensors in composite media used in aircraft.

During the conference we will give some possible results associated of the main conducted researches during all the WP's. We will present designs, realized prototypes with simulation, experimental results and antenna test measurements provided by SATIMO Company. Some guidelines for the future will be presented.

Acknowledgements, We would like to thank the French Ministry of Finances, DGA, Regional and Departmental Agencies for supporting this large 3 years program. We would like to thank the Aeronautic French Cluster ASTECH for giving the label for this project.

REFERENCES

1- C.T. Manh, H.H.Ouslimani and A.C.Priou, "Resonance characterization of high impedance surface properties by suspended stri-line method", Metamaterials 2010, September 13-18, 2010, Karlsrulhe, GE

2- F.Meng, H.H.Ouslimani, A.C.Priou and Y.Duval, " Multi-function and multipolarization patch antennas with metamaterial high impedance surfaces", Metamaterials 2010, September 13-18, 2010, Karlsrulhe, GE

3 - X.Han, H.H.Ouslimani and A.C. Priou, 'Reduction of the E-plane coupling between microstrip antenna arrays using high impedance surfaces", Metamaterials 2010, September 13-18, 2010, Karlsrulhe, GE

4 - C.T.Manh, X.Han, H.H.Ouslimani, A.Priou, A. Marteau and G. Collignon," Redcution of the coupling between microstrip antennas using high impedance surface (HIS) structures", EuMC 2010, 26 septembre au 1 octobre 2010, Paris, France

5 - T.Yuan, L.Zhou, H.H.Ouslimani, A.C.Priou, P. Besnard, G.Collignon and A. Marteaux, " A compact broadband omnidirectional vertically polarized VHF antenna for aircraft", EuMC 2010, 26 septembre au 1 octobre 2010, Paris, France

6- X.Han, H.H.Ouslimani, A.C.Priou, G. Collignon and A. Marteau, " Low profile antenna arrays and mutual coupling reduction", PIERS 2011, Marrakech, 19-23 March 2011,

7 - C.T.Manh, X.Han, H.H.Ouslimani, A.Priou, " Characterization of high impedance surface (HIS) properties for low profile antenna applications", PIERS 2011, Marrakech, 19-23 March 2011,

8 - T.Yuan, L.Zhou, H.H.Ouslimani, A.C.Priou, G.Collignon and A. Marteau, " Ultra compact VHF vertically polarized antenna for aircraft, PIERS 2011, Marrakech, 19-23 March 2011,

9 - X.Han, H.H.Ouslimani, A.Priou, A. Marteau and G. Collignon, "Understanding the coupling reduction effect in microtrip array antennas using high impedance surface (HIS)," APS-S/URSI 2011, Spokane,USA

Magnetic Charge and Problems Condensed Matter Physics

O. Kuvandikov, E. U. Arzikulov*
[1]Samarqand State University, 140104, university blvd. 15, Samarqand, Uzbekistan
*corresponding author: e-mail: eshquvat@mail.ru

Abstract

Experimenter physicists more than hundred years searched for a magnetic charge and a last they have found it in the condensed matter, in "earthly matters".

Problems of magnetic charges - magnetic monopolies was discussed in the classical Maxwell theory by a number of famous scientists such O. Heviside (1884), H. Hertz (1893) and Henri Poincaré (1896).

P. A. Dirac in 1931 has given new values for magnetic charges. He connected this problem to other, basic from the point of view of the quantum theory, problem by integer quantization of an electrical charge of particles. Dirac has shown that from a hypothesis of existence of monopolies the quantization of an electrical charge follows also. His analysis is based on the basic principles of the quantum mechanics. If to assume, following Dirac, existence of a magnetic pole with a charge ***g*** and linear singularity ***l*** of a field of a vector of potential ***A***, a single-valuedness condition of wave function ***ψ,*** at tracking on the closed contour covering a line ***l***, results in the following rule of quantization: $g \cdot q = n/2$, where ***n*** - integer, ***q*** - electrical charge.

Dirac has proved, that the hypothesis of magnetic poles complemented by a condition quantization, does not result neither to any to the contradictions nor with the Maxwell's equations with the modern quantum theory. He has told: "… from this point of view it would be surprising, if the Nature did not use this opportunity". In 1948 Dirac considers the general theory of the charged particles and poles interaction with each other via an electromagnetic field. The lines break of vector potential also will be "Dirac string". Obviously also that "Dirac string" can have the any form and direction in space.

It is necessary to note, that in all these unsuccessful searches it was supposed to find out a Dirac's monopolies, and these particles saw by the researchers by extremely exotic.

Monopolies or arrived to us from other worlds, or were born in extreme conditions, for example on accelerators.

The data of numerous experimental researches on a problem of magnetic particles have convinced that magnetic charges is not exotic, and real component of atoms and substance. Here it is important to note, that in the literature there are papers by definition of quantity a magnetic charge. For example in 1945 F. Ehrenhaft has determined quantity of a magnetic charge on particles were of the same order, as quantities of their electrical charge.

Sizov in 1970 studying magnetic scattering of neutrons in ferrite has established, that magnetic charges enters in structure substance.

In 2009 group of the scientists from Germany, France investigating magnetic scattering of neutrons in magnetic ordering substances (for example: $Ho_2Ti_2O_7$, $Dy_2Ti_2O_7$) have confirmed existence of a magnetic monopolies and "Dirac strings".

The opportunity of separation northern and southern magnetic poles is proved; the opening of such surprising statuses has extreme importance for physics both by way of showing of new especial properties, and as a direction of development of potential technologies. The examples fractalization (separateness) are extremely rare and one and two-dimensional systems practically only to systems, so the three-dimensional lattice pyro-chlore represents promising a direction for the further researches both in magnetic and in exotic metals.

Nanoguiding of Light and Matter Waves by Negative Refraction Media: New Problem Definition and Applications

Vasily Klimov
Lebedev Physical Institute, Russia
vklim@sci.lebedev.ru

Abstract: We derive exact analytical solutions for the focusing of Maxwell photons and massless Dirac particles by half space and other domains (slabs, spheres, cylinders, wedges) with negative refraction. These novel paradoxical solutions show that half space with negative refraction cannot be simply considered as a superlens. Instead of a 2D focus spot it results in the creation of a sink of complicated spatial structure. Our analytical solutions also show substantial differences in the focusing of Maxwell and Dirac field within this geometry. We find a new manifestation of the Klein paradox which is the creation of sinks in negative refraction area. The found solutions pave a natural way to provide effective excitation transfer from one atom to another. Possible applications and generalizations of our approach are discussed.

Despite huge interest in negative refraction phenomena, no nontrivial analytical solution of this problem was found until now neither for Maxwell nor for Dirac fields. In this talk, I shall present exact analytical solutions both for matter and light waves outgoing from a point source and suffering negative refraction in a half-space, in a slab or in domains of other shape (sphere, cylinder, wedge, etc.). It is a unique feature that for a lossless negative refraction material, the analogue of the theory of images can be applied allowing one to find an exact solution in spatial domain as different combinations of sources, sinks, and free propagating surface plasmon waves or localized plasmons. It is very important that solutions found contain both REAL sources (emitter) and REAL sinks (detector, sensor, receiving nanoantenna etc).

As an example, in Fig.1 energy flows for light (left panel) and massless electrons (right panel) found within our analytical solutions, are shown.

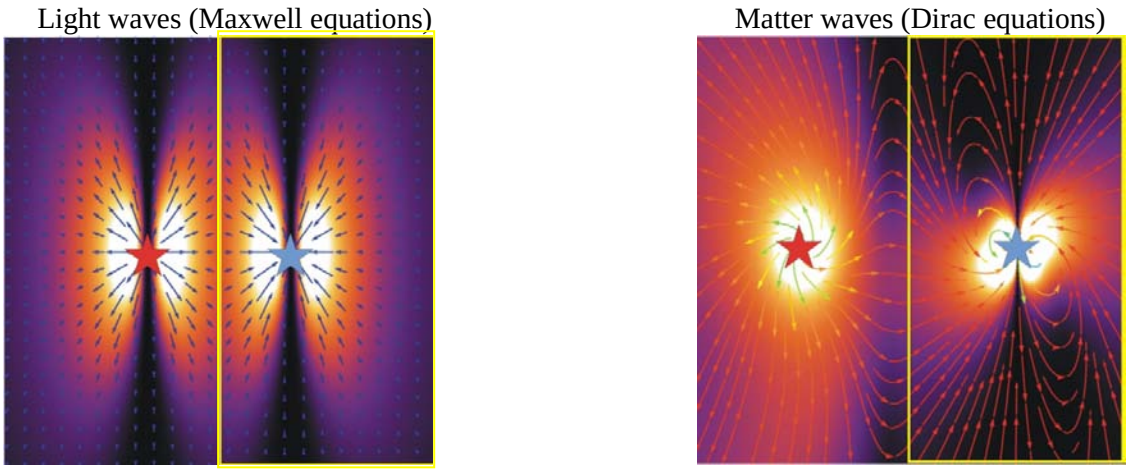

Figure.1. Energy flows from source to sink for light (left panel) and matter (right panel) waves in the presence of a negative refraction half-space. The yellow box indicates the negative refraction half-space. The source and sink are labeled by red and blue stars correspondingly.

From these figures, one can see that the behavior of energy flows differs for photons and electrons. While for the light we have straight stream lines with a sharp bend at the interface of the negative refraction half-space, for the electrons we have more complicated curves. Moreover, negative refraction for electrons, in fact, begins slightly before the negative refraction half-space. It is very important that found solutions are based on source-sink pairs that are analogous to particle-antiparticle pairs explaining the Klein paradox. So, our results are another manifestation of the Klein paradox. The effects predicted can be verified more easily in the case of massless electrons in graphene. Analogous solutions were also obtained for some other negative refraction domains (sphere, cylinder, wedge, etc see Figure 2).

In the case of arbitrary small losses, the previous solutions remain valid, but in this case there are also other solutions where the singular sink of energy is replaced by a distributed sink of energy, that is, by surface plasmon waves propagating along interface. It is very important that our approach allows tracing appearance of both solution with point singularities and surface plasmon waves as a result of bifurcation of the unique

analytical solution. As a result of this bifurcation, creation of a pair of source-sink or a pair of surface plasmons propagating in opposite directions, takes place.

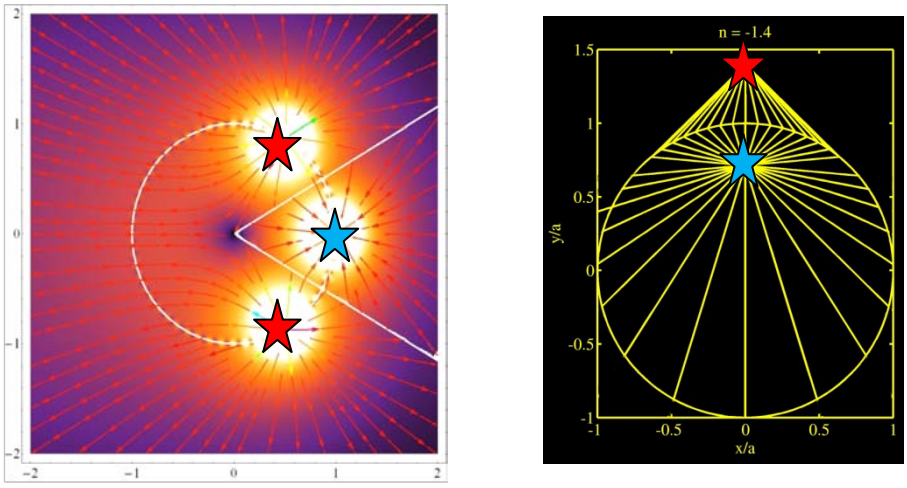

Figure.2. Energy flows from sources (red stars) to sinks (blue stars) for light for nontrivial geometries. Left panel - wedge with refractive index $n=-1$. Right panel - sphere of radius a with refractive index n=-1.4, $r_{source} = a|n|, r_{\text{sink}} = a/|n|$.

The found solutions pave a natural way to provide effective energy and excitation transfer from the point source (an excited atom or a molecule) to the point sink (an atom or a molecule in ground state). Several possible applications of such energy guiding (preparation of entangled pairs of atoms, effective excitation of atom or molecules, etc.), will be also discussed.

Conclusion: New paradigm for subwavelength waveguiding and focusing by negative refraction domains is proposed. Main feature of this paradigm is that both source and receiver are needed to provide effective operation of nanodevices. New paradigm can be applied for different geometries and wave phenomenon where negative refraction is present.

Acknowledgements, the author thanks the Russian Foundation for Basic Research (grants # # 11-02-91065, 11-02-92002, 11-02-01272) for financial support of this work.

REFERENCES

1. Klimov,V.V., Baudon, J. and Ducloy, M., "Comparative focusing of Maxwell and Dirac fields by negative refraction half-space," *Europhysics Lett.*, Vol. 94 , 20006, 2011.
2. Klimov,V.V., "Novel approach to a perfect lens," *JETP Lett.*, Vol. 89, No. 5, 270-273, 2009.

Plasmonic metasurfaces for tandem thin-film solar cells

C. R. Simovski and D. C. Morits

[1] Radio Science Dept, ELEC School, Aalto University

[*]corresponding author: Konstantin.simovski@aalto.fi

Abstract-We suggest a new design solution for an anti-reflecting coating based on a plasmonic metasurface dedicated to reduce the reflection from a thin-film solar cell (TFSC) over the whole band of its operation. The comparison with a usual optical blooming for TFSC shows better efficiency of our metasurface which is nearly equivalent to a multi-layer coating. Moreover, for tandem TFSC the bottom cell together with the metasurface can compose a standing-wave Fabry-Perot resonator for the frequency range of the top cell. This approach allows the complete absorption of the light in the top cell with the thickness of the photovoltaic layer as thin as 100 nm.

Thin-film solar cells represent the third generation of solar cells, which are dramatically cheaper and/or more efficient than other known types of solar cells. The main difficulty for a thin-film solar cell (TFSC) is trapping the incident light. Really, multilayer anti-reflection coatings (ARC) used for more expensive thick-film solar cells are not suitable for TFSC due to their fragility and low resistance to abrasion. Practically, such ARC need to be protected themselves by optically thick glass sheets. This is not acceptable for TFSC fabricated on flexible substrates. Such TFC are usually bloomed by a single nanolayer of MgF_2 or SiN depending on the frequency range of operation. A single blooming layer reduces the reflectance from a semiconductor to $R<0.05$ in a narrow (<10%) frequency range. However, low cost of such ACR justifies their use in the case when the thickness of the photovoltaic layer d is substantial enough, practically $d >500$-600 nm. If $d<400$ nm and the TFSC is single-junction a simple ACR cannot work due to the total light reflection by the lower contact electrode. For a tandem TFSC the reflection can be reduced by a simple ACR however the tandem cannot operate because the light is weakly absorbed in the band of the top solar cell since it is transmitted into the bottom cell and dissipated there. The main problem for $d<300$ nm becomes how to concentrate the incident light energy in a so optically thin photovoltaic layer. For the tandem TFSC we have to avoid both reflection of solar light in the frequency range of the top TFSC and its transmission to the bottom solar cell. For a simple TFSC we have to prevent the reflection in presence of the mirror on the bottom of an absorbing layer which is too thin to absorb the incident energy for a usual optical blooming. This situation justifies the use of plasmonic arrays for trapping the light for ultimately thin photo-absorbing layers. Planar plasmonic arrays (plasmonic metasurfaces) are capable to concentrate the light energy inside a very thin layer. In the literature, however, there we did not find a satisfactory explanation why plasmonic metasurfaces can be better than any ARC. Analyzing the numerical data we noticed that in the case of a semi-transparent substrate (modeling the bottom cell of the tandem TFSC) a metasurface placed on top of the structure together with this substrate can form a Fabry-Perot resonator for the standing wave. Then the maximum of the field at the resonance frequency is located at the center of the top photo-absorbing layer. This prevents both reflection and transmission at the resonance frequency and makes possible a nearly full absorption of light (at this frequency) even in a so thin layer as $d=100$ nm. However, in the available literature the reported enhancement is very modest due to two factors: a narrow frequency band of Plasmon resonance (even for multi-resonant metasurfaces) and strong absorption losses of plasmonic nanoparticles. In fact they are usually of the same order as the reflection losses in an uncoated TFSC.

In this paper we report numerical results obtained for a new structure which will allow the strong enhancement of a CIGS TFSC treated as a tandem top cell. We suggested a design solution based on a recently invented cheap technology, which allows fabrication of large-area metasurfaces printed on a polyethylene or another cheap plastic film. Two significant advantages of our ARC schematically shown in Fig.1 are very broad frequency range of light trapping and low plasmonic dissipation because the hot spots are mostly formed outside plasmonic nanoantennas. The last advantage feature is connected with the collective resonances of the metasurface. We claim the theoretically achieved enhancement for the top cell short-circuit current 46% that dramatically exceed results claimed for known analogues [1].

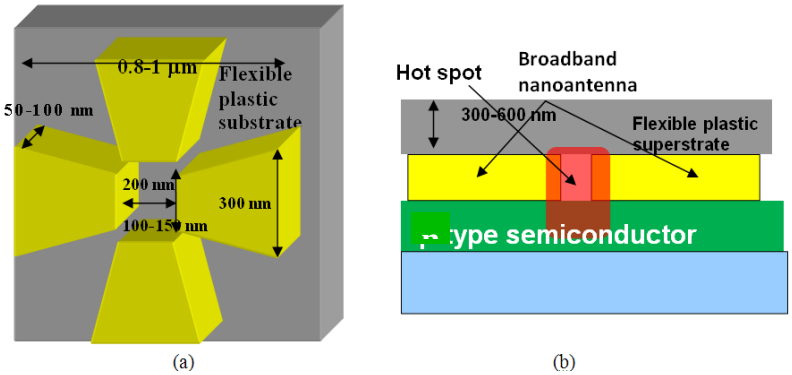

Fig. 1: A unit cell of the metasurface of broadband nanoantennas of gold patches printed on a plastic film and used as an ARC for a tandem TFSC: (a) – top view, (b) – cross section. A blue layer is the remainder of the tandem.

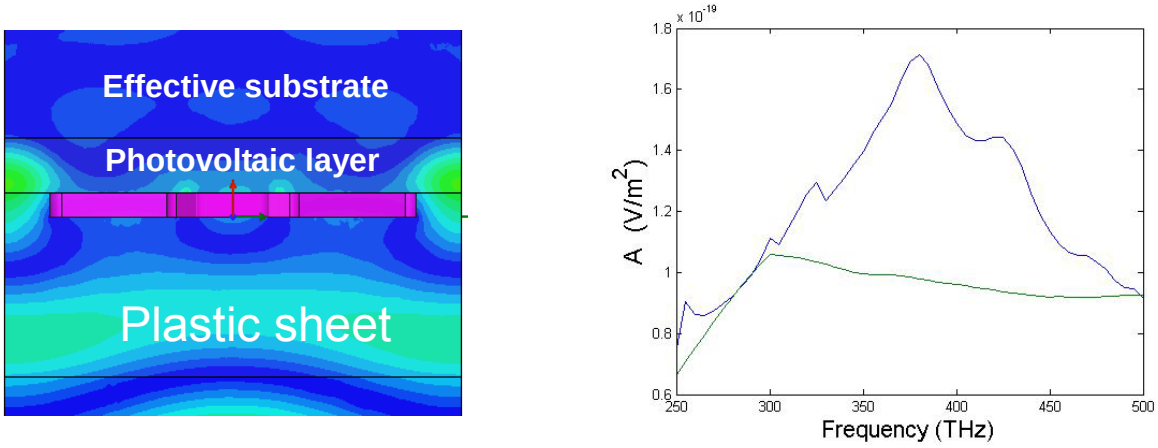

Fig. 2: A unit cell of the metasurface (cross section) and the field intensity distribution (a). Hot spots are located between nanoantennas. (b) – Photovoltaic absorption coefficient A versus frequency for d=110 nm thick n-doped $CuInSe_2$ layer. Green line – A in absence of the metasurface.

Acknowledgement, this conference attendance has been supported by the UK Navy grant No. 62909-11-1-1082

REFERENCES

1. Atwater, H. A. “Plasmonics for improved photovoltaic devices,” *Nature Mat.*, Vol. 9, No. 2, 205–208, 2010.

Scanning near-field optical polarimetry of plasmonic metamateials

M. R. Shcherbakov[1], **B. B. Tsema**[1,2], **Yu. B. Tsema**[1], **A. T. Le**[1], **A. A. Ezhov**[1], **and A. A. Fedyanin**[1]

[1]Faculty of Physics, Lomonosov Moscow State University, Russia
[2]Moscow State Institute of Radioengineering, Electronics and Automation, Russia
shcherbakov@nanolab.phys.msu.ru

Abstract— Polarization properties of planar optical metamaterials are studied by means of scanning near-field optical dynamic polarimetry. Local field maps of linear and circular diattenuation measured with a scanning near-field optical microscope and calculated using the finite-difference time-domain method demonstrate strong polarization sensitivity of the metamaterials in the nanoscale regime which makes them a notable candidate for subwavelength polarization control.

The progress of contemporary nanolithography techniques allowes one to structure media on the submicron scale. Varying the geometry of the structuring makes the media acquire different optical properties which are not specific to the host media. Among the most remarkable properties are magnetic response of nanostructures at optical frequencies and negative refraction [1], extraordinary optical transmission [2], light nanofocusing with nanostructured metallic films [3], artificial optical anisotropy [4] and chirality [5]. The latter two became possible with thin metallic films structured with patterns of certain types of asymmetry. Nevertheless the thicknesses of the films are much less than the wavelength of the visible light, these metamaterials are capable of competing with the conventional bulk polarization optics in specific linear birefringence and dichroism and chirality. In this work local-field analogues of the linear and circular diattenuation effects are numerically and experimentally found in these metamaterials. High in-plane spatial variation of these effects indicates the key role of plasmons in establishing of the polarization-sensitive response of metamaterials.

The samples of polarization-sensitive optical metamaterials were prepared using the electron beam lithography and ion beam lithography methods out of thin opaque noble metal films. The nanowire array sample comprised of a set of 100 golden nanowires with the length of 30 μm and cross-section of 80x40 nm^2 and period of 300 nm. The sample demonstrates high optical anisotropy in the spectral vicinity of the local plasmon-polariton resonance [6]. The dynamic polarimetry technique was applied to the near-field optical microscopy to obtain the local values of the linear diattenuation effect. Two-dimensional map of the linear diattenuation measured for the nanowire array sample in the local-plasmon resonance is presented in Fig. 1. The map displays the distribution of the ratio of the field transmission coefficients for the light polarized along and perpendicularly to the wires $\rho_{nf} = T_H/T_V$. The image shows the inhomogenious distribution of the said effect with the maxima situated above the nanowires. The redistribution of the diattenuation effect demonstrates the possibility of the polarization-controlled spatial localization of the electromagnetic fields in plasmonic nanostructures.

Using the finite-difference time-domain simulations and near-field dynamic polarimetry we show that achiral, i.e. having the mirror symmetry in its plane, ensemble of elliptical nanoholes with planar 3-fold rotational symmetry made in an opaque thin golden film exhibits mirror symmetry breaking in the near-field when illuminated with either right- or left-handed circularly polarized light. Fig. 2 shows the distribution of the electromagnetic field intensity collected at a fixed subwavelength distance from the film. The surface plasmon modes are seen to be launched in three directions away from the nanoholes position which is a consequence of interference between three point-like polarization-sensitive plasmon emitters. The phase between the emitted plasmons is controlled by the handedness of the impinging circularly polarized light. As a result, the direction of the plasmon propagation is handedness-sensitive in spite of the structure being handedness-insensitive. This makes a near-field circular polarization filter—a near-field probe placed in a particular place in the of the sample detects light only if it is polarized with a certain way of handedness. The maximum local-field diattenuation between the right-hand circularly polarized and the left-hand one is estimated as high as 35 dB.

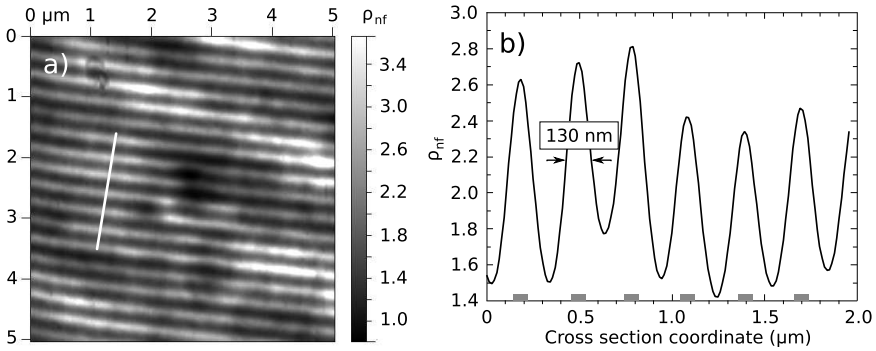

Figure 1: a) The distribution of linear diattenuation in the $\lambda/25$ vicinity of the sample. b) The cross-section of the map to the left. Grey rectangles denote the position of the nanowires.

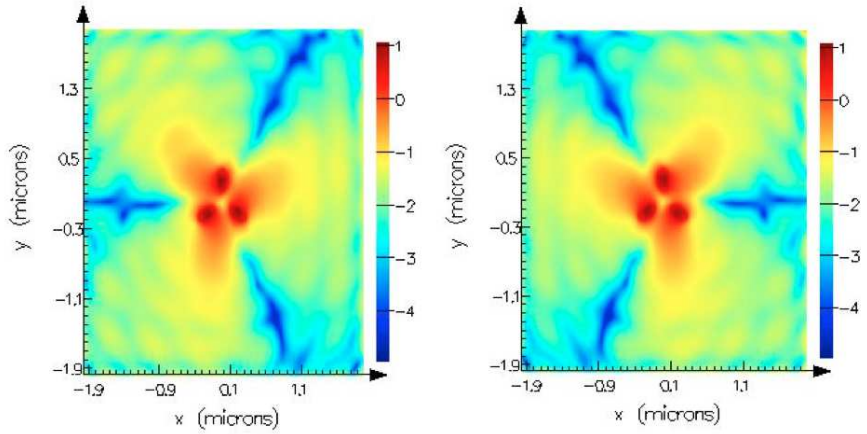

Figure 2: The distribution of the electromagnetic field intensity near the surface of the 300 nm-thick golden film with three elliptic nanoholes illuminated with right-hand (left panel) and left-hand (right panel) circularly polarized light. The interference fringes occur due to the finite computational volume.

In conclusion, it is shown experimentally and numerically that strong linear and circular diattenuation in the near-field of plasmonic nanostructures leads to the polarization-controlled redistribution of the local plasmonic fields. This characteristic of low-symmetry nanostructures is expected to find numerous applications in novel plasmonic circuitry devices.

REFERENCES

1. V. M. Shalaev, "Optical negative-index metamaterials," *Nat. Photonics,* vol. 1, p. 41, 2007.
2. T.W. Ebbesen et al., "Extraordinary optical transmission through sub-wavelength hole arrays," *Nature*, vol. 391, p. 667, 1998.
3. D. K. Gramotnev et al., "Plasmonics beyond the diffraction limit," *Nat. Photonics* vol. 4, p. 83, 2010.
4. M. R. Shcherbakov et al., "Full Poincaré sphere coverage with plasmonic nanoslit metamaterials at Fano resonance, " *Phys. Rev. B*, vol. 82, p. 193402, 2010.
5. M. Kuwata-Gonokami et al., "Giant optical activity in quasi-two-dimensional planar nanostructures," *Phys. Rev. Lett.* vol. 95, p. 227401, 2005.
6. M. R. Shcherbakov et al., "Plasmonic enhancement of linear birefringence and linear dichroism in anisotropic optical metamaterials," *JETP Lett.* vol. 90, p. 433, 2009.

Light diffraction from opal-like photonic structures: transition from 2D to 3D regimes

K. B. Samusev*, A. K. Samusev, I. S. Sinev, E. Yu. Trofimova, D. A. Kurdyukov
Ioffe Physical-Technical Institute, Russian Academy of Sciences, St. Petersburg, 194021, Russia
*corresponding author: K.Samusev@mail.ioffe.ru

We present an overview of the diffraction of visible light from opal-like photonic structures. A special attention is paid to the transformation of diffraction patterns upon building up the opal structure from two-dimensional (2D) single layer of silica particles *a*-SiO_2 towards bulk three-dimensional (3D) opal structure. We also discuss the selective switching of (*hkl*) reflections in diffraction patterns of thick opal films depending on the value of permittivity of infiltration material (filler) ε_f.

The Bragg diffraction is a key optical phenomenon in photonic crystals (PhC). Bragg diffraction gives rise to energy stop-bands in the spectrum for the electromagnetic wave propagation in a periodic structure. The presence of photonic stop-bands along certain directions of electromagnetic wave propagation or the formation of a completely three-dimensional photonic band gap is the major feature of PhC.

Opal-like structures are PhC that possess stop-bands in the visible range due to the typical size of the constitutive particles of some hundreds of nanometers. This provides a unique chance to study photonic properties not only by traditional methods like registering transmission or reflection with a spectrometer, but also by directly observing diffraction patterns on a screen disposed behind or around the sample.

The key feature of our studies is the experimental data presentation [1]. Most commonly, 2D diffraction patterns are presented as recorded on a flat screen. Here an alternative approach is used: a collection of a large number of the cylindrical screen color photographs are presented as a function of the angle of light incidence θ and the angle of diffracted light registration Θ. The diffraction patterns are collected for the angles of incidence within the range $-90^\circ \le \theta \le 90^\circ$ with the angular step size of $\Delta\theta = 2.5^\circ$. Hereby, 72 narrow «strip-patterns» are obtained and joined together into a single image.

The advantage of this presentation is that one can easily distinguish 2D and 3D diffraction, along with singling out a variety of effects induced by the disorder in the opal sample. Indeed, in the case of 2D diffraction one has a complex dependence between Θ and θ angles for the allowed, i.e., experimentally observed, reflections. At the same time, the case of 3D Bragg diffraction reduces to the specular reflection of the beam from a set of (*hkl*) crystallographic planes, and is thus described by a simple equation $\Theta = 2(\theta - \theta_{hkl})$. Therefore, in the (θ, Θ) coordinates the allowed 3D Bragg reflections will be represented by parallel straight lines, and any deviation or broadening of the lines will be associated with some kind of sample disorder.

The light diffraction from a six-layers-thick opal film has a vivid 2D nature. The zeroth order diffraction corresponds to specular reflection from the hexagonal plane on all wavelengths and is observed experimentally as a bright white stripe at $\Theta = 2\theta$. Theoretical dependences $\Theta = f(\theta, \lambda)$ for a non-zero order of diffraction represent nested closed curves (ovals); with the ovals corresponding to a higher order of diffraction lying within the ovals of the lower order for the given wavelength.

Increasing the specimen thickness leads to a transition from 2D to 3D diffraction. With increasing number of layers, certain regions of both the ovals and the diagonal fade out. First, the closed ovals break up into bands, then the bands narrow down, and finally, in the case of the bulk specimen these regions turn into a set of straight segments parallel to the $\Theta = 2\theta$. As a result, the expected Bragg diffraction pattern is indeed reached.

For the light diffraction from 3D bulk opal sample, the effect of the selective weakening of the {*hkl*} reflections appears to be the most important experimental result. The intensity of all reflections of the {111} and {220} families exhibit pronounced dependence on the filler permittivity ε_f. The intensities of {111} and {220} reflections have minima at ε_f = 1.86 and ε_f = 2.05 respectively [2]. At the same time the {200} reflections keep almost constant intensity in the investigated diapason of filler permittivity values.

Therefore, one can conclude a possibility of selective control over the intensity of Bragg diffraction reflections in low-contrast opal-based PhC.

The authors are grateful to V. G. Golubev for providing with opal films and for numerous fruitful discussions. We thank M. F. Limonov and M. V. Rybin for their help in conduction of the experiments and useful discussions of the work.

The work is supported by the RFBR (project No. 10-02-01094).

REFERENCES

1. Samusev, A. K., K. B. Samusev, M. V. Rybin, M. F. Limonov, E. Yu. Trofimova, D. A. Kurdyukov, and V. G. Golubev. "Two-dimensional light diffraction from thin opal films", *Phys. of Solid State*, Vol. 53, No. 5, 1056-1061, 2011.
2. Samusev, A. K., K. B. Samusev, I. S. Sinev, M. V. Rybin, and M. F. Limonov. "Selective control of light beams in diffraction experiments on synthetic opals", *Phys. of Solid State*, Vol. 53, No. 7, 1415-1424, 2011.

Spectral-luminescent characteristics styrylcyanine dye Sbt and homodimers in solutions

E.N.Kurtaliev
Samarkand State University, University blvd. 15, 140104 Samarkand, Uzbekistan
e-mail: kurtaliev@rambler.ru

Abstract. The influence of concentration, solvent nature on the intermolecular interaction and its spectroscopic manifestations in solutions of styrylcyanine dye Sbt and its homodimers was studied. It was established that, depending on the concentration, the structure of dye molecules, the nature of the solvent produced various forms of associated molecules, each in its own way is manifested in the spectra of absorption and fluorescence.

Relevance of the study of spectral luminescence, photophysical and photochemical properties of organic dyes in recent years has increased dramatically. This is due to the fact that organic dyes are widely used in various branches of science and technology. In particular, in medicine and biology in recent years styrylcyanine dyes are widely used as fluorescent probes and labels. The aim of this work is to study the effect of concentration, the nature of the solvent on the intermolecular interaction and its spectroscopic manifestations in solutions of styrylcyanine dye Sbt and its homodimers. It was established that for all studied dyes in the concentration range 10^{-6}-10^{-5}M the shape of the absorption and fluorescence remains constant, and they belong to the free (unaggregated) form of dyes molecules. Based on experimental measurements data for aqueous solutions of the studied dyes, the main spectral-luminescent characteristics of dyes in free form were determined: extinction coefficient (ε), oscillator strength (f_e), radiative lifetime of the excited state (τ), the frequency of purely electronic transition (ν_{0-0}) and Stokes shift (SS). The quantum yield of aqueous solutions of the studied dyes is 0.01-0.02%. Dye Sbt is monomeric, and Dbt-5 and Dbt-10 are homodimers of dye Sbt, chromophores of which are covalently linked in polymethylene chain with long chain n=5 and n=10, respectively. From table, the maximum of absorption and fluorescence spectra of dyes Dbt-5 and Dbt-10 is hypsochromically shifted on the 8-21 nm as compared with the maximum of the absorption spectrum and fluorescence of dye Sbt. The increase in the polymethylene chain of dyes Dbt-5 and Dbt-10 leads to decrease in the extinction coefficient in 1.9 and 6 times respectively as compared with the dye Sbt. For the monomeric dye Sbt with increasing concentration the absorption intensity of the monomer band with λ_{max}=511 nm falls and from the shorter wavelengths there observed a new band with λ_{max}=498 nm. For dye Dbt-5 with increasing concentration in the absorption spectra there observed a decrease in the intensity of the absorption, while for the dye Dbt-10 the form and the intensity of the absorption remains constant. Intensity of fluorescence of aqueous solutions of all studied dyes falls with increasing concentration. Observed phenomena in the absorption and fluorescence spectra in aqueous solutions can be explained in terms of formation of non-luminescent aggregates of dye molecules with solvent molecules. Established that the transition from water to binary mixtures of water+ethanol, water+DMF and water+dioxane the absorption spectra of dye Sbt and homodimers undergo bathochromic shifts in the 9-26 nm, and fluorescence spectra of 2-4 nm. The intensity of the absorption decreases, while the shape is markedly broadened. The shape of the fluorescence spectrum remains constant, and light intensity is increased by a half order. This change in the absorption and fluorescence spectra is due to change of the solvation shells surrounding the dye molecules, which is due to universal and specific interactions of dye molecules with solvent molecules.

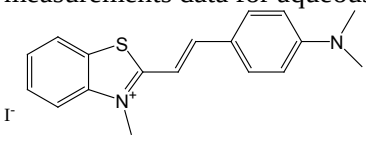

Sbt

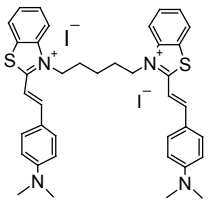

Dbt-5

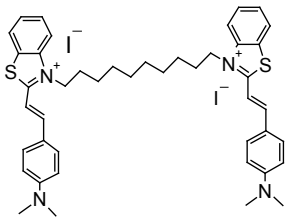

Dbt-10

Fano resonance in photonic crystals: experiment and theory

M. F. Limonov* and M. V. Rybin
Ioffe Physical-Technical Institute of the Russian Academy of Sciences, St.Petersburg, Russia
*corresponding author: M.Limonov@mail.ioffe.ru

We present a study of a Fano resonance between a narrow Bragg band and disorder-induced continuum in photonic crystals where the continuum is either of the broad band Fabry-Pérot scattering in an imperfect one-dimensional photonic crystal or Mie scattering in an imperfect three-dimensional photonic crystal. Our experimental studies of synthetic opals have demonstrated how the Fano resonance may lead to a transmission spectrum exhibiting a Bragg dip with an asymmetric profile or a Bragg rise.

Fano resonance [1] takes place when a narrow band of virtually any origin is superimposed onto a featureless background spectrum. Fano resonance arises when a scattered projectile exhibiting a wave-like nature may reach the same final state via two different paths. The first scattering path corresponds to the formation of a narrow band, where the wave phase changes by ~π. The second scattering path corresponds to a broad background, where the wave phase and amplitude are nearly constant in the spectrum range of interest.

In this report we consider a Fano resonance involving interference between a narrow band Bragg scattering and a broad band disorder-induced scattering. The underlying mechanism of the latter is strongly dependent on the dimensionality of the system. For example, for a 1D photonic crystal (PhC) composed of slabs or a 3D PhC composed of spherical particles, the disorder-induced scattering is Fabry-Pérot or Mie scattering, respectively. We demonstrate that 3D opal-based PhC exhibit a Fano resonance of the same nature and propose a theoretical ‘‘quasi-3D’’ model that incorporates both Bragg and disorder-induced Mie scattering mechanisms in a way that naturally leads to their coupling.

We present experimental and theoretical study of a Fano resonance between a narrow Bragg band and the disorder-induced Mie continuum in three-dimensional opal-based photonic crystals [2,3]. The resonance leads to a transmission spectrum exhibiting a Bragg dip (photonic stop-band) with an asymmetric profile, which can be tunably reversed to a Bragg rise (photonic pass-band). The Fano asymmetry parameter is linked with the dielectric contrast between the permittivity of the filler and the specific value determined by the opal matrix. In other words, in contrast to general expectations, photonic crystals under certain conditions were shown to exhibit enhanced transmission of light at the Bragg’s wavelength instead of the expected enhanced disorder induced scattering resulting to enhanced reflection or diffusion. The theoretical model produces results in excellent agreement with the experimental data.

We also develop a new picture of optical spectra transformation in disordered 1D PhC [3]. We demonstrate that the optical phenomena in 1D PhC dramatically depend on the character of the disorder. Variation in the dielectric constant of the constituents of the 1D PhC gives rise to the disorder-induced Fabry-Pérot background in transmission spectra. We reveal the existence of two different types of scattering mechanisms that result in formation of a Fano-type resonance. At the same time, one can observe a distinct transformation picture of the spectrally narrow band specific for the Fano resonance, which manifests as of the photonic band gap in transmission spectra, i.e., its transformation from the stop-band to the pass-band.

In John's pioneering work [5] on light scattering in disordered PhC it was predicted that localization of photons may occur in the vicinity of band edges. Since then such interplay between Bragg diffraction and disorder-induced scattering was considered only as a way to localize light and as a mechanism capable to suppress transmittance and increase backscattering. We demonstrate that it is not always so and at some particular conditions Fano interference between scattered background radiation and Bloch waves gives rise to anomalous increase of the optical transmittance near photonic band edges or when the Bragg condition is satisfied.

This work was supported in part by the RFBR, Grant No.10-02-01094.

REFERENCES

1. Fano, U., "Effect of configuration interaction on intensities and phase shifts," *Phys. Rev*, Vol. 124, No. 6, 1866–1878, 1961.
2. Rybin, M. V., A. B. Khanikaev, M. Inoue, K. B. Samusev, M. J. Steel, G. Yushin and M.F.Limonov, "Fano resonance between Mie and Bragg scattering in photonic crystals," *Phys. Rev. Lett.*, Vol. 103, 023901, 2009.
3. Rybin, M. V., A. B. Khanikaev, M. Inoue, A. K. Samusev, M. J. Steel, G. Yushin and M.F.Limonov, "Bragg scattering induces Fano resonance in photonic crystals," *PNFA*, Vol. 8, Issue 2, 86-93, 2010.
4. Rybin, M. V., M. F. Limonov, A. B. Khanikaev and C. Soukoulis, "Optical properties of 1D disordered photonic crystals," in *Optical properties of photonic structures: interplay of order and disorder*, Ed. M.Limonov and R. De La Rue, CRC Press Taylor & Francis, in press.
5. John, S., "Strong localization of photons in certain disordered dielectric superlattices," *Phys. Rev. Lett.*, Vol. 58, No. 23, 2486–2489, 1987.

Manipulating the Light Transmission and Faraday Rotation through Periodic Metamaterials by Applying an External Field and by Changing the Nano-structures Shapes

Y. M. Strelniker[1], **D. J. Bergman**[2], **Y. Fleger**[1], **M. Rosenbluh**[1], **A. O. Voznesenskaya**[3], **A. P. Vinogradov**[4], and **A. M. Merzlikin**[4]

[1]Department of Physics, Bar-Ilan University, IL-52900 Ramat-Gan, Israel
[2]Raymond and Beverly Sackler School of Physics and Astronomy, Faculty of Exact Sciences, Tel Aviv University, IL-69978 Tel Aviv, Israel
[3]St. Petersburg State University of Information Technologies, Mechanics and Optics, 197101, St. Petersburg, Russia
[4] Institute for Theoretical and Applied Electromagnetics,125412, Moscow, Izhorskaya 13, Russia

Abstract— The light transmission through metallic films with different types of nano-structures was studied both theoretically and experimentally. It is shown, analytically, numerically and experimentally, that the positions of the surface plasmon resonances depend on the nano-structural details. Those can be changed from sample to sample or in given sample by applying an external dc electric or magnetic field. The dependence of transmission spectrum on the shape of nanostructures and external fields can be used for manipulation of the light transmission, as well as the polarization, Faraday rotation and other optical properties. Two complementary situations are considered: a metal film with dielectric holes and a dielectric film with metallic islands.

We discuss some phenomena which can be used for manipulating the transmission of light through thin metal (with dielectric inclusions) and dielectric (with metal inclusions) films by applying an external magnetic field [1-3]. The optical properties of such systems strongly depend (at some frequency region) on coupling of light to plasmons on the surface of the patterned metal film. Continuing this idea, the effect of an applied static magnetic field on the optical properties of the metamaterials has been discussed. It was shown there that the applied static magnetic field shifts the surface plasmon resonance and the peaks in optical spectra. Quite recently our predictions were verified experimentally [4]. Now the influence of a magnetic field on the optical properties of the metamaterials is under intensive study. It was also found that the magneto-induced anisotropy of the optical properties of metamaterials with periodical nano-structures depend strongly on direction of the applied field. This is similar to the anisotropic magnetoresistance recently found in periodic conducting composites [5, 6]. It also was shown that the nanostructured metallic films can be used as systems with strong polarization [7] and Faraday rotation effect, when the magnetic field is applied perpendicular as well as parallel to the surface of the film.

In our approach, the local electric potential $\phi^{(\alpha)}(\mathbf{r})$ is the solution of the partial differential equation $\nabla \cdot \hat{\varepsilon}_F \cdot \nabla \phi^{(\alpha)} = \nabla \cdot \theta_I \delta\hat{\varepsilon} \cdot \nabla \phi^{(\alpha)}$, with the boundary condition $\phi^{(\alpha)} = r_\alpha$. Here r_α is the α-component of $\mathbf{r}$, $\hat{\varepsilon}_I$ and $\hat{\varepsilon}_F$ are the electrical permittivity tensors of the *inclusions* and the host (*film*) respectively, $\delta\hat{\varepsilon} \equiv \hat{\varepsilon}_F - \hat{\varepsilon}_I$, and $\theta_I(\mathbf{r})$ is the characteristic function describing the location and the shape of the inclusions ($\theta_I = 1$ inside the inclusions and $\theta_I = 0$ outside of them)[1-3,7-9]. Next, we compute, approximately, the tensor $\hat{\varepsilon}_e(\omega)$, which is defined by the relation $\hat{\varepsilon}_e \cdot \langle \mathbf{E}(\mathbf{r}) \rangle = \langle \hat{\varepsilon}(\mathbf{r}) \cdot \mathbf{E}(\mathbf{r}) \rangle$, where $\langle ... \rangle$ denotes a volume average and $\hat{\varepsilon}(\mathbf{r})$ is the local electric permittivity tensor. In the dilute limit and for the case of zero magnetic field, $H = 0$, and when the light electric field $\mathbf{E}_0$ and the coordinate axes are directed along the symmetry axes of the ellipse, $\hat{\varepsilon}_e$ is diagonal and takes the form $\varepsilon_{ii}^{(e)} = \varepsilon_{ii}^{(F)} \left[1 - p\delta\varepsilon_{ii}/(\varepsilon_{Fii}^{(F)} - n_i\delta\varepsilon_{ii})\right]$ in the dilute limit, i.e., when the volume fraction of inclusions p is much less than 1, where n_i are the depolarization factors and $i = x, y, z$. The frequency of the surface plasmon (SP) resonance, $\omega_{sp,i}$, (for the electric field polarized in the i-direction) is the one for which $\varepsilon_{ii}^{(e)}$ becomes very large even for a very small applied field. This condition is satisfied when $\varepsilon_{ii}^{(F)}(\omega_{sp,i}) - n_i\delta\varepsilon_{ii}(\omega_{sp,i}) = 0$. In limit $\omega_p\tau \to \infty$, one obtains

$$\begin{aligned} \omega_{sp,i} &= \omega_p\sqrt{(1-n_i)/[(1-n_i)+n_i\varepsilon_{ii}^{(I)}]}, && \text{when the film is metallic,} \\ \omega_{sp,i} &= \omega_p\sqrt{n_i/[\varepsilon_{ii}^{(F)}(1-n_i)+n_i]}, && \text{when the inclusions are metallic.} \end{aligned} \quad (1)$$

This resonance is known also as the *localized surface plasmon resonance* and/or *quasistatic surface plasmon resonance*. The Maxwell Garnett (MG) or Clausius-Mossotti (CM) approximation, for ε_e and ω_{sp} can be obtained directly from the dilute approximation just by the formal substitution $n_i \to n_i(1-p)$ [8]. The MG approximation is valid for volume fractions p that are considerably larger than required for the dilute limit to be valid.

An alternative possibility to manipulate light transmission through a perforated metal film is to fill the holes with a uniaxially anisotropic dielectric, such as a nematic liquid crystal (NLC)[8]. Since the frequency of the surface plasmon resonance depends strongly on the light polarization with respect to the principal axis of the NLC, known as the director, and the latter can be rotated by applying a static magnetic $\mathbf{H}_0$ (or electric $\mathbf{E}_0$) field (so-called Freedericksz effect), this result implies that the transmission can be controlled simply by rotating $\mathbf{H}_0$ (or $\mathbf{E}_0$) even if this magnetic field has no effect on the plasma frequency ω_p of the metallic film.

In order to verify our predictions but not to deal with magnetic field, we study optical properties of several samples with metallic particles (as well as metallic films with holes) of different aspect ratios [9]. We studied the optical density, $\mathrm{OD} = -\log_{10} T$ (where T is the transmission coefficient) of a dielectric film with a periodic array of metallic islands. In the case of metallic islands, we propose two ways of controlling plasmon resonance frequency: changing the aspect ratio of the elliptical (or rectangular) islands and changing their mutual distances. For this case a new analytical asymptotic approach for calculating the optical properties of such plasmonic systems is developed. The results of our analytical and numerical studies are in good qualitative agreement with experiment.

ACKNOWLEDGMENT

This research was supported in part by grants from the U.S.-Israel Binational Science Foundation, the Israel Science Foundation, the Russia-Israel Science Foundation (RFBR), and the KAMEA program of the Ministry of Absorption of the State of Israel.

REFERENCES

1. Strelniker, Y. M. and D. J. Bergman, "Optical transmission through metal films with a subwavelength hole array in the presence of a magnetic field," *Phys. Rev. B*, Vol. 59, R12763–R12766, 1999.
2. Bergman, D. J. and Y. M. Strelniker, "Anisotropic ac electrical permittivity of a periodic metal-dielectric composite film in a strong magnetic field," *Phys. Rev. Lett.*, Vol. 80, 857–860, 1998.
3. Strelniker, Y. M. and D. J. Bergman, "Magnetic-field-induced transparency of conducting films," *Phys. Rev. B*, Vol. 77, 205113-1–205113-5, 2008.
4. Ou, N., J. Shyu, J. C. Wu, and T. Wu, "Extraordinary optical transmission through dielectric hole-array coated with TbFeCo thin film," *IEEE Transactions on Magnetics*, Vol. 45, 4027–4029, 2009.
5. Tornow, M., D. Weiss, K. v. Klitzing, K. Eberl, D. J. Bergman, and Y. M. Strelniker, "Anisotropic magnetoresistance of a classical antidot array," *Phys. Rev. Lett.*, Vol. 77, 147–150, 1996.
6. Bergman, D. J., and Y. M. Strelniker, "Exact asymptotics for the strong-field macroscopic magnetotransport of a composite medium," *Phys. Rev. B*, Vol. 82, 174422-1–174422-19, 2010.
7. Strelniker, Y. M., "Theory of optical transmission through elliptical nanohole arrays," *Phys. Rev. B* , Vol. 76, 085409-1—085409-6, 2007.
8. Strelniker, Y. M., D. Stroud, and A. O. Voznesenskaya, "Control of extraordinary light transmission through perforated metal films using liquid crystals," *Eur. Phys. J. B*, Vol. 52, 1–7, 2006.
9. Fleger, Y., M. Rosenbluh, Y. M. Strelniker, D. J. Bergman, and A. N. Lagarkov, "Controlling the optical spectra of gold nano-islands by changing the aspect ratio and the inter-island distance: theory and experiment," *Eur. Phys. J. B*, Vol. 81, 85-93, 2011.

All-dielectric horn antennas based on woodpile structures

I. Khromova[1*], R. Gonzalo[1], I. Ederra[1], J. Teniente[1] , K. Esselle[2]
[1]Public University of Navarra, Spain
[2]Macquarie University, Australia
[*]corresponding author: irina.khromova@unavarra.es

Abstract- This paper is devoted to EBG horn antennas. This novel type of all-dielectric horn antennas is based on complex hollow defects in woodpile structures and can be used for creating compact arrays and provide a promising solution for millimeter and terahertz devices. A novel concept of feeding EBG horn antennas via evanescent fields existing in periodic structures is presented. The principle of creating all-dielectric pyramidal horn antennas based on woodpile structure with hollow defects is proposed. Different horn antennas based on woodpile structures were designed, fabricated and measured.

The scientific and technological interest towards electromagnetic band gap (EBG) structures has been growing rapidly since their discovery. The essence of any EBG structure, a periodical dielectric struc-ture with certain geometry and dimension, is that it is a resonance structure. Due to this fundamental property different interesting well-known effects, such as band gaps, controllable dispersion, defect-based waveguiding, field localization or resonant transmission are observed [1-3]. In recent years EBGs have been widely exploited for the purpose of shaping and improving the radiation characteristics of antennas of different types. Following the analogy with classical metallic horn antennas, introducing a horn-shaped hollow defect can make the EBG-based system work as a horn antenna [4-6].

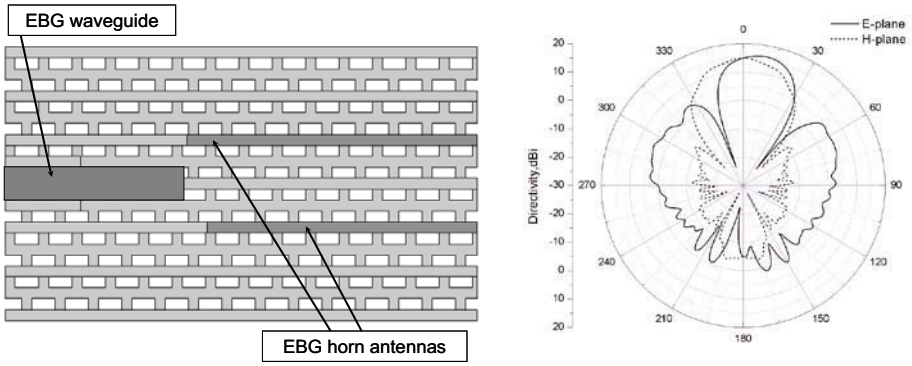

Fig.1 (left) Side-view of the evanescently-fed double EBG horn antenna. (right) Radiation pattern of a double evanescently-fed EBG horn antenna radiation pattern (at 110GHz).

An EBG horn antenna can be realized as a hollow pyramidal-shaped defect of the ideal periodic structure. This paper demonstrates a new concept of evanescent feeding for EBG horn antennas. It is shown that such horn antennas, realized as hollow defects in a three-dimensional (3D) periodic structure can be coupled to an EBG waveguide via evanescent fields existing in the embedding medium. This concept allows one to design compact arrays of EBG antennas, where horns can share feeds. A woodpile-based evanescently fed horn antenna operating in the F band (at around 110GHz) was designed (Fig.1): the horn throats and the EBG waveguide end

are separated by a slab of periodic structure. With its operating bandwidth of 8.3% and directivity and gain equal to 16.1 dBi and 14.83 dBi, respectively, this antenna demonstrates a competitive performance. The double evanescently fed EBG horn antenna was fabricated and measured at Ku band. Experimental results have shown a very good agreement with the numerical simulation data.

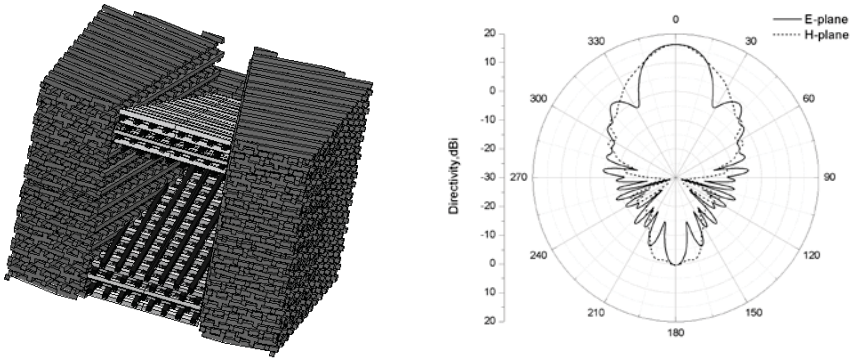

Fig.2. (left) EBG EH-horn antenna. The woodpile sections are turned at the antenna flare angle. (right) Radiation pattern of the EBG EH-horn antenna at 107GHz.

This paper also presents the design and the concept of a novel symmetric EH-horn antenna based on EBG structures. The main idea lies in turning the EBG structure at the antenna flare angle and thus forming the EBG ”walls” of the horn. The adiabatic transition between the feeding EBG waveguide and the free space, provided by such antenna is possible thanks to the gradual shift of the periodic lattice nodes (Fig.2). The antenna presented in Fig.2 was designed for the F band, however it is also perfectly scalable and the same configuration can be used in different frequency ranges. Unlike its woodpile-based “predecessors” this antenna possesses a symmetric radiation pattern in both E- and H-planes. The reported pyramidal woodpile-based horn antenna possesses a symmetrical radiation pattern and a wide operating bandwidth of 10.2% in the F band. The directivity and radiation efficiency of the reported antenna are equal to 16.35 dBi and -0.55 dB, respectively. It is also significantly robust towards small errors in such parameters as flare angle and antenna throat position.

This work was supported by the Spanish Ministry of Science and Innovation Project Nos. TEC2009-11995 and CSD2008-00066.

REFERENCES

1. R.D. Meade et al, “Photonic bound states in periodic dielectric materials”, *Phys Rev.B*, 44, 24, 13772-12774, 1991.

2. S. Noda, A. Chutinan, and M. Imada, “Trapping and emission of photons by a single defect in a photonic bandgap structure”, *Nature*, 407, 6804, 608-610, 2000.

3. I. Khromova et al, “Resonance Frequency Behavior of 3D EBG Cavities", *J. Appl. Phys*. 106, 014901-01498, 2009.

4. R. L. Moore et al, US Patent 5,689,275, 1997.

5. A. R. Weily, K. P. Esselle, B. C. Sanders, *Phys. Rev. E*., vol. 70, pp. 037602-4, 2004.

6. I. Khromova et al, “Evanescently-fed electromagnetic band gap horn antennas and arrays”, submitted to IEEE TAP, 2010.

7. I. Khromova et al.,”Symmetrical Pyramidal Horn Antennas Based on EBG Structures”, *PIER B*, 29, 1-22, 2011.

Transmission and Reflection Spectra of Photonic Crystal with Plasmonic Defect

Sergey G. Moiseev

Kotelnikov Institute of Radio Engineering and Electronics of Russian Academy of Sciences, Ulyanovsk Branch, Russia

Features of the behavior of electromagnetic eigenmodes in an artificial layered periodic structure with a finite number of periods and a plasmonic defect are analyzed. The plasmonic defect consists of a dielectric medium with metallic nanoparticles. It is shown that the presence of a defect in a layered periodic structure causes the appearance of a narrow passband corresponding to the mode associated with the defect (defect mode) in the stopband of the nondefective structure. The capability of control of the transmission and reflection spectra by changing the parameters (concentration and shape of nanoparticles) and position of the defect is discovered.

Terahertz detection in a gated planar plasmonic crystal with an asymmetric unit cell

D. V. Fateev[1,6,*], **V. V. Popov**[1,6], **T. Otsuji**[2], **Y. M. Meziani**[3], **D. Coquillat**[4], **W. Knap**[4], **S. A. Nikitov**[5,6]

[1]Kotelnikov Institute of Radio Engineering and Electronics (Saratov Branch) of RAS, 410019 Saratov, Russia

[2]Reseach Institute of Electrical Communication, Tohoku University, 2-1-1Katahira, Sendai 980-8577, Japan

[3]Dpto. de Fisica Aplicada, Universidad de Salamanca, Pza de la Merced s/n, 37008 Salamanca, Spain

[4]Laboratoire Charles Coulomb UMR5221, CNRS&Université Montpellier 2, 34095 Montpellier, France

[5]Kotelnikov Institute of Radio Engineering and Electronics of RAS, 125009 Moscow, Russia

[6]Saratov State University named after N.G. Chernyshevsky, 410012 Saratov, Russia

[*]corresponding author: FateevDV@yandex.ru

Abstract – We propose a double-grating-gate transistor structure with two-dimension electron channel and an asymmetric unit cell for detection of the terahertz radiation by plasma waves. We calculate photovoltaic terahertz response of the transistor structure under consideration as a function of the asymmetry.

The detection of the terahertz (THz) radiation in the field effect transistor (FET) structure with two-dimensional (2D) electron channel originates from a nonlinear dynamics of 2D electron fluid described by the hydrodynamic equations (the Euler equation and the continuity equation) [1]. There are two different nonlinear terms in the hydrodynamic equations: the nonlinear electron convection term in the Euler equation and the current term in the continuity equation. Time average of the nonlinear current yields the detection signal.

Detection of THz radiation based on plasmonic nonlinearities in the grating-gate FET structure with 2D electron channel has been investigated recently [2-5]. In such type of plasmonic detectors, the grating gate of a large area (comparable with a typical cross-section area of a focused THz beam) acts as an effective aerial matched antenna and hence such device can effectively operate without using supplementary antenna elements. In essence, the grating-gate FET structure with 2D electron channel can be considered as a gated planar plasmonic crystal strongly coupled to THz radiation. Since THz photovoltaic response is zero in the grating-gate FET structure with a symmetric unit cell, required asymmetry in the grating-gate FET channel is commonly introduced by applying dc bias current in the FET channel. However, strong dc current causes large voltage drop in the long FET channel and hence the gate voltage value is effectively different in different unit cells of a large-area grating-gate FET structure. As a result, the net responsivity of the grating gate FET plasmonic detector remains quite low (below 50 mV/W [5]). In this paper, we calculate the photovoltaic THz response of a double-grating-gate (DGG) FET structure with an asymmetric unit cell [Fig. 1 (a)]. Lateral shift between two different sub-gratings (having metal fingers of different width) introduces a required asymmetry in the unit cell of the entire DGG-FET structure. Individual gate voltage (U_1 and U_2) can be applied to each sub-grating. The equilibrium electron density in 2D electron channel is a periodic function of the coordinate across the DGG fingers (the x-coordinate): $N^{(0)}(x) = N^{(0)}(x+L)$, where L is the DGG period. The electric field of incident THz wave is polarized across the DGG fingers. We solve the Maxwell equations and the hydrodynamic equations for 2D electron fluid self-consistently in a perturbation approach describing the induced THz electric field $E(x,t)$,

induced electron-density perturbations, and the electron-velocity perturbations in the 2D electron channel by the series over powers of the external THz electric-field amplitude.

Calculated photovoltaic THz response of the InGaP/InGaAs DGG-FET with an asymmetric unit cell and density modulated 2D electron channel is shown on Fig. 1 (b). Calculation shows that the responsivity of the DGG-FET THz plasmonic detector with aperture area of 80×30 μm^2 can exceed 100 V/W.

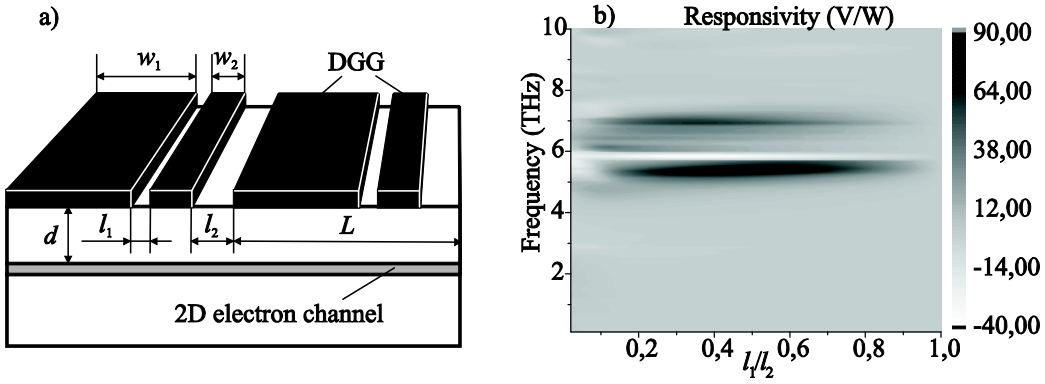

Figure. 1. (a) Schematic view of the double-grating-gate FET structure (two unit cell of the structure are shown). External THz radiation is incident normally from the top. (b) Calculated responsivity of InGaP/InGaAs DGG-FET detector as a function of the frequency and asymmetry factor l_1/l_2 for L = 900 nm, w_1 = 600 nm, w_2 = 200 nm, d = 30 nm for U_1 = –1V and U_2 = 0 V at room temperature.

Acknowledgements. This work has been supported by the Russian Foundation for Basic Research (Grant Nos. 10-02-93120 and 11-02-92101), by the Russian Academy of Sciences Program "Fundamentals of Nanotechnology and Nanomaterials", and by the Grant of the Government of the Russian Federation for supporting scientific research projects supervised by leading scientists at Russian institutions of higher education (Contract No. 11.G34.31.0030).

REFERENCES

1. Dyakonov, M. and M. Shur, "Detection, mixing, and frequency multiplication of terahertz radiation by two dimensional electronic fluid," *IEEE Trans. Electron Devices*, Vol. 43, No. 3, 380-387, 1996.
2. Peralta, X. G., S. J. Allen, M. C. Wanke, N.E. Harff, J. A. Simmons, M. P. Lilly, J. L. Reno, P. J. Burke, J. P. Eisenstein, "Terahertz photoconductivity and plasmon modes in doublequantum-well field-effect transistors," *Applied Physics Letters*, Vol. 81, No. 9, 1627-1629, 2002.
3. Coquillat, D.,S. Nadar, F. Teppe, N. Dyakonova, S. Boubanga-Tombet, W. Knap, T. Nishimura, T. Otsuji, Y. M. Meziani, G. M Tsymbalov, and V.V. Popov, "Room temperature detection of sub-terahertz radiation in double-grating-gate transistors," *Optics Express*, Vol. 18, No. 6, 6024-6032, 2010.
4. Marem'yanin, K. V, D. M. Ermolaev, D. V. Fateev, S. V. Morozov, N. A. Maleev, V. E. Zemlyakov, V. I. Gavrilenko, V. V. Popov and S. Yu. Shapoval, "Wide-aperture detector of terahertz radiation based on GaAs/InGaAs transistor structure with large-area slit grating gate," *Technical Physics Letters,* Vol. 36, No. 4, 365-368, 2010.
5. Aizin, G.R., D.V. Fateev, G.M. Tsymbalov, V.V. Popov, "Terahertz plasmon photoresponse in a density modulated two-dimensional electron channel of a GaAs/AlGaAs field-effect transistor ," *Applied Physics Letters,* Vol. 91, No. 16, 163507, 2007.

Quarter-wavelength wire lens for subwavelength imaging at terahertz frequencies

A. E. Ageyskiy[1], **S. Yu. Kosulnikov**[1], **S. I. Maslovski**[2], **P. A. Belov**[1,3], **Yu. S. Kivshar**[4]

[1]National Research University of Information Technologies, Mechanics and Optics (ITMO)
[2]Instituto de Telecomunicações, Universidade de Coimbra
[3]Queen Mary College, University of London
[4]Nonlinear Physics Centre, Australian National University
alex.ageyskiy@phoi.ifmo.ru

Abstract— A quarter-wavelength metal-backed wire lens for subwavelength imaging with resolution not worse than $\lambda/8$ in the terahertz range is proposed and studied both numerically and analytically. The operation of the lens is based on the internal imaging effect in the half-wavelength wire medium slab reported earlier.

Wire lenses are slabs of uniaxial wire media of resonant thickness $L = n\lambda/2$ where, typically, $n = 1$ [see Fig. 1(a)]. In optics, the resonance employed in these lenses is known as the Fabry-Perot resonance (of the first order when $n = 1$). As is known, this resonance corresponds to a minimum in the reflectivity and a maximum in the transmittivity of a material slab under the normal plane wave incidence. At the same time the electromagnetic field *inside* the Fabry-Perot cavity may experience a resonant growth. Moreover, in slabs of uniaxial wire media that support propagating modes with large transverse wavenumbers, such a growth of the field inside the slab accompanied with a low reflectivity at the slab interfaces happens also for the plane waves that are evanescent in free space. This effect is responsible for the amplification of the evanescent waves in the internal imaging phenomenon in wire lenses [1, 2, 3].

In this phenomenon a subwavelength image is formed inside the half-wavelength wire lens at its middle cross-section, as shown in Fig. 1(a). At this cross-section the magnetic field and the wire currents of the P-polarized wire medium modes are maximized, similarly to the magnetic field and the current in a resonant half-wavelength segment of a transmission line open at both ends. It can be shown that the electric field of the P-polarized modes almost vanishes at the middle cross-section, therefore, the image is encoded in the distribution of the wire currents.

One may notice that vanishing of the electric field at the middle of the half-wavelength wire lens allows to place there a metallic screen (with wires electrically connected to the screen) without disturbing the conditions that are vital for the resonance of the wire currents. In this case, the lens thickness may be reduced by a factor of two. Additionally, there appears a possibility to register the wire currents at the points where the wires are attached to the ground screen. This can be done differently, for example, the wires could be put through holes in the screen and terminated with small grounded wire loops, the purpose of which would be to couple the wire currents to the near magnetic field on the back side of the screen.

In this work we consider the metal-backed quarter-wavelength wire lens the geometry of which is shown in Fig. 1(b). The lens is formed by a periodic array of metallic nanowires with the radius $r = 200$ nm. The array period is $a = 2$ μm. The length of the nanorods (the thickness of the lens) is $L = 15$ μm that is about $\lambda/4$ at 5 THz. The array has 21×21 nanorods in total and is terminated by a metal screen. We excite the lens with a pair of point electric dipoles aligned with the nanorods and placed at the distance of 10 μm from the face of the lens. The dipoles are separated by 8 μm (which is about $\lambda/8$ at 5 THz). The results of the full-wave simulations performed in Microwave CST Studio$^{\text{TM}}$ that are shown in Fig. 1(d) confirm that the operation of the quarter-wavelength lens is similar to the operation of the half-wavelength lens in the internal imaging mode [see Fig. 1(c)].

In the frames of the effective medium model, the nanowire array may be described by the uniaxial relative permittivity tensor with $\varepsilon_{yy} = \varepsilon_{zz} = 1$ and $\varepsilon_{xx} = 1 - k_p^2/(k^2 - k_x^2)$ where $k = \omega/c$ and $(k_p a)^2 \approx 2\pi/(\ln \frac{a}{2\pi r} + 0.5275)$ (the x-axis is along the nanowires). As is known, there are two types of P-polarized waves in wire media: the TM waves with the dispersion $k^2 = k_x^2 + k_y^2 + k_p^2$ and the TEM waves with the dispersion $k^2 = k_x^2$ (we assume $k_z = 0$). Thus, there exist four independent

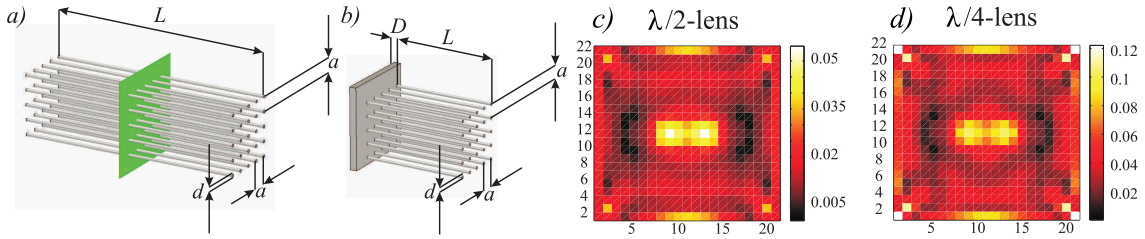

Figure 1: The subwavelength imaging by a half-wavelength [panels (a) and (c)] and a quarter-wavelength [panels (b) and (d)] lenses formed by metallic nanorods. (a) The geometry of the half-wavelength lens. (b) The geometry of the metal-backed quarter-wavelength lens. (c) The image of a pair of electric dipoles aligned with the nanorods and placed at 10 μm distance from the face of the half-wavelength lens as encoded in the nanorod currents at the middle cross-section of the lens. (d) The image of the same sources formed by the quarter-wavelength metal-backed lens as encoded in the nanorod currents at the points where the nanorods touch the metal screen. In both cases the array is formed by 21×21 metallic nanorods with the radius $r = 200$ nm and the array period $a = 2$ μm. The operating frequency is 5 THz. The results are obtained with full-wave simulations in Microwave CST Studio$^{\text{TM}}$.

P-polarized waves in a nanowire slab for a fixed transverse wavenumber k_y at a given frequency (in contrast to only two such waves in a slab of a local dielectric). The higher number of independent waves requires additional boundary conditions (ABCs) at the interfaces of the nanorod array, i.e., at the points where the nanorods meet the metal screen and at the free ends of the nanorods. The ABCs at these points may be formulated in terms of the nanorod current J_x. At the free ends of the nanorods the nanorod current must vanish: $J_x = 0$, while at the points where the nanorods are attached to the metal screen the surface change density on the nanorods must vanish which results in a condition $\partial J_x/\partial x = 0$.

Assuming an incident P-polarized plane wave of a unit amplitude and using the standard Maxwellian boundary conditions for the tangential electric and magnetic fields and the ABCs, the amplitudes of the two TM waves $A_{\pm}^{\text{TM}}$ and of the two TEM waves $A_{\pm}^{\text{TEM}}$ in the slab, and the amplitude of the reflected wave R in the air region are found from a 5×5 system of linear equations:

$$\begin{pmatrix} -1 & 1 & 1 & 1 & 1 \\ i\kappa_x & -\gamma_{\text{TM}} & \gamma_{\text{TM}} & ik & -ik \\ \kappa_x^2 & \gamma_{\text{TM}}^2 & \gamma_{\text{TM}}^2 & -k^2 & -k^2 \\ 0 & -\gamma_{\text{TM}}e^{-\gamma_{\text{TM}}L} & \gamma_{\text{TM}}e^{\gamma_{\text{TM}}L} & ike^{ikL} & -ike^{-ikL} \\ 0 & -\gamma_{\text{TM}}^3e^{-\gamma_{\text{TM}}L} & \gamma_{\text{TM}}^3e^{\gamma_{\text{TM}}L} & -ik^3e^{ikL} & ik^3e^{-ikL} \end{pmatrix} \cdot \begin{pmatrix} R \\ A_-^{\text{TM}} \\ A_+^{\text{TM}} \\ A_-^{\text{TEM}} \\ A_+^{\text{TEM}} \end{pmatrix} = \begin{pmatrix} 1 \\ i\kappa_x \\ -\kappa_x^2 \\ 0 \\ 0 \end{pmatrix}, \qquad (1)$$

where $\gamma_{\text{TM}} = \sqrt{k_p^2 + k_y^2 - k^2}$ and $\kappa_x = i\sqrt{k_y^2 - k^2}$. Solving this system the transfer function of the lens is found as

$$T = A_-^{\text{TM}} + A_+^{\text{TM}} + A_-^{\text{TEM}} + A_+^{\text{TEM}} = \frac{4\kappa_x \text{sech}(\gamma_{\text{TM}}L)\left(k_y^2 + k_p^2\text{sinh}(\gamma_{\text{TM}}L)/\cos(kL)\right)}{ikk_p^2\tan(kL) - \kappa_x(k_p^2 + k_y^2) - i\gamma_{\text{TM}}k_y^2\tanh(\gamma_{\text{TM}}L)}. \qquad (2)$$

This analytical expression has been compared with the transfer function of the half-wavelength wire lens obtained earlier. It has been found that when $k \ll k_p$, Eq. (2) results in a value of T which is twice higher than the corresponding $T_{1/2}$ of the half-wavelength wire medium lens [3]. The same is also seen from the results of the numerical simulations represented in Figs. 1(c,d).

REFERENCES

1. P. Belov, Y. Zhao, and Y. Hao, "Subwavelength internal imaging by means of a wire medium," *Journal of Optics: Pure and Applied Optics*, Vol. 11, P. 075101, 2009.
2. P.A. Belov, Y. Zhao, Y. Hao, and C. Parini, "Enhancement of evanescent spatial harmonics inside media with extreme optical anisotropy," *Optic Letters*, Vol. 34, No. 4, P. 527, 2009.
3. A.E. Ageyskiy, S.Yu. Kosulnikov, and P.A. Belov, "Resonant exitation of evanescent spatial harmonics in medium formed by parallel metallic nanorods," *Optics and Spectroscopy*, Vol. 110, P. 572, 2011.

Thin smart multilayer microwave absorber based on hybrid structure of polymer and carbonated nanoparticles

Yann Danlée, Christian Bailly, Isabelle Huynen
Universite cathalique de Louvain, Belgium

A thin multilayer sheet was created in order to absorb electromagnetic waves in the GHz range. Submillimetric conductive and dielectric layers based respectively on carbon nanotubes and polymer were successively stacked. This smart periodic arrangement with increasing charges concentration shows an especially high absorption index despite its overall millimetric thickness.

Experimental studies of light reflection from the boundary with a chiral medium

A. A. Khyshov, V. V. Ivanov, S. S. Ustavschikov, and M. A. Novikov
Institute for Physics of Microstructures RAS, Russia
khysh@ipm.sci-nnov.ru

The experiments on the investigation of polarization plane rotation and circular dichroism at reflection of light from the boundary of chiral crystal and chiral liquid are carried out by means of different methods of measurement. Experimental studies with good accuracy showed that at normal incidence on the boundary of the chiral medium the optical chirality does not occur. The experimental results show that the symmetrical recording of constitutive equations while maintaining the traditional boundary conditions is the most appropriate description of chiral optical effects.

The problem of correct selection of constitutive equations and corresponding boundary conditions in the chiral optics is remains unsolved so far. There are several forms of constitutive equations, but in practice only two of them are uses most often. In one form to describe the optical chirality only the equation relating the electric induction and electric field, including its spatial derivatives is used [1]. In another approach the electric and magnetic contribution in these equations are separated [2]. As shown in a number of publications, e.g. [3], in describing the homogeneous chiral optical effects, both approaches lead to the same result. However, this is not true for the chiral optical effects in optically inhomogeneous media, in particular, on the boundary. For both forms of the constitutive equations the choice of boundary conditions is nontrivial and requires serious justification [4]. Another aspect of the problem lies in the fact that there is still not enough experimental data on basis of which one could give preference to a certain point of view, and the results of existing experiments contradict each other. Thus, one of the authors studied the polarization effect at normal light reflection from the boundary of the lithium iodate crystal, whose optical axis was normal to its boundary [5]. This case is equivalent to the case of chiral liquid. The experiment showed that in this configuration in the absence of absorption, the optical chirality is absent within experimental error; i.e. light at the reflection does not change its polarization. This result is corresponding to the conclusion emanating from the symmetrical forms of the constitutive equations and the traditional recording of boundary conditions. At the same time, in [6] it was observed the polarization plane rotation (10^{-4}-10^{-5} rad) in a similar configuration at light reflection from a uniaxial crystal of cinnabar under conditions of strong absorption. Nontriviality of proposed by the authors of this paper the interpretation of their results is that it contradicts the theorem of reciprocity in its traditional interpretation, as in this case in a medium which is symmetric in time, there is a non-reciprocal optical effect.

We have created a sensitive polarimeter (similar to that used in [6]), with which experiments to measure of the polarization plane rotation of reflected light from a chiral $CdAs_2$ crystal at normal incidence on the z-cut were carried out. The same measurements were made using the original method of a polarization ring interferometer of zero area, which is sensitive only to the difference between the nondiagonal reflection matrix elements, i.e. only to nonreciprocal polarization plane rotation at the reflection from the sample. Up to a measurement error

(10^{-6} rad) in both cases the polarization plane rotation was not observed. Our experiments disprove the results obtained in [6]. It is showed that in methodology of the experiment that used in [6] a parasitic anisotropy of optical elements or sample (e.g. mechanical stress or a slight deviation from the normal to the optical axis of the sample) will result to the same effect.

The measurement of circular dichroism at the reflection from the $CdAs_2$ crystal was carried out using an original photothermal method with a modulation of light polarization ellipticity at the frequency range from Hz to kHz. By varying the modulation frequency of the pumping, you can change the penetration depth of the heat wave in the sample, and thus separate the signals from the volume and surface absorption. The results of measurements showed no circular dichroism in reflection from the sample at normal incidence with an accuracy of 10^{-5} rad.

With the help of the original modulating circular dichrometer on depolarized light, we measured the circular dichroism at normal reflection from the chiral liquid - air boundary. As the liquid used mirror isomers of limonene. The use of depolarized light to illuminate the samples reduced the parasitic effects connected with birefringence in the modulator. The measurements were performed at a wavelength of 500 nm in the effective bandwidth of 50 nm. Angle of incidence on the samples was about 30 angular minute. The measured difference of the circular dichroism of R-and S-limonene was $6\times10^{-7}\pm2.4\times10^{-6}$, which corresponds to the nondiagonal terms of the reflection matrix limonene $1.5\times10^{-8}\pm6\times10^{-8}$. At the operating wavelength the gyration constant of limonene is 1.2×10^{-6}, so that our result is strong evidence in favor of the absence of the circular dichroism at normal reflection from isotropic chiral medium.

Our experimental data confirm that observed in [6] the polarization plane rotation at reflection is not associated with the manifestation of chirality. Thus, carried out various experiments confirm the implementation of the Onsager relations at reflection from chiral media and show that the symmetrical recording of constitutive equations while maintaining the traditional boundary conditions is the most appropriate description of chiral optical effects.

This work was supported by Russian Foundation for Basic Research, grant No 07-02-01449.

REFERENCES

1. Landau, L. D. and E. M. Lifshits, *Electrodynamics of continuous media*, Pergamon, New York, 1960.
2. Condon, E. U., “Theories of optical rotatory power”, *Rev. Mod Phys*, Vol. 9, 432–457, 1937.
3. Hornreich R. M. and S. Shtrikman, “Theory of gyrotropic birefringence”, *Phys. Rev.*, Vol. 171. No 3, 1065–1074, 1968.
4. Vinogradov A. P. “On the form of constitutive equations in electrodynamics”, *Phys. Usp.*, Vol. 45, 331–338, 2002.
5. Luk'yanov, A. Yu. and M. A. Novikov, “Reflection of light from the boundary of chiral gyrotropic medium”, *JETP Lett.*, Vol.51, No 11, 673-675, 1990.
6. Bungay A. R., Yu. P. Svirko and N. I. Zheludev, “Experimental observation of specular optical activity”, *Phys.Rev.Lett*. Vol. 70, No. 20, 3039-3042, 1993.

Optical and magneto-optical resonances in nanostructured ferromagnetic films

M. V .Sapozhnikov[1*], S. A. Gusev[1], B. B. Troitskii[2], L. V. Khokhlova[2]

[1]Institute for Physics of Microstructures RAS, Nizhny Novgorod, Russia

[2]G. A. Razuvaev Institute of Organometallic Chemistry Russian Academy of Sciences, Nizhny Novgorod, Russia

[*]corresponding author: msap@ipm.sci-nnov.ru

Abstract -We report here on experimental investigations of optical and magnetooptical (MO) spectra of nanostructured Co and Ni films deposited on the top of PMMA colloidal crystal. The resonance peculiarities were observed both the spectra in visible and near IR range, their positions are scaled with the PMMA sphere diameter and depend on incident angle. To explain the above results both the surface plasmon resonances (SPR) and interference between the reflections from the colloidal crystal and from the nanostructured film should be considered.

The samples were prepared by magnetron deposition of the metal on the top of PMMA colloidal crystal. The morphology of the films was studied by electron and atomic force microscopy. The particles were packed into a dense hexagonal lattice, the period of the structures determined by a size of PMMA particles and lies within 125 - 500 nm. As the thickness of the deposited films (10 - 60nm) was sufficiently less than the diameter of the particles, the film became corrugated in two dimensions.

The following distinguished features have been found in the MO spectra of the nanocorrugated Co and Ni films: spectra have lost a monotonic character which is typical for the flat films and has two valleys which we will

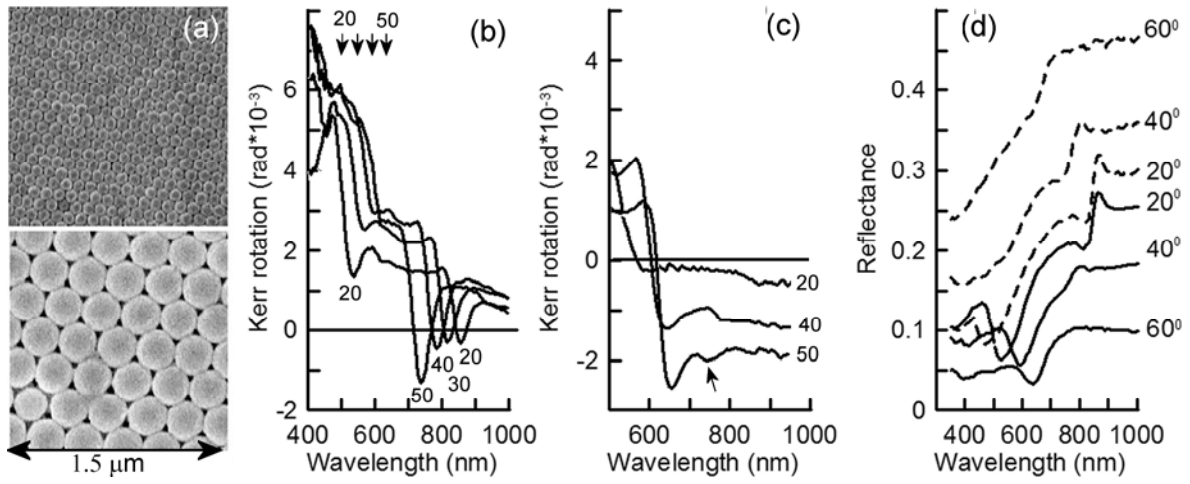

Fig.. (a) SEM images of the nanocorrugated Ni films with the periods 125 nm and 370 nm. (b) Measured MO spectra of 30 nm thick nanocorrugated Co film for p-polarization of the light for different incident angles. Arrows denote the calculated positions of the corresponding SPR. (c) MO spectra of the 60nm thick Ni films for p-polarization of the light. Arrow indicates the remnants of the lw-resonance (d) The optical reflectance spectra of the 30 nm Ni film for s- (dashed lines) and p-polarization (solid lines). with the period 410 nm

refer as long-wave (lw) and short-wave (sw) minima. To understand the observed intriguing difference of MO properties between flat and nanostructured films we have investigated the spectra of the structures with different periods, film thicknesses, for various light polarisations and incident angles. The main results are summarised here: (*i*) the shape of the spectra for s- and p- polarisation of the incident angle are practically the same, although the valleys are more pronounced for p-polarisation; (*ii*) the lw-minimum blueshifts as the incident angle increases in the same manner for s- and p-polarizations. On the contrary the sw-minimum redshifts, in the same conditions; (*iii*) the MO spectra of nanocorrugated films are scaled with a colloidal particle diameter which determined the period of the structure. Both the position of lw- and sw- minima show monotonous red-shift as the structue period increases; (*iv*) with the increase of the film thicknes upto 60 nm the lw-minima become less prononced, while the sw-minima remains unchanged; (*v*) Quite often one or both minima become so deep, that the direction of the polarisation rotation even changes it sign; (*vi*) the lw-minimum become less prononsed in the case of thick films. Qualitatively, the MO spectrum of the Ni nanocorrugated films has the same dependence on experimental parameters as in the case of the Co films. The main differences is related to the fact that the coefficient of the MO rotation is less for Ni and changes its sign at approximately 800 nm even in the case of flat film.

The mirror reflection spectra of the nanocorrugated Ni films for different light polarizations and incident angles show their complete identity with the reflection spectra of the nanocorrugated Co films measured earlier[2]. The reason for such similarities, obviously, is the fact that the dielectric constants of these materials are very similar in magnitude in the optical range. The both reflection spectra of the nanocorrugated Co and Ni films have two peculiarities, which positions are strongly correlated with the positions of the MO spectra valleys.

The dispersion of the resonance with the incident angle and scaling of the spectra with the period of the structure are fingerprints of surface plasmon (SP) excitations. For estimations we used a simplest model with the dispersion relation for SP on the flat metal-dielectric interface. Actually we found a good agreement between measured sw-resonance positions and calculated positions for SP resonance for metal-air interface even in this simplest model. The observed decrease and even the change of the sign of MO rotation near the resonance is due to the fact that probably the MO rotation in the reflectance channel connected with the SPP excitation has the sign opposite to MO rotation at the nonresonant reflection. If the contribution of SPR channel to the reflection is significant enough, then there is a change in the MO rotation sign. The similar effects were observed in the hexagonal lattice of Co antidots[2]. As for lw-resonance in the reflection of the nanocorrugated films, its position coincides with the position of the Bragg peak in the reflection of the initial colloidal crystal and has the same angular dependence. The initially symmetric Bragg resonance lineshape in the reflection of the colloidal crystal become more and more asymmetric as the deposited film thickness increases. In this case asymmetric Fano-like the lineshape is the result of interference of two reflection processes: the resonant Bragg reflection from the 3D colloidal crystal and the reflection from the nanocorrugated film.

ACKNOWLEDGEMENTS

This research was supported by RFBR, RF Agency for Education (Rosobrazovanie) and RF Agency for Science and Innovation.

REFERENCES

1. G.Ctistis, E.Papaioannou, P.Patoka, J.Gutek, P.Fumagalli, M.Giersig, Nano Lett., **9**, 1, (2009).
2. M.V.Sapozhnikov, S.A.Gusev, V.V.Rogov, O.L.Ermolaeva, B.B.Troitskii, L.V.Khokhlova, D.A.Smirnov, Appl. Phys. Lett. **96**, 122507 (2010).

Design of Multiple Spiral Frequency Selective Double-Negative MetamaterialDesign of Multiple Spiral Frequency Selective Double-Negative Metamaterial

Iarj Arghand Lafmajani

Semnan University Iran

In this paper; a multiple spiral unit cell to the modeling of double negative metamaterial (MTM) structures is presented. At the unit-cell level, the properties of the metamaterial are described by a multiple spiral with different curves and a stimulation cute wire on both side of a dielectric. The proposed metamaterial is designed based on the methods of the chirality. With choosing different curve of spiral, it is possible to change the properties of metamaterial. In addition to, a multilayered form of the metamaterial are found to be suitable for use as ultrathin polarization rotators and circular polarizer for practical applications.

Competing Interactions and Cluster Dynamics in Doped Rare-earth Manganites

Wiqar Hussain Shah

King Faisal University, Hofuf, 31982 SAUDI ARABIA, Saudi Arabia

The magnetic and transport behavior of $La_{1-x}Ca_xMnO_{3+}$ (x=0.48, 0.50, 0.52 and 0.55 and =0.015) compositions close to charge ordering, was studied through resistivity DC magnetization and AC susceptibility measurements. With time and thermal cycling (T<300 K) there is an *irreversible* transformation of the low-temperature phase from a partially ferromagnetic and metallic to one that is less ferromagnetic and highly resistive. For instance, an increase of resistivity can be observed by thermal cycling, where no effect is obtained for lower Ca concentration. The time changes in the magnetization are logarithmic in general and activation energies are consistent with those expected for electron transfer between Mn ions. The data suggest that oxygen non-stoichiometry results in mechanical strains in this two-phase system, leading to the development of *irreversible* metastable states, which relax towards the more stable charge-ordered and antiferromagnetic microdomains. This behavior is interpreted in terms of strains induced charge localization at the interface between FM/AFM domains in the antiferromagnetic matrix. Charge, orbital ordering and phase separation play a prominent role in the appearance of such properties, since they can be modified in a spectacular manner by external factor, making the different physical properties metastable. Here we describe two factors that deeply modify those properties, viz. the doping concentration and the thermal cycling. The metastable state is recovered by the high temperature annealing. We also measure the magnetic relaxation in the metastable state and also the revival of the metastable state (in a relaxed sample) due to high temperature (800) thermal treatment.

THE ROLE OF THE SURFACE ENERGY IN THE FORMATION OF UNIQUE PROPERTIES OF THIN-FILM MATERIALS

Erkin N. Shermatov, Bahrom N. Shermatov

Physics Department, Samarkand State University, 15, University blvd., Samarkand, 104103, Uzbekistan (E-mail: erk-shermatov@yandex.ru)

Taking into account the field-substance interaction we discussed the mechanism of formation of the surfaces energy in condensed matter, and its role in the formation of various properties of substances. For small quantities of the substance the role of the surface energy significantly increases, which leads to the unique properties of thin-film materials. Taking into account these circumstances, we propose a systematic approach to explaining the mechanism of simultaneous coexistence of electric and magnetic properties of multiferroics. "Frozen structural instability" in multiferroics leads to the formation of a double-well potential, and, as a result, they acquire the properties of a switch. According to modern ideas, all the particles and bodies are formed as a result of vortex processes and condensation of the physical vacuum.

Formation of the surface energy of the particles is accompanied by the formation of WFR of the surface energy of the particles in the system, and its transition to the condensed state. Experimental studies show that the thickness of the coherent shell on the surface of materials depends on the homogeneity of the substances. Depending on the surface energy of the system as a whole and its internal energy structure the different properties of materials are formed. The material properties remain practically independent on their size, when their number exceeds the spatial dimensions of the WEF of components of their systems or particles.

Formation of the surface energy of the particles and WFR, respectively, in a system of particles appears as a maximum in the wavelength region in the energy structure of the WFR of the material. In the study of electronic spectra in homogeneous crystals in liquid helium, there is extremely narrow or giant resonance line with a width of 10^{-3} $cm^{-1} \div 10^{-7}$ cm^{-1}.

These data indicate that the thickness of the coherent layer or the surface energy of materials may differ significantly from each other; to destroy it it's necessary to make the magnetic fields of various magnitudes. Based on these data, we can assume that the destruction of the coherence shell or surface energy of materials with tremendously high energies requires applying a giant magnetic field, and this is manifested in the form of a giant magnetic resistance.

It is known that multiferroics are produced by stretching or compressing the lattice. It uses materials that originally do not have any magnetic or ferroelectric properties. Stretching is caused by growing a thin film of the same material on the surface of another substance having the same crystal lattice with a little more distance between the atoms. Increasing the surface of the structure of the film of another material will tend to adjust the distance between the atoms of its crystal structure in the "substrate" distance, which creates a mechanical stress and strain of the crystal structure of the grown material. At the same time stretching the lattice is about 1%. Deformation of the equilibrium state of the crystal structure leads to the induction of magnetic spins, which have three degrees of freedom. As a result, the materials forming the conditions under which it is possible the simultaneous coexistence of ferromagnetic and ferroelectric properties are comparable with the properties of materials that exhibit these properties individually. It seems to us that formation in various ways of distorted crystal structure can be considered as "frozen structural instability" in the crystal structure of the material. The situation can be represented as the formation of the double-well potential in the energy structure of the material, which, depending on the nature of external influence, can switch from one type of ordering to another. The influence of the external field changes the energy surface of the material and symmetry of breaking interactions, and, respectively, the nature of the ordering system as a whole. This process is accompanied by the magnetoelectric properties of materials.

Generation of non-diverging beams by negative refraction.

M. Kaliteevski
[1]*Ioffe Institute,26 Polytechnicheskaay, 194021, St-Petersburg, Russia*
Academic University, 3/8 Khlopina, St-Petersburg, Russia

Diffraction causes a beam of radiation with wavelength λ and width w to diverge by an angle δ which satisfies the relation $\sin\delta = \lambda / \pi w$. In an attempt to eliminate, or at least to reduce the divergence of beams, Bessel [1] and Airy beams [2], have been employed. Both Bessel and Airy beams are eigenfunction of wave equations with specific wavevector $\vec{k}$, and to achieve true non-divergence these beams should have infinite size in the direction perpendicular to direction of propagation $\vec{k}$. Recently alternative approach of generation of the beam of reduced divergence based on formation surface mode on structured surface near small opening has been proposed [3]. Here we demonstrate how the beam which do not experience divergence over large distance can be generated using slab of negatively refracted material [4]. Negative refraction can occur near an optical resonance in conventional material with positive magnetic permeability, in quasi-homogeneous metamaterials and in photonic crystals .There are branches in dispersion relation of photonic crystals for wich group velocity is negative, as shown in figure 1a. If wave of the corresponding frequency is incident of the boundary of photonic crystal it can be refracted natively. Near the top of band of negative refraction, equifrequency surfaces have a shape of ring with radius (Bloch wavevector) which is much smaller than light wavector in the vacuum. In other words effective refractive index n in this case is scalar, "negative" and $|n|<1$, which make possible total internal reflaction of light incident from vacuum, and the angle of total internal reflection α_{tot}, given by $\sin\alpha_{tot} = |n|$.

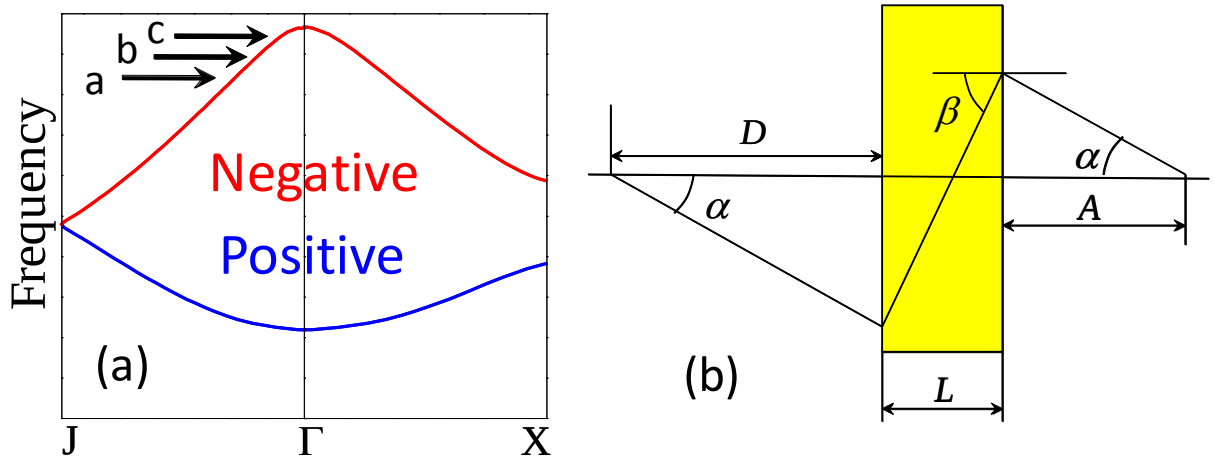

Fig 1. (a) Dispersion relation for metallic photonic crystal. Arrows indicate frequencies, for which field profiles in figure 2 are shown. (b) Ray propagation in flat lens of negative index material.

Consider a propagation of the rays originated from a point source incident on the slab of "negative" index material (see fig. 1b). If the magnitude of refractive index of slab and surrounding material are equal, than any ray, originated from source cross optical axis on other side of the slab at the same point, and the system will work as well known flat lens. But if $|n|$ is different from those of surrounding material, that axis will cross optical axis in different points.

For small angles of incidence, rays cross the optic axis near $D_0 = L/|n| - A$, but when the incident angle corresponds to α_{tot}, $D_0 \to \infty$. Hence, the image of the point source will not be a single point, but will be stretched from the point D_0 to infinity. Since D_0 can be made arbitrarily large by reducing $|n|$, the result suggests that it should be possible to use a slab with a negative effective refractive index of small magnitude to produce an essentially non-divergent beam of radiation from a point source. Figures 2(a-c) show the field patterns formed by a flat slab of photonic crystal irradiated with line sources of frequencies marked as "a","b" ,and "c" in figure 1a. It can be seen that the closer frequency to the top of band (i.e. the smaller $|n|$), the larger the distance, at which beam does dempnstrate divergence.

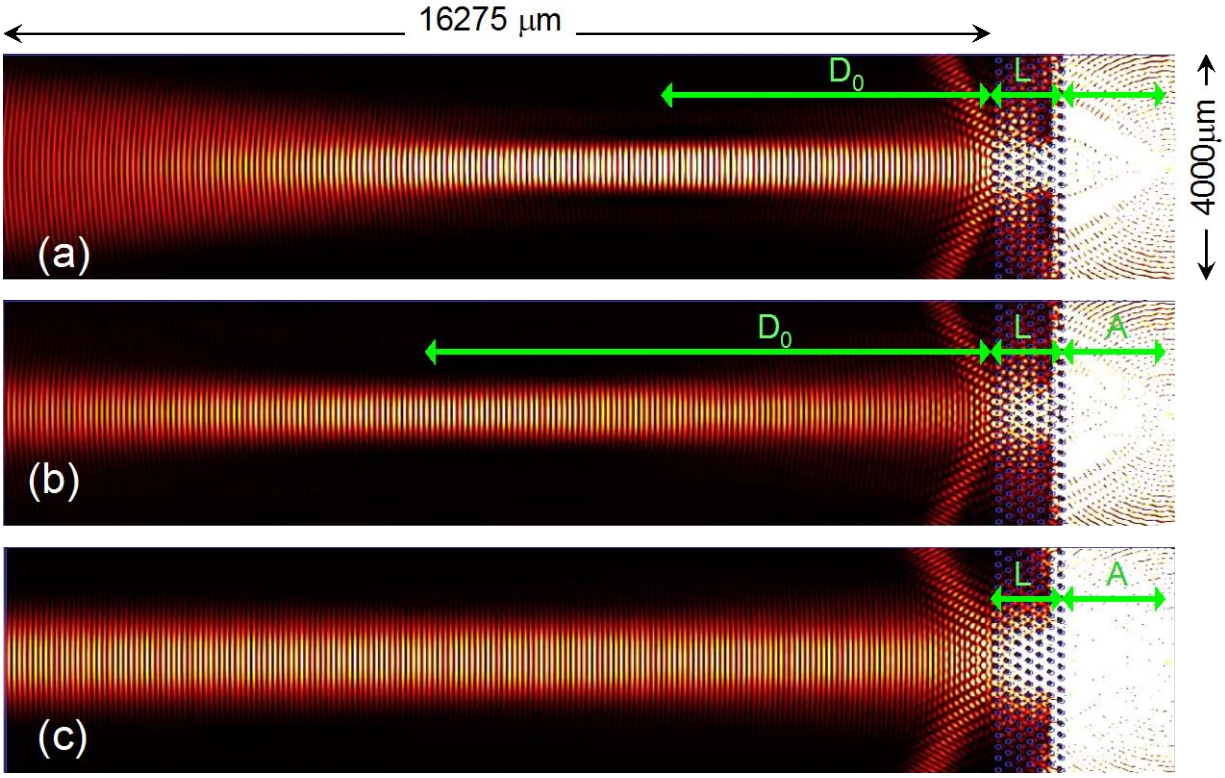

Figure 3. The patterns formed when a line source irradiates the photonic crystal slab at frequencies of (a), (b), and (c) in figure 1a. [See [4] for details.]

During the presentation various methods of generation of non-diverging beams and their physical bases will be analysed and compared with the method described above.

References

[1] J Durnin, J J Mieceli, and J H Eberly, *Phys. Rev. Lett.* **58**(15)1499 (1987)

[2] G A Siviloglou, J Broky, A Dogariu, and D N Christodoulides, *Phys.Rev.Lett.*, **99** 213901 (2007)

[3] P. Kramper et al, *Phys.Rev. Lett.* **92**, 113903 (2005)

[4] M. Kaliteevski, et al, *Optics express* **16** (19) 14582 (2008)

Theory and Efficient Integration of Random Nanoparticle Layers in Photovoltaic Devices

C. David[1*], J. P. Conolly[2], A. Griol[2], C. Ramos[2], J. Hurtado[2], F. J. García de Abajo[1], G. Sánchez[2]

[1]Nanophotonics Group, Instituto de Óptica, CSIC, Serrano 121, 28006 Madrid, Spain

[2]Nanophotonics Technology Center, Universidad Politécnica de Valencia, 46022 Valencia, Spain

[*]corresponding author: christen.david@csic.es

Abstract Aiming at a theoretical description of the optical properties of random metal nanoparticle distributions as obtained with the nanosphere self-aggregation method (NSA), we develop a simple procedure based on rigorous solutions of Maxwell's equations to yield optical spectra of fully interacting random particles. The results of the numerical method are directly compared to optical characterization of exact copies made from the modeling input distributions by exploiting electron beam lithography (EBL). Using only the particle size and spacing distributions of a sample, the model can be applied to arbitrary random particle distributions.

In the European FP7-248909-LIMA [1] project an industrially feasible solar cell design is developed exploiting state-of-the-art techniques to go beyond the state-of the art to improve light management. Based on integrated back contact (IBC) cells, enhancement of the quantum efficiency is achieved by using silicon nanocrystals as a photoluminescence (PL) down shifter [2]. Furthermore, a plasmonic particle layer (PPL) is designed to overall increase light-matter-interaction. Increased scattering and a high plasmon mode density increase the effective absorptivity by efficiently coupling the light to the underlying structure [3].

One challenge is the production of nanoparticle layers with a cost-effective fabrication process. This work indicates a cheap and CMOS-compatible process allowing integration of metallic nanoparticle (MNP) layers in photovoltaic solar cell manufacturing, exploiting the nanosphere self-aggregation (NSA) method. Here, thin silver films self-aggregate into a sheet of randomly distributed nanoparticles upon annealing. Different processing parameters such as anneal temperature and time as well as Ag precursor thickness enable us to predict final geometrical parameters and influence particle homogeneity and density to some extent.

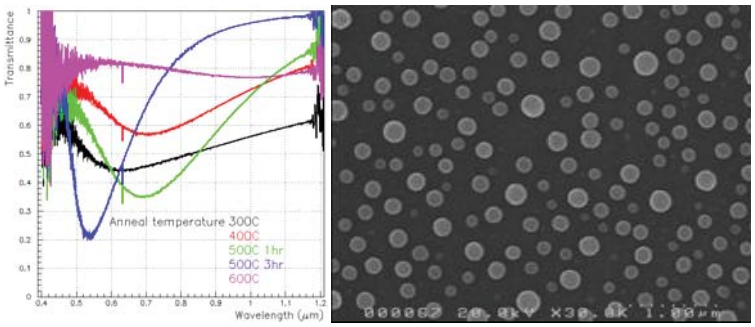

Figure 1: (*Left*) Optical characterization results for NSA samples using various anneal temperatures and times and (*Right*) SEM image of a sample fabricated at 500ºC, annealed for 3 hours with an initial Ag film thickness of 20 nm.

Desirable particle diameters to obtain highest scattering efficiencies in accordance to theoretical modeling are well within the wide range of parameters achievable with the NSA technique. The resulting NSA samples are investigated by appropriate scanning electron microscopy, and by spectrally resolved transmission and reflection measurements. Measurements on PL intensity enhancement of combined Silicon nanocrystals and PPL layer are performed and demonstrate the improved light trapping by applying the PPL.

A further challenge is the theoretical modeling of random PPLs. We introduce a random electron beam lithography technique. EBL is a standard nanofabrication technique allowing for high control and systematic study of previously defined geometries. Therefore, it can give valuable feedback to theoretical modeling, also on random samples provided numerically and in accordance to geometrical parameters found for random NSA samples. Parallel optical characterization and further calculation of optical properties with the numerical sample gives best insights into physical behaviour of the random PPL and quality of the theoretical modeling. The theoretical results are based on exact electrodynamic modeling using a multiple scattering approach [4].

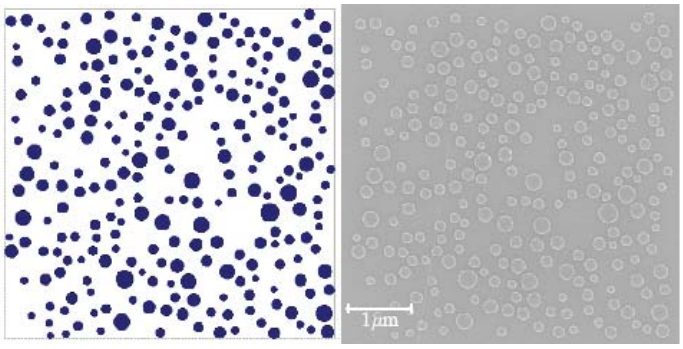

Figure2: Comparing numerical sample and resulting real sample fabricated with electron beam lithography (EBL) covering an area of 5 × 5μm^2. The achieved agreement is very good and enables direct comparison of optical characterization and simulation.

Acknowledgement. This work is supported by the European Commission FP7-ICT-2009-4-248909-LIMA.

REFERENCES

1. Detailed project information provided on www.limaproject.eu.
2. Yuan Z., Pucker G., Marconi G., Sgrignuoli F., Anopchenko A., Jestin Y., Ferrario L., Bellutti P., Pavesi L., "Silicon nanocrystals as a photoluminescence down shifter for solar cells", *Solar Energy Materials and Solar Cells,* 95, 1224, 201.
3. Catchpole , K. R., Polman A., "Plasmonic solar cells", *Opt. Express,* 16, 21793, 2008.
4. García de Abajo, F. J.,"Multiple scattering of radiation in clusters of dielectrics", *Phys. Rev. B,* 60, 6086, 1999.

Stochastization of light polarization in random system

A.M. Merzlikin[1], A.I. Ignatov[1], A.P. Vinogradov[1] and G. Samelsohn[2]

[1] Institute for theoretical and applied electromagnetics RAS, Moscow, Izhorskaya 13/19 Russia,

[2] Holon Institute of Technology, Holon 58102, Israel

Recently the electrodynamics of inhomogeneous media has been experienced rapid development. The rapid development is partially determined by a possibility of translation (so-called “mapping”) of wave phenomena from quantum theory of solids into electrodynamics. This mapping results in appearance of theories of photonic crystal, diffusion of light, backscattering and the Anderson localization of light.

However in spite of the similarity of wave phenomena in different areas of physics, there is a difference between electrodynamics and quantum theory of solids: the electron wave function is scalar (neglecting effects associated with spin) whereas the electric and magnetic fields are the vector quantities.

Most clearly vectors nature of electromagnetic field reveals itself in anisotropic or gyrotropic properties. We have considered the polarized light travelling in random system of uniaxial layers. It is assumed that the layers are identical whereas the directions of the axis are random.

It is shown that the light “forgets” the initial polarization during propagation through the system. It means that the distribution function of polarization tends to one that is independent of incident polarization. Such a “forgetting” is characterized by new geometrical scale different from localization length.

Diamagnetism phenomenon in theory of wave multiple scattering on random discrete dielectric media

Yu.N.Barabanenkov[1], M.Yu.Barabanenkov[2*], and S.A.Nikitov[1]

[1] V.A. Kotelnikov Institute of Radioengineering and Electronics, Russian Academy of Sciences,
Mohovaya 11, 103907 Moscow, GSP-3, Russia

[2] Institute of Microelectronics Technology, Russian Academy of Sciences,
142432 Chernogolovka, Moscow Region, Russia

[*]corresponding author: barab624@mail.ru

Abstract - We show that technique of Dyson equation in wave multiple scattering on spatially disordered media statistical theory leads directly to an effective dielectric permittivity tensor, which is characterized by spatial dispersion and obeys the generalized Lorentz-Lorenz formula. Introduced via this spatial dispersion by Lindhard rule effective magnetic permeability demonstrates the diamagnetic property, including the ideal diamagnetism, in simple limit of independent non-magnetic small spherical particles. Applying the earlier Dyson equation technique elaborations enables us to study the diamagnetism properties of random discrete dielectric media in the case of dependent particles also, taking into account the effect of space group resonance between particles as well as the effect of particle correlation.

Increasing attention on metamaterials has been paid due to their exciting physical behaviors and potential applications. While most of such artificial material structures have been developed on base of metallic resonant structure, Mie resonances of dielectric particles opened a simple and more versatile route for construction of isotropic metamaterials with higher operating frequencies (see, e.g., review [1]). One does need to remark that usually above metallic or dielectric composites are thought as periodic structures, with Maxwell's equations averaging over crystal unit cell and applying some intuitively appropriate Clausius-Mossotti relations for both effective dielectric permittivity and magnetic permeability.

Here we report the recent progress in study the Mie resonance-based dielectric random (not periodic) composites, using general theory of wave multiple scattering in random discrete media [2], with Maxwell's equations averaging over statistical ensemble of particles and providing consistent description of underlying physical mechanism of diamagnetism phenomenon. In summary our basic equations are according to [3] , firstly, the generalized Lorentz-Lorenz formula

$$\frac{\varepsilon_{eff}^{t,l}(k)-\varepsilon_0}{\varepsilon_{eff}^{t,l}(k)+2\varepsilon_0}=-\frac{\tilde{M}^{t,l}(k)}{3k_0^2} \qquad (1)$$

for transversal $\varepsilon_{eff}^{t}(k)$ and longitudinal $\varepsilon_{eff}^{l}(k)$ components of effective dielectric permittivity tensor with respect to a wave vector $\vec{k}$ and, secondly, the Lindhard rule [4] for

effective magnetic permeability, $1-1/\mu_{eff}=(\omega^2/c^2)[\varepsilon^t_{eff}(k)-\varepsilon^l_{eff}(k)]/k^2$, in the limit $k\to 0$. The Dyson equation transformed mass operator $\tilde{M}$ in the right hand side (rhs) of (1) is given in the second order of the particle number density $f_1 = f_1(\vec{r}_1)$ by symbolic expression

$$\tilde{M} \approx \int d1\, f_1 T_1 + \frac{1}{2}\iint d1d2\, f_2(1,2)(T_{12} - T_1 - T_2 - T_1\tilde{G}T_2 - T_2\tilde{G}T_1) + \iint d1d2\, g_2(1,2)T_1\tilde{G}T_2 \quad (2)$$

where $f_2(1,2)$ and $g_2(1,2)$ are two particle distribution and correlation functions, respectively, as well as T_1 and T_{12} are scattering operator of a single particle and of a pair of particles; symbol $\tilde{G}$ denotes the principal part of the electric wave field tensor Green function in the host medium. The first term in the rhs of (2) describes the independent particles and leads in the case of small spherical silicon and gold particles to diamagnetism phenomenon in visible and terahertz frequency ranges, respectively, when only the magnetic dipole scattering gives contribution into effective magnetic permeability. The second term in the rhs of (2) is used to take into account the effect of space group resonance between dependent particles [5], because of which the electric dipole scattering can also give contribution into effective magnetic permeability. At last the third term in the rhs of (2) can cause decrease in imaginary part of effective magnetic permeability at special correlation functions between particles according to old discussion [6] on extinction decreasing by wave multiple scattering in dense discrete media.

Acknowledgements. The work was supported in part by Russian Foundation for Basic Research, Grants 09-02-00920-a and 09-02-12433-OFIM, by the Russian Academy of Sciences project " Passive multichannel human radio- and acousto-thermotomography in near zone" .

REFERENCES

[1] Zhao, Q., J. Zhou, F. Zhang and D. Lippens, "Mie resonance-based dielectric metamaterials", Materials today , Vol. 12, No. 12, 60-69, 2009.

[2] Barabanenkov, Yu. N., "Asymptotic limit of the radiative transfer theory in problems of multiple wave scattering in randomly inhomogeneous media", Physics-Uspekhi", Vol. 52, No.5, 502-506, 2009.

[3] Barabanenkov, Yu. N., M. Yu. Barabanenkov and S. A. Nikitov, "Artificial magnetism in theory of wave multiple scattering by random discrete non-magnetic conducting media", arXiv:1009.4770v1 [cond-mat.dis-nn] 24 Sep 2010.

[4] Lindhard, J, "On the properties of a gas of charged particles", Dan. Mat. Fys. Medd., Vol. 28. No. 8, 3-57, 1954.

[5] Barabanenkov, Yu. N. and V. V. Shlyapin, "Space group resonance in electromagnetic wave multiple scattering", Phys. Lett. A, Vol. 170, No.3, 239-244, 1992.

[6] Barabanenkov, Yu.N., "Energetic criterion of coherence and incoherence of multiple scattering of waves in randomly inhomogeneous medium", Izv. Vyssh. Uchebn. Zaved. Radiofiz., Vol. 28, No. 9, 1136-1143, 1985.

STUDY OF MAGNETIC PROPERTIES OF COMPLEX SYSTEM ($La_{0.8}Ag_xMnO_3$) AT HIGH TEMPERATURES.

O.K.Kuvandikov, H.O.Shakarov, Z.M.Shodiev, B.U.Amonov

Samarkand State University, Dpt. of Physics, Samarkand, Uzbekistan

E-mail: quvandikov @rambler.ru

This work is devoted to experimental study of temperature dependence of the magnetic susceptibility [$\chi(T)$] of Ag-doped $La_{0.8}Ag_xMnO_3$ (x=0.03; 0.1; 0.15; 0.2) manganites in a wide temperature interval (20-850^{0}C), as well as to determination of their magnetic parameters on the base of obtained experimental results.

The samples were synthesized in the problem laboratory of new materials at the Moscow State University.

Dependencies $\chi^{-1}(T)$ of the studied samples were measured by the Faraday's method with the help of the balance magnetic scales in Al_2O_3 crucible in a surplus purified helium atmosphere. Maximal relative error of measurement of the magnetic susceptibility did not exceed 3%.

Analysis of the obtained experimental results shows that the magnetic susceptibility of manganites decreases monotonically with rising temperature, and it increases with rising stechiometric ratio of Ag atoms.

Analysis $\chi^{-1}(T)$ dependencies of the samples show that the dependencies are of linear character with two breaks. This testifies that each linear part of the $\chi^{-1}(T)$ dependens follows the Curie-Weiss law $\chi = C/(T-\theta_P)$. We should not here that the slope of $\chi^{-1}(T)$ dependence (tgα=dχ^{-1}/dT) increases after each break, i.e. the magnetic susceptibility of the sample decreases.

The reason of anomalous behavior of $\chi^{-1}(T)$ dependence (i.e. the reason of breaks) can be explained by polymorphic transformations in crystalline structure of the lattice of studied manganites that depend of their composition and temperature.

On the base of the experimental $\chi^{-1}(T)$ dependencies the allotropic phase diagram of the studied manganites was constructed.

Analysis of the obtained magnitudes of magnetic parameters shows that the magnetoactive atom (Mn) in the studied manganites is in state, which is close to the state of Mn^{3+} ion.

EPR spectroscopy of nanostructured units in iron-containing alkali-borate glasses obtained by the thermoradiation founding.

M.M. Mirkamalov, A.N. Salakhitdinov, M.K. Salakhitdinova*, A.A. Yusupov
Samarkand State University, Uzbekistan,
e-mail: smaysara@yandex.ru

Thermoradiation founding [1] of the oxygen-containing glasses in an intense radiation field of ^{60}Co with the dose rate of ≥ 10 Gr/s represents a qualitatively new way of effect on materials, because this greatly improves their complex physical and chemical properties, and there is a modification of the nanostructure of the solid.

Previously [1-2] we have shown the experimental evidence of the fact that the in optical borate glasses with additives of oxides of Fe_2O_3, CuO and in laser phosphate glasses with protective additives of CeO2 the degree of aggregation of activator ions (Fe^{3+}, Fe^{2+}, Cu^{2+}, Cu^{+}, Ce^{3+}, Ce^{4+}, Nd^{3+}) during a normal heat treatment, synthesis and thermoradiation founding and processing changes in the opposite way: in the first case, the dimensions of areas of the chemical differentiation grow, and, consequently, there is an increase in the degree of aggregation of microparticles, clusters of nanostructures. In the second case, according to the optical and EPR spectroscopy, as well as to direct magneto-chemical measurements it was shown the opposite effect, i.e. a decrease in the size of these structures.

In this paper we continue the experimental and theoretical studies of the radiation-induced paramagnetic centers in alkali-borate glass of the optimal composition ($22K_2O$, $78B_2O_3$) without (pure) and with additions of Fe_2O_3 (0,1, 0,25; 0.5 mass.% over 100%). The main objective of the work is to clarify the conditions of preservation of useful thermoradiation effects in their synthesis in the γ-field of ^{60}Co ((≥ 10 Gr/s), to study the effect of duration (dose), dose rate and the temperature of re-founding in γ-field, as well as to study the mechanisms of the thermoradiation impact.

Original glasses were obtained from the charge at (1273 ± 10) K in the laboratory conditions in corundum crucibles. Remelting from the alkali-borate glass is carried out at (1273 ± 1) K in quartz crucibles.

For pure alkali-borate glass the analysis of data obtained at various kinds of heat treatment in and out of the γ- field (thermal annealing, tempering) after the synthesis in and out of the γ-field was carried by the Griscom-Bishay model with respect to radiation-induced “Bore oxygen-hole center” (“BOHC”).

For the alkali-borate glass with additions of Fe_2O_3 there appears a complex radiation-induced center, which characterizes the interaction of Fe^{3+} ions with BOHC as the ion protector, and also as a modifier ion, with the inherent oxygen environment.

On the basis of the obtained data, theoretical analysis and comparison of study we have found that:

a) the thermoradiation conditions are equivalent to the strong oxidizing conditions with a high efficiency of radiation-chemical reactions involving atmospheric oxygen;

b) the thermoradiation effect leads to the emergence of new peroxide nanostructures [=B-O-$O^{\bullet}$], [≡B-O-$O^{\bullet}$], [=Fe^{3+}-O-$O^{\bullet}$], [≡Fe^{3+}-O-$O^{\bullet}$];

c) the thermoradiation effect of small doses was observed;

d) the interpretation of the observed effects is proposed.

The developing dynamic-evolutionary concept has led to a fundamental conclusion that by the thermoradiation effects on oxide glasses one can obtain more balanced, more compacted and more disordered system of the short-range order than that of usual founding.

1. Salakhitdinov A.N., Boboev A.H., Umarova D.R. Physics and chemistry of radiation treatment of the glass. Tashkent, Fan, 1992, 132.
2. Salakhhitdinov A.N. Book of abstracts of 14-th Simposium on Thermophysical Properties. June 25-30, 200, Boulter, Colorado, USA, p.127.

An application of second-generation magnetic abrasive polishing

C. G. Park[1*] and J. S. Kwak[2*]

[1]Graduate School of Manufacturing and Automation, Pukyong National University, Republic of Korea

[2]Department of Mechanical Engineering, Pukyong National University, Republic of Korea

[*]corresponding author: jskwak5@pknu.ac.kr

Abstract - In this study, simulations and experimental verification were carried out to increase the magnetic force by determination of optimal arrangement of electro-magnet array. Moreover, experimental evaluation and optimization of process parameters for MAP of AZ31B plate that is one of the non-magnetic materials were performed by a design of experiments and the response surface method.

INTRODUCTION

A conventional magnetic abrasive polishing (MAP) is not suitable for non-magnetic materials, because the polishing process is fundamentally possible by help of a magnetic force but the magnetic force is very low in these materials [1, 2]. A system with an electro-magnet array table installed under the workpiece, which is called second generation magnetic abrasive polishing, can help to enhance the magnetic force. This study verified the effect of the electro-magnet array table for MAP of AZ31B.

EXPERIMENTS AND RESULTS

The electro-magnet array table was installed on the bed of MAP apparatus on a level with the magnetic tool. The electro-magnet array table used in this study includes thirty-two electro-magnets. Each electro-magnet was arranged at regular interval and could change the magnetic flux density by changing of a mount of current applied into coil. Moreover, that could reverse the magnet pole by using array table controller.

Figure 1 shows comparison of simulated magnitude with measured magnetic flux density. As results of experimental verification in case of that identical magnet pole was arranged, measured magnitudes were some different from simulated magnitudes. However, distribution of magnetic flux density was very similar to simulation results. On the other hand, in case that different magnet pole lined up alternately, both of distribution and maximum magnitude of measured magnetic flux density coincide well with those of the computer simulation. In these figures, minus sign means S pole of electro magnet.

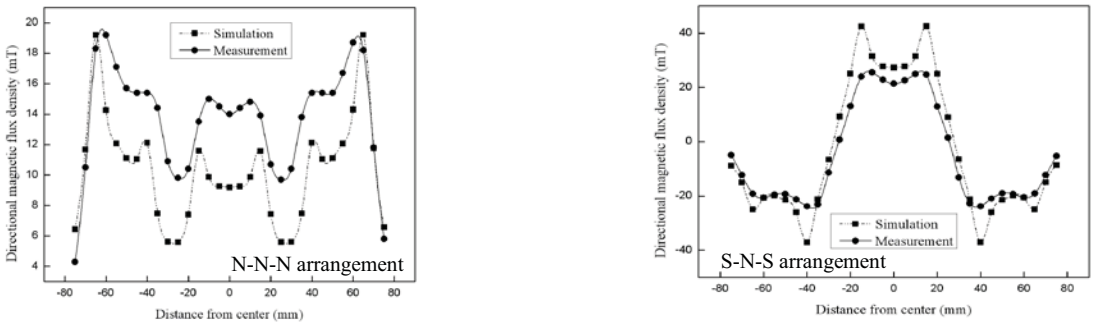

Figure 1 Experimental verification for magnetic flux density

It is desirable to be able to forecast improved surface roughness according to the MAP conditions. Second-older response surface model using the current of table, the current of tool, spindle speed and abrasive weight was developed as blow.

$$\begin{aligned}\Delta Ra = &-0.677525238 + 0.046606A + 0.2633557B + 0.00113841C - 0.05471886D \\ &+ 0.0606419A^2 - 0.056942335B^2 - 0.000000523C^2 + 0.063218003D^2 \\ &- 0.029700025AB + 0.000294894AC - 0.145297703AD \\ &+ 0.0000123BC - 0.023207141BD - 0.0000592CD\end{aligned} \quad (1)$$

Where, the symbol ΔRa (μm) was the value of improved surface roughness and, A, B, C and D are the process parameters. Figure 2 represents an example of the response surface and contour plots of the improved surface roughness according to change of the current of table and the spindle speed. In these plots, the current of tool and weight of abrasive were fixed as 2.0A and 2.5g respectively. The 3D plot seems to rapidly change according to the change of the spindle speed more than current of table. Moreover, from the contour plot it is seen that improved surface roughness was increased linearly when the current of table was increased and the spindle speed was fixed.

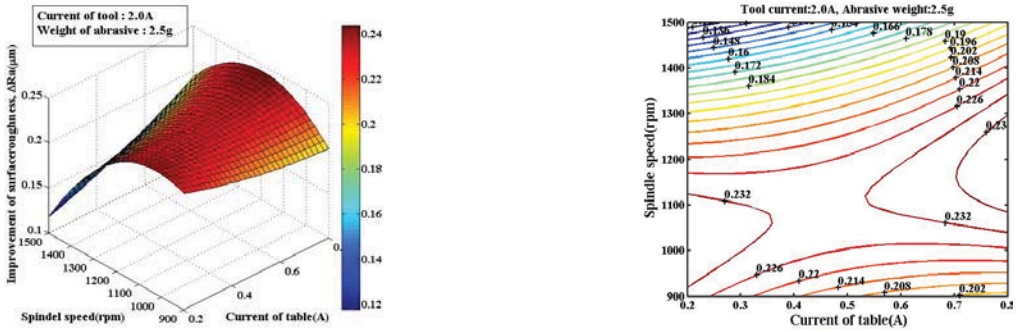

Figure 2 3D plot and contour plot of second-order RSM for predicting improvement of surface roughness

CONCLUSIONS

To increase magnetic force on the surface of magnesium alloy, electro-magnet array table was installed in MAP. As results of simulation and experimental verification in case of that different magnet pole lined up alternately, both of distribution and maximum magnitude of magnetic flux density were larger than in case of arrangement of identical magnet pole. The prediction models were developed by response surface model and signal-to-noise ratio. Based on the results, the response surface model is suitable for predicting surface roughness after second generation MAP of AZ31B more than prediction model using signal-to-noise ratio.

ACKNOWLEDGEMENT

This work is the result of the "Human Resource Development Center for Economic Region Leading Industry" Project, supported by the Ministry of Education, Science & Technology(MEST) and the National Research Foundation of Korea(NRF).

REFERENCES

1. Kim, S. O. and Kwak, J. S., "Magnetic force improvement and parameter optimization for magnetic abrasive polishing of AZ31," *Transactions of Nonferrous Metals Society of China*, Vol. 18, 369-373, 2008.
2. Kwak, J. S., "Enhanced magnetic abrasive polishing of non-ferrous metals utilizing a permanent magnet," *International Journal of Machine Tools and Manufacture*, Vol. 49, 613-618, 2009.

Analysis for behavior of keyhole and plasma in aluminum laser welding using optical measurement of plasma generation

Dongyoon Kim[1] **and Young Whan Park**[2*]

[1]Department of Manufacturing and Automation, Pukyong National University, Busan, Korea

[2]Department of Mechanical Engineering, Pukyong National University, Busan, Korea

[*]corresponding author: parkyw@pknu.ac.kr

Abstract-The laser welding is very useful process to joining metals. For mass production line quality assurance is very important for reliability, so monitoring system to judge weld quality is necessary. In this paper, as the basic research of laser weld phenomenon such as behavior of keyhole, optical measurement system by photodiode was developed and analyzed light-emitted characteristics. The behavior of plasma was also analyzed dependent on welding conditions. The light intensity of plasma was altered by heat input and wire feed rate conditions, and it showed the stability of plasma and keyhole.

Laser welding is widely used in the many industries because it has a lot of advantages such as increasing productivity, precise, and high quality welding and a deep penetration. To maximize the productivity applying laser welding and to automate a welding process, a monitoring system to judge the welding quality is essential. There are typical phenomena during welding process such as an acoustic sound emission, light emission, optical imaging, stress wave and so on. To measure these, microphone, ultra-violet (UV), visible, or infra-red (IR) photodiode, a charge coupled device (CCD) or complementary metal-oxide semiconductor (CMOS) cameras and an acoustic emission transducer. Many researchers tried to figure out the relation between welding conditions and monitoring method or signals. [1-5]

In this study, we suggested the laser weld monitoring system using optical sensor. In order to select the sensor to detect plasma and keyhole, the spectral analysis was carried out as shown in Fig. 1. Fig. 1 showed emission properties of plasma during Nd:YAG laser irradiation to AA5182 aluminum alloy. It has 370 - 710 nm wave length shown in Fig. 1. Further, it has 10 peak spectrums during emission area. We also observed the peak spectrum at the right part of the figure, and this peak spectrum come from Nd:YAG laser.

A photodiode was used as a sensor for measuring light intensity of the keyhole and plasma during welding.

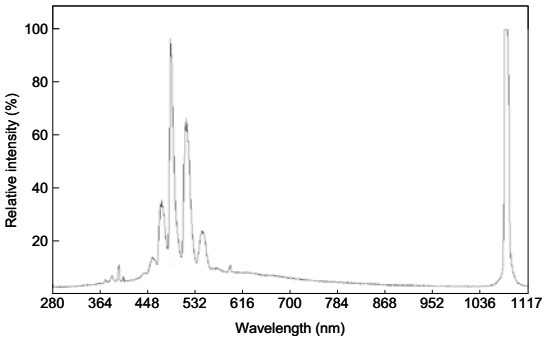

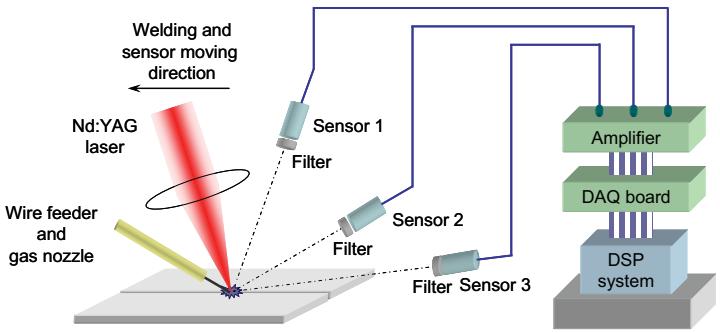

The spec of sensor was the response range with 190 - 680 nm. As the wavelength range of plasma light emission was from 370 to 710 nm as shown in Fig. 1, the sensor response range was coincide with plasma light and the sensor was good for monitoring the aluminum laser welding in this study.

Using this sensor, the laser weld monitoring system was equipped at the experimental system as shown in Fig. 2. Laser welding experiments were performed according to the weld properties of input heat and feeding. Variables were a laser power (LP) and a wire feed rate (WFR). Laser outputs were 4, 3.5, and 3kW and feed rate of the filler wire were 2, 3 and 4 m/min.

Plasma measurements during welding process were showed in Fig. 3. The conditions represented 4 kW of laser output and 2 m/min of feed rate. As shown in the figure, the keyhole and light intensity of plasma showed strong when the laser output was high, but it showed low when the laser ouput was small. These phenomena was observed by the sensors and described in Fig. 4.The average values from the each welding were described in Fig. 4. As shown in Fig. 4, the light intensity of a sensor was increased as the laser output was increased. However, we could observe the different patterns in the feed rate. If the heat input was enough to melt both a wire and materials, the average was getting bigger, but if not, the higher melting wire amount had a lower light intensity of the laser. This affected much to the weld shape and strength.

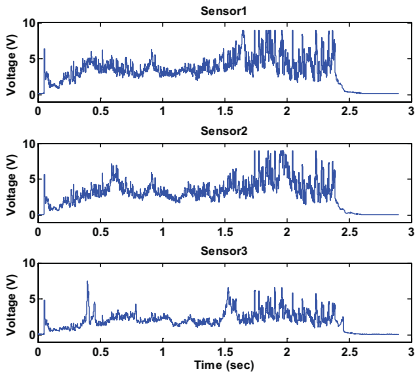

Fig. 3 Sensor signals

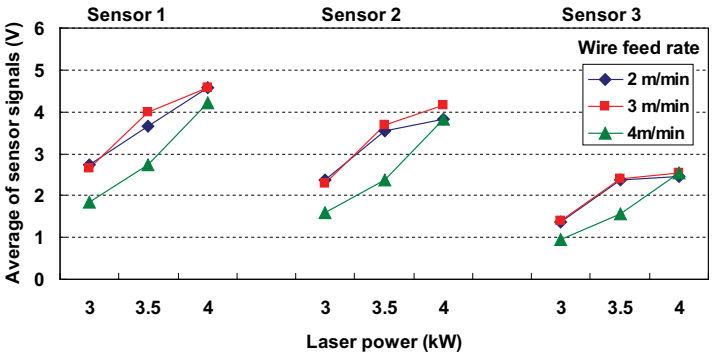

Fig. 4 Average of signals according to welding condition

Acknowledgements Following are results of a study on the "Human Resource Development Center for Economic Region Leading Industry" Project, supported by the Ministry of Education, Science & Technology (MEST) and the National Research Foundation of Korea (NRF).

REFERENCES

1. Sibillano, T., Ancona, A., Berardi, V. and Lugarà, P.M. "A real time spectroscopic sensor for monitoring laser welding processes," *Sensors*, Vol. 9, No. 5, 3376–3385, 2009.
2. Sibillano, T., Ancona, A., Berardi, V. and Lugarà, P.M. "Correlation analysis in laser welding plasma," *Opt. Comm.*, Vol. 251, 139–148, 2005.
3. Farson, D., Ali, A. and Sang, Y., "Relationship of optical and acoustic emission to laser weld penetration", *Welding Journal*, Vol. 77, No. 4, 142s–148s, 1998.
4. Park, Y.W., Park, H., Rhee, S. and Kang, M., "Real time estimation of CO_2 laser weld quality for automotive industry", *Optics and Laser Technology*, Vol. 34, No. 2, 135–142, 2002.
5. Beersiek, J., "A CMOS camera as a tool for process analysis not only for laser beam welding", in *Proceeding of ICALEO 2001*, Jacksonville, Florida, USA, October, 15-18, Vol. 90, 1185–1193, 2001.

A Study on Magnetic Abrasive Polishing in Concave Type of Al6061

S. O. Kim[1] and J. S. Kwak[2*]

[1]Grauated School of Manufacturing and Automation, Pukyong National University, Republic of Korea

[2]Department of Mechanical Engineering, Pukyong National University, Republic of Korea

[*]corresponding author: jskwak5@pknu.ac.kr

Abstract- Automatic magnetic abrasive polishing which can be applied after machining of the mold on a machine tool without unloading is very effective for finishing a free form surface such as a complicated injection mold. This study aimed to improve the efficiency of MAP of non-ferrous mold surface. So, the magnetic array table and control of the electro-magnets polarity was applied into MAP of free form surface. In this study, firstly, the simulation of magnetic flux density on the mold surface was carried out to develop the optimal condition of polarity array. Lastly, the estimation of MAP's efficiency for polishing of non-ferrous mold surface was performed according to change of radius of curvature and magnetic flux density. As a result, the most improved surface roughness was observed not only in the upward tool path but in working area of larger magnetic flux density.

In the present technological world many products require a surface roughness of the order of a micro/nanometer. Magnetic Abrasive Polishing(MAP) is one of the advanced finishing processes, which produces a high level of surface quality. MAP is a process in which workpiece surface is smoothened by removing the material in the form of micro chips by abrasive particles in the presence of magnetic field in the finishing zone. The working gap between workpiece and inductor is filled with mixture of ferromagnetic particles and abrasive powder popularly known as magnetic abrasive particles. These particles form a flexible magnetic abrasive brush which does not require dressing. Magnetic abrasive particle are either bonded (fabricated by compacting and sintering of the mixture) or unbounded (mechanical mixture of ferromagnetic and abrasive particle). This flexible tool can remove a very small amount of materials on a curved surface such as a complicated injection mold and then a better surface can be produced after polishing the workpiece without damages on the surface[1,2]. Nevertheless, it is very difficult to polish non-ferrous materials off using the MAP process because this process is fundamentally through the help of magnetic forces[3,4]. Therefore, it is necessary to develop the improvement strategy of magnetic force in MAP of non-ferrous materials. In this study, to improve the magnetic force, the electro-magnet array table which could changed magnetic polarity by help of controller, was developed. To evaluate the characteristic of magnetic flux density in accordance with arrangement of magnet pole, computer simulation was performed and then experimental verification was occurred.

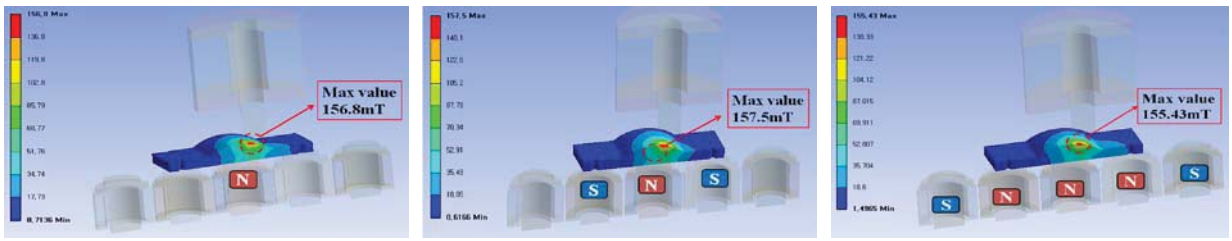

Figure 1. Magnetic flux density according to the change of electro-magnet array

Figure 1 shows simulation results for magnetic flux density on the curved surface. As shown these results, the higher magnetic flux density was observed in S-N-S electro-magnet array. Based on the simulation results, the experimental verification was performed. As results, the same magnetic flux density was calculated on the surface of workpiece. Therefore, to improve the magnetic flux density, this combination of the electro-magnet array was used in MAP of curved surface. In this study, to evaluate the capacity of MAP on curved surface according to change of pole arrangement, some experimental verification was carried out. Workpiece was aluminum alloy(Al6061) and radius of curvature was 39mm. To observe the characteristic of MAP on the curved surface, the tool path was generated as shown in Figure 2 (a). This tool path was consist of three steps(upward - top of hill - downward). The used abrasives are a mixture of iron powder of 150㎛, GC grain of 6㎛ and silicone gel medium. The applied working gap is 1.5mm. Tool path was repeated 20 times.

Figure 2 (b) shows results of experiments. The variation of surface roughness was measured on each route. As shown this figure, as S-N-S electro-magnet array was adopted during MAP, the largest improvement of surface roughness was measured because of the larger magnetic flux density than other polarity array. Therefore, the larger improvement of surface roughness was observed during route1(tool path of upward). This result indicated that the higher working pressure was transmitted to magnetic abrasive on the tool path of upward.

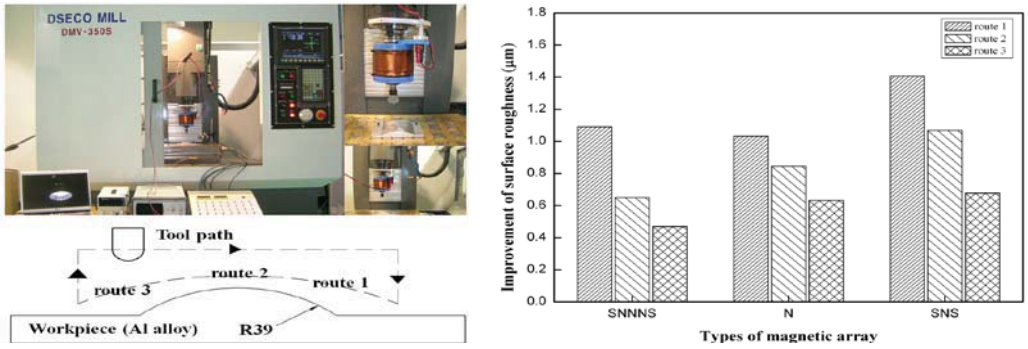

(a) Experimental setup (b) Experimental results

Figure 2. Experimental setup and improvement of surface roughness after MAP

Acknowledgements

This study was supported by Basic Science Research Program through the National Research Foundation of Korea (NRF) funded by the Ministry of Education, Science and Technology (Grant No. 2010-0015271).

REFERENCES

1. Hirota, M. T. and Kawashima, Y., "Clarification of Magnetic Abrasive Finishing Mechanism," *Int. J. Materials Processing Tech.*, Vol. 143~144, 682–686, 2003.
2. Shimura, T. and Aizawa, T., "Development of Plane Magnetic Abrasive Finishing Apparatus and its Finishing Performance (2nd Report, Finishing Apparatus Using a Stationary Type Electro-magnet)," *Int. J. J SPE*, Vol. 54, No. 5, 928–933, 1988.
3. Kim, S. O. and Kwak, J. S., "Improvement of Magnetic Force and Experimental Verification for Magnetic Abrasive Polishing of Aluminum Alloy," *Trans. of KSMTE*, Vol. 17, No. 5, 23–29, 2008.
4. Kwak, J. S., "Enhanced Magnetic Abrasive Polishing of Non-ferrous Metals Utilizing A Permanent Magnet," *Int. J. Machine Tool Manufact*, Vol. 49, No. 7~8, 613–618, 2009.

Scuffing wear monitoring using acoustic emission

D.C. Choi[1], **and T. W. Kim**[2*]

[1]Graduate School of Mechanical Engineering, Pukyong National University, South Korea

[2]Department of Mechanical Engineering, Pukyong National University, South Korea

[*]corresponding author: tw0826@pknu.ac.kr

Abstract- Scuffing experiments are conducted by an indirect sensing approach using Acoustic Emission(AE) measurement to detect scuffing failure. The results show AE signals is provide a valuable indication about the state of the friction and wear processes on the contacting surfaces in real time. The FFT(Fast Fourier Transform)analyses of the AE signal are used to understand the interfacial interaction.

INTRODUCTION

Scuffing failure is an important problem for machine element, but it is very difficult work that forecast scuffing onset because so many factors are related. Acoustic Emission signal has been widely utilized to monitor the interaction at the friction interface [1-2]. This paper is concerned with the measurement and subsequent analysis of the AE raw signals under the boundary lubricated sliding contacts and will be shown that the AE raw signals have some relation to the friction behavior and scuffing damage.

EXPERIMENT

We used a ball-on-plate tribometer to reciprocate 6.3mm diameter 52100 steel balls against the 1040 steel plate. The experiments were carried out in air, at room temperature and under boundary lubricated sliding condition. Normal force and friction force between ball and plate are measured by built-in load cell. AE signals were detected by a resonance type transducer (resonance frequency: 300kHz, band pass: 125~750kHz) attached in wear tester. Specimens are carried out with SM45C that it is used plentifully in machine structural steel. All plate is processed identical roughness of Ra=2μm.

RESULTS

Figures 1 and 2 show the raw signals under experiment condition of sliding speed 1Hz and load 400N. For the steady state(Figure 1(a)), the signals are continuous type and the FFT analysis results(Figure 1(b)) of the AE signal show that particular frequency band is not detected. However, Figure 2 shows a case of severe wear, which appears burst emissions signal with increased amplitude.

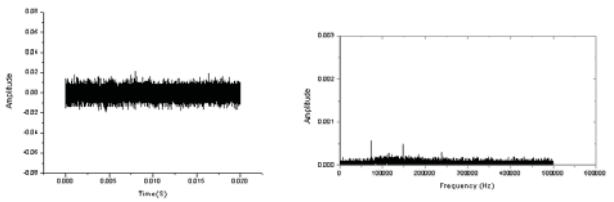

(a) Time domain (b) Frequency domain

Figure 1 AE raw signal with steady

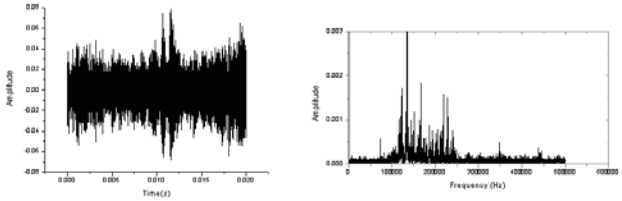

(a) Time domain (b) Frequency domain

Figure 2 AE raw signal with scuffing

Figure 3 presents the variation of AE count and friction coefficient just before occurrence of scuffing failure as a function of time. The lower curve in Figure 3 shows plots of AE count that the number of times an acoustic emission signal exceeds the threshold voltage of 0.05 V. It was found that AE count increases rapidly earlier than the friction coefficient increases. Therefore, AE count is more sensitive to the detection of scuffing failure than the friction coefficient.

In addition, the monitoring of the value of AE RMS may be useful to investigate the wear processes. Typical RMS acoustic emission signals for boundary lubricated experiments obtained from the ball-on-plate test rig are illustrated in Figure 4. This results show RMS voltage, plotted against time for a constant load of 300N and sliding speed of 1Hz. It was realized that the measurement of the RMS of the AE signal contained considerable information concerning the wear mechanism (running in - smoothing - scuffing) in sliding contacts. There is an initial increase in the RMS signal at 220s, followed by a gradual decrease between 220s and 600s, higher peak occurring until scuffing occurring.

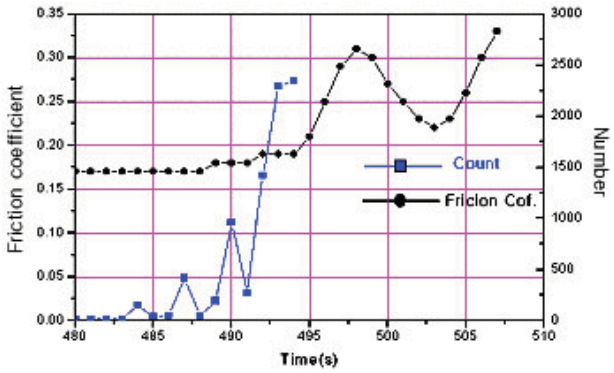

Figure 3 Relation between friction coefficient & AE count

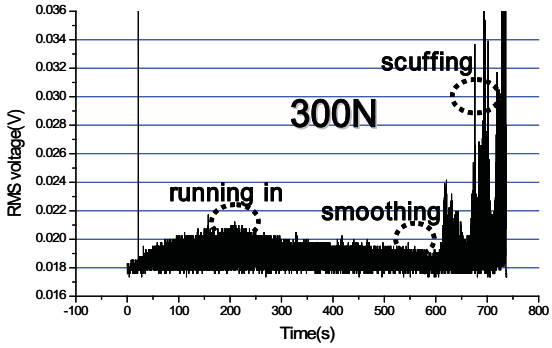

Figure 4 Variation in RMS signal with time

CONCLUSIONS

In this study, scuffing experiments are conducted using Acoustic Emission (AE) measurement by an indirect sensing approach to detect scuffing failure. Using AE signals we can get an indication about the state of the friction processes and the quality of solid and liquid layers on the contacting surfaces in real time. The FFT analyses of the AE signal are used to understand the interfacial interaction. This result will be shown that there is the specific frequency regime of acoustic emission corresponding to scuffing failure. The measurement of AE RMS also shows the usefulness in explanation of the scuffing wear mechanism occurring in sliding contacts.

ACKNOWLEDGEMENTS

This work is the result of the "Human Resource Development Center for Economic Region Leading Industry" Project, supported by the Ministry of Education, Science & Technology(MEST) and the National Research Foundation of Korea(NRF).

REFERENCES

1. Hanchi, J. and Klamecki, B. E. “Wear process description based on acoustic emission,” *Journal of Tribology*, Vol. 112, 468-476, 1990
2. Boness, R. J. and Hawthorne, H. M., “Acoustic emission from the unlubricated sliding wear of steel and silicon nitride,” *Tribology Transactions*, Vol. 38, 293-298, 1995

Control of Braking Velocity on Vehicle using ABS Slip Ratio

J. H. Choi[1], **D. H. Lee**[2]
[1]Education Center for Vehicle Safety Component Technology, Pukyong National University, Korea
[2]Department of Mechanical Engineering, Pukyong National University, Korea
*corresponding author: choijh2007@pknu.ac.kr

Abstract-Anti-lock Braking System(ABS) in the passenger car is a safety device, which adds hydraulic system to the existing brake system to prevent wheel from locking, so we can obtain maximum braking force on driving. On braking in ABS vehicle, the braking force that is described by slip ratio function can be maximum value when slip ratio is from 0.1 to 0.3. In this paper, the aim is that the braking velocity is stable decreased by control of slip ratio. The 1/4 vehicle model is used and slip ratio is controlled by PWM and SMC based on vehicle dynamics in the same way a two-level control scheme.

On operating the brake system in ABS vehicle, the friction force between the tire and the road surface is generated and the velocity of vehicle decrease slowly. The friction force that is the main braking force depends on the road condition and the value of the wheel slip ratio that is defined as the ratio of the linear velocity to the angular velocity. The hydraulic modulator in this paper is constructed using one solenoid valve with 3way-2position. The valve operates on the modulated signal due to PWM method and SMC based on the vehicle dynamics is applied on the braking torque. In this paper, a hydraulic modulator is composed of one solenoid valve with high responsibility shown in Fig.1.

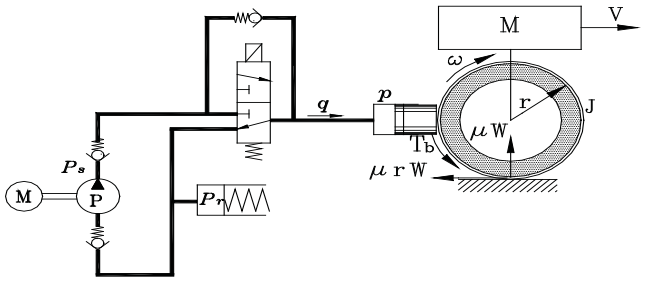

Fig. 1 1/4 Vehicle model

The valve can be in two positions, closed or open. The pressure in the wheel cylinder increases if the valve is open and if the valve is closed the pressure decreases due to the fluid flow in the direction of the low-pressure accumulator. The movement of valve can be approximated to first order time delay and the open area can be considered as a constant gain. For vehicle motion on braking, the model consists of linear dynamics and the rotational dynamics. The linear dynamics and the rotational dynamics can be described by Newtonian equation of motion.

$$M\,\dot{v}(t) = -F_t - F_a = -\mu(\lambda)W - \frac{1}{2}C_a\,\rho_a\,A_a\,v^2 \tag{1}$$

$$J\,\dot{w}(t) = -r\,F_t - T_b = -r\,\mu(\lambda)W - C_b\,\mu_b\,\frac{r_e}{r}A_p\,p \tag{2}$$

The friction coefficient between the tire and the road depends on the road condition and the value of the wheel slip ratio. According to a typical m-l curve, a mathematical description is described by Peng and Tomizuka[3] as follow;

$$\mu(\lambda) = \frac{2\,\mu_p\,\lambda_p\,\lambda}{\lambda_p^2 + \lambda^2} \tag{3}$$

The control input applied Sliding-Mode-Control method is described Eq.(4) to make the system trajectory along the sliding surface and reached the original point. The control input can be

$$u = k_p e + k_d \dot{e} + k\,sat\left(\frac{S}{\Phi}\right) \tag{4}$$

The PWM method can modulated error signal using a carrier wave with a high frequency, a periodically tooth wave. The duty ratio is defined as the ratio of the time of switching ON state to the period of the carrier wave. And the control input generated SMC is added to braking torque. Fig. 2 shows the velocity of vehicle and the angular velocity of wheel. The angular velocity of wheel is oscillated in large due to switching ON and OFF state. But, applied SMC on the braking torque the value of variation of angular velocity is small and the reduction ratio of vehicle velocity is large in comparison with operating ON/OFF state. For controlling slip ratio the variation of angular velocity can be decreased and the velocity can be reduced in a rapid time.

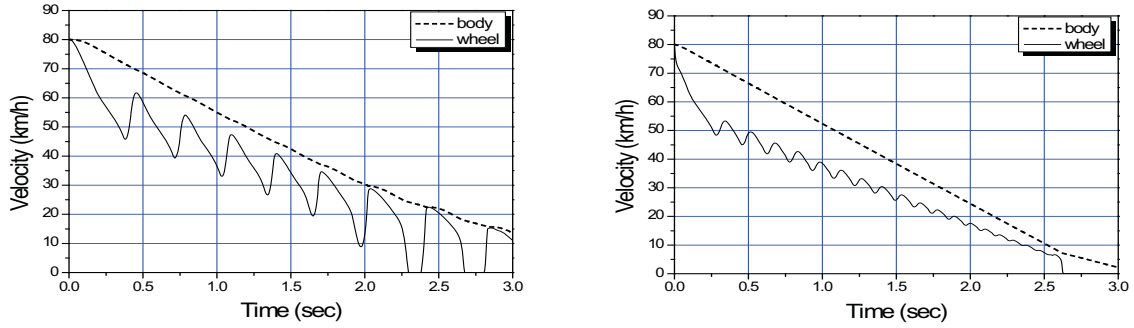

(a) PWM (b) SMC

Fig. 2 Results of simulation

REFERENCES

1. J. L. Harned et al., "Measurement of tire brake force characteristics as related to wheel slip control system design", SAE Trans., vol. 78, no. 690214, pp. 909-925, 1969.
2. S. Drakunov et al., "ABS Control Using Optimum Search via Sliding Modes", IEEE Trans. Control System Technology, vol. 3, pp. 79-85, 1995.
3. H. Peng and M. Tomizuka, "Vehicle lateral control for highway automation", Pro. Amer. Contr. Conf., San Diego, CA, pp. 788-794, 1990.
4. C. Ünsal and P. Kachroo, "Sliding Mode Measurement Feedback Control for Antilock Braking Systems", IEEE Trans. Control System Technology, vol. 7, pp. 271-281, 1999.

Magnetic properties of arrays of magnetostatically coupled glass-covered microwires for design new metamaterial family

[4]J. González[1*], V. Rodionova[1,2,3], M. Ipatov[1], M. Ilyn[1], V. Zhukova[1], N. Perov[2], J.J. Del Val[1], and A. Zhukov*

[1]Department Materials Physics, faculty

[1]Department of Materials Physics, Faculty of Chemistry, University of the Basque Country, Paseo Manuel de Lardizabal 3, 20018 San Sebastián, Spain

[2]Faculty of Physics, Moscow State University, Leninskie Gory, Moscow, Russia

[3]Institute for Theoretical and Applied Electromagnetics of Russian Academy of Sciences, Moscow, Russia

[4]TAMAG Ibérica S.L., Parque Tecnológico de Miramón, Paseo Mikeletegi 56, 1a Planta, 20009 San Sebastián, Spain

[*]corresponding author: julianmaria.gonzalez@ehu.es

Abstract-Magnetization reversal process in arrays consisting of different numbers of $Co_{67}Fe_{3.9}Ni_{1.5}B_{11.5}Si_{14.5}M_{1.6}$ and $Fe_{74}B_{13}Si_{11}C_2$ amorphous microwires with different shape of the hysteresis loops is analysed. $Fe_{74}B_{13}Si_{11}C_2$ microwires have rectangular hysteresis loops, while $Co_{67}Fe_{3.9}Ni_{1.5}B_{11.5}Si_{14.5}M_{1.6}$ with vanishing magnetostriction constant possess inclined hysteresis loops with low coercivity. The presence of a neighboring microwire (Fe- or Co-based) significantly modifies the hysteresis loop of the whole microwire array. In microwire arrays containing Fe-based microwires we observed splitting of the initially rectangular hysteresis loop with a number of Barkhausen jumps correlated with the number of Fe-rich microwires. In arrays consisting of Co-based microwires a change of inclination of the overall hysteresis loop and consequently the magnetic anisotropy field was observed. In the case of mixed arrays containing Fe- and Co-rich microwires it was able to obtain irregular hysteresis loops with unusual shape. In this case, a considerable increase of harmonics has been observed. The observed dependences have been interpreted through magnetostatic interaction between the microwires with different magnetic–domain structures. Besides the conventional methods, such as thermal treatment, designing arrays containing different types of microwires can serve to tailor their magnetic properties.

Recently, a new family of metamaterials in the microwave range has attracted the attention owing the potential applications as wireless communication, antenna engineering, non-destructive testing of civil structures, multifunctional structural materials, and biomedical engineering, the investigations into innovative designs of electromagnetic materials continue to be an important issue. This new metamaterial family is, basically, a composite containing elongated metallic inclusions (microwires) can be designed to have specific frequency spectra. Therefore, investigations of the magnetic behaviour of arrays with these glass coated microwires can be of enormous interest to design new metamaterials. Consequently, certain efforts have been made to tailor the magnetic properties through creation of artificial magnetic structures using partial devitrification and/or crystallization of the metallic nucleus, creating the microwire arrays, changing the geometrical characteristics,

and even the material of the glass coating or creation of additional metallic layers with different thermal expansion coefficients [1-3].

In this paper we present novel results on the magnetic properties of arrays containing not only the identical Fe- or Co-based microwires but also different combinations of them (see Fig.1). The observed magnetic properties have been explained taking into account the magnetostatic interaction between the microwires with different magnetic domain structure. Together with conventional methods, such as thermal treatment, the design of arrays containing different types of microwires can be used for tailoring their magnetic properties.

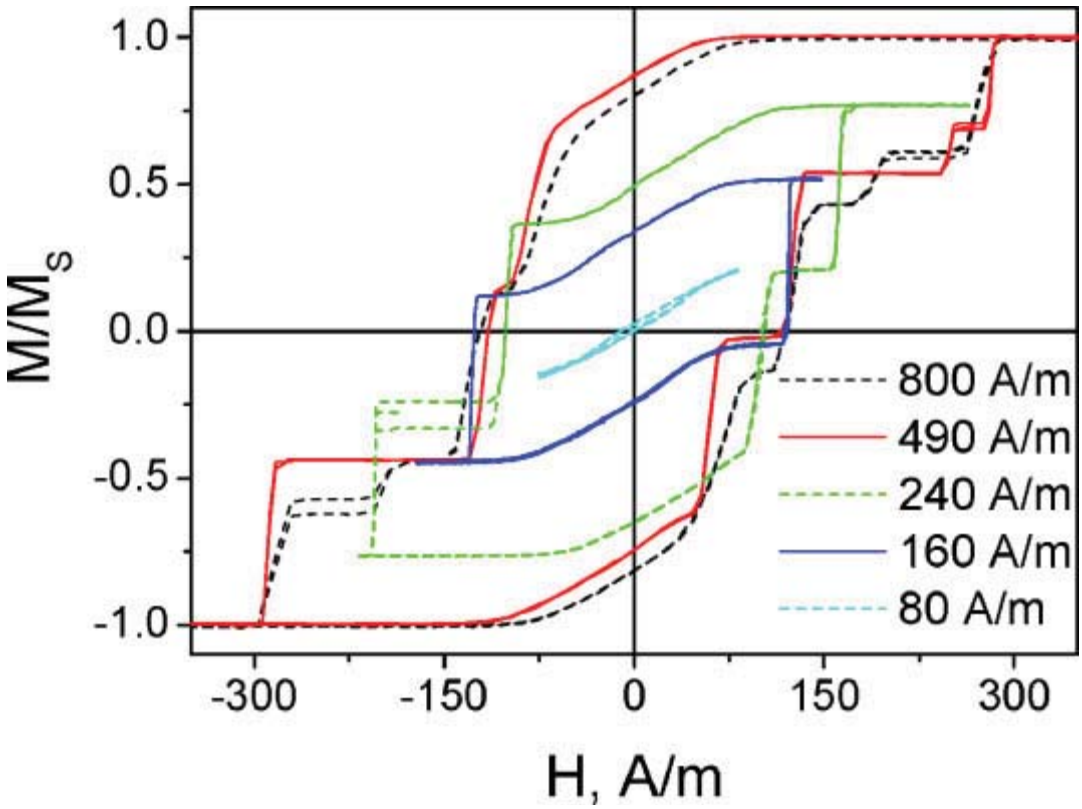

Fig. 1. Hysteresis loops of the array containing three $Fe_{74}B_{13}Si_{11}C_2$ and $Co_{67}Fe_{3.9}Ni_{1.5}B_{11.5}Si_{14.5}M_{1.6}$ microwires.

Acknowledgements, This work is supported by EU ERA-NET under project "SoMaMicSens" (MANUNET-2010-Basque-3) and by Spanish Ministry of Science and Innovation MICINN under project MAT2010-18914

REFERENCES

1. A. Zhukov and V. Zhukova, "*Magnetic Properties and Applications of Ferromagnetic Microwires with Amorphous an Nanocrystalline Structure*", Nova Science Publishers, Inc., New York, 2009

2. H. Chiriac and T. A. Ovari, *Prog. Mater. Sci*. Vol. 40, 333, 1996.

3. A. Zhukov, M. Ipatov, V. Zhukova, C. Garcı´a, J. Gonzalez, and J. M. Blanco, *Phys. Status Solidi A*, Vol. 205, 1367, 2008.

List of presenting authors

	Name	email	Affiliation	Page
1	Ageyskiy Alexander	alex.ageyskiy@phoi.ifmo.ru	Saint-Petersburg State University of Information Technologies Mechanics and Optics	68-69
2	Amonov B. U.	a_baxtiyor@samdu.uz	Samarkand State University, Uzbekistan	85
3	E. S. Andrianov	14159262006@yandex.ru	Institute for Theoretical and Applied Electromagnetics, 13 Izhorskaya, Moscow 125412, RF	19-20
4	A.K. Arzhnikov	arzhnikof@bk.ru	Physical-Technical Institute, Ural Division of RAS, Izhevsk, Russia	46
5	E.Arzikulov	eshquvat@mail.ru	Samarkand State University, Uzbekistan	36
7	Yurii N Barabanenkov	barab624@mail.ru	V.A Kotelnikov Institute of Radioengineering and Electronics, Russian Academy of Sciences, 125009 Moscow, Russia	83-84
8	Belov P. A.	belov@phoi.ifmo.ru	Queen Mary University of London, London, UK; National University of Information Technologies, Mechanics and Optics, St. Petersburg, Russia	30-31
9	Bergman David J.	bergman@post.tau.ac.il	Raymond and Beverly Sackler School of Physics and Astronomy, Faculty of Exact Sciences, Tel Aviv University, Israel	29
10	Yann Danlée	yann.danlee@uclouvain.be	Universite catholique de Louvain, Belgium	70
11	A. V. Dorofeenko	asdf00@mail.ru	Institution of the Russian Academy of Sciences Institute for theoretical and applied electromagnetics RAS (ITAE RAS), 125412, Russia, Moscow, ul. Izhorskaya, d. 13	17-18
12	C. David	christin.david@csic.es	Nanophotonics Group, Instituto de Óptica, CSIC, Serrano 121, 28006 Madrid, Spain	80-81
13	Fateev Denis Vasilievich	FateevDV@yandex.ru	Kotelnikov Institute of Radio Engineering and Electronics (Saratov Branch) of Russian Academy of Science, 410019 Saratov, Russia;Saratov State University named after N.G. Chernyshevsky, 410012 Saratov, Russia	66-67

14	Fedyanin Andrey	fedyanin@nanolab.phys.msu.ru	Quantum Electronics Department Faculty of Physics Lomonosov Moscow State University Moscow 119991, RUSSIA	39-40
15	Fedyanin Dmitry Yu.	feddu@mail.ru	Laboratory of Nanooptics and Femtosecond Electronics, Moscow Institute of Physics and Technology (State University), Dolgoprudny, Russian Federation	22-23
16	Gonzalez J.	julianmaria.gonzalez@ehu.es	Department of Materials Physics, Faculty of Chemistry, University of the Basque Country, Paseo Manuel de Lardizabal 3, 20018 San Sebastian, Spain	97-98
17	Granovski Alexander	granov@magn.ru	Faculty of Physics, Moscow State University, Moscow, 119991 Russia;	37-38
18	M. Kaliteevski	mikhail.kaliteevski@durham.ac.uk	Ioffe Institute,26 Polytechnicheskaay, 194021, St-Petersburg, Russia Academic University, 3/8 Khlopina, St-Petersburg, Russia	78-79
19	Khromova Irina	irina.khromova@unavarra.es	Public University of Navarra, Spain	63-64
20	Khyshov Andrey	khysh@ipm.sci-nnov.ru	Institute for Physics of Microstructures RAS, Russian Federation	71-72
21	T. W. Kim		Department of Mechanical Engineering, Pukyong National University, Republic of Korea	93-94
22	Klimov Vasily Vasilievich	klimov55@mail.ru	P.N. Lebedev Physical Institute Moscow, Russia	50-51
23	Kosulnikov S. Yu.	serg.kosulnikov@phoi.ifmo.ru	National University of Information Technologies, Mechanics and Optics, St. Petersburg, Russia	32-33
24	Kurtaliev Eldar	kurtaliev@rambler.ru	Samarkand State University, Uzbekistan	58
25	O.K. Kuvandikov	quvandikov @rambler.ru	Samarkand State University, Dpt. of Physics, Samarkand, Uzbekistan	49
26	J. S. Kwak		Department of Mechanical Engineering, Pukyong National University, Republic of Korea	91-92
27	Lafmajani Iarj Arghand	irajarghand@gmail.com	Semnan University, Iran	75

28	M. F. Limonov	M.Limonov@mail.ioffe.ru	Ioffe Physical-Technical Institute of the Russian Academy of Sciences, St.Petersburg, Russia	59-60
29	Mikhail Lapine	mikhail.lapine@gmail.com	Nonlinear Physics Centre, Research School of Physics and Engineering, Australian National University, Canberra ACT 0200, Australia	45
30	D. H. Lee		Department of Mechanical Engineering, Pukyong National University, Republic of Korea	95-96
31	Milton G.	milton@math.utah.edu	Department of Mathematics University of Utah, USA	28
32	Merzlikin Alexander Mikhailovich	merzlikin_a@mail.ru	Institution of the Russian Academy of Sciences Institute for theoretical and applied electromagnetics RAS (ITAE RAS), 125412, Russia, Moscow, ul. Izhorskaya, d. 13	82
33	Moiseev Sergey G.	serg-moiseev@yandex.ru	Kotelnikov Institute of Radio Engineering and Electronics of Russian Academy of Sciences, Ulyanovsk Branch, Russia	65
34	Nizomov Negmat	nnizamov@yandex.ru	Samarkand State University, Uzbekistan	24-26
35	Y. W. Park		Department of Mechanical Engineering, Pukyong National University, Republic of Korea	89-90
36	Popov Alexander K	apopov@uwsp.edu	Department of Physics & Astronomy, University of Wisconsin-Stevens Point, Stevens Point, WI 54481-3897	43-44
37	Priou Alain	alainpriou@orange.fr alain.priou@u-paris10.fr	University Paris Ouest Nanterre la Défense, Energy, Mechanics and Electromagnetic Lab.(LEME) 50 rue de Sevres, 92410 Ville d'Avray, France	47-48
38	Ruzimurodov J. T.	ruzimurodov_j@samdu.uz	Samarkand State University, Department of Physics, 140104, University blvd. 15, Samarkand, Uzbekistan	27
39	Salakhitdinova Maysara Kamolidinovna	smaysara@yandex.ru	Samarkand State University, Uzbekistan	86
40	Sapozhnikov Maksim V.	msap@ipm.sci-nnov.ru	Institute for Physics of Microstructures RAS, Nizhny Novgorod, GSP-105, Russia	73-74
41	Shah Wiqar Hussain	wiqarhussain@yahoo.com	King Faisal University, Hofuf, 31982 SAUDI ARABIA	76

42	K. B. Samusev		Ioffe Physical-Technical Institute, Russian Academy of Sciences, St. Petersburg, 194021, Russia	56-57
43	Shcherbakov Maxim	shcherbakov@nanolab.phys.msu.ru	Faculty of Physics, Lomonosov Moscow State University	54-55
44	Shermatov Erkin N	erk-shermatov@yandex.ru	Samarkand State Univesrsity, Uzbekistan	77
45	Simovski Constantin	konstantin.simovski@aalto.fi	Radio Science Dept, ELEC School, Aalto University, Finland	52-53
46	Stockman M.	mstockman@gsu.edu	Department of Physics and Astronomy Georgia State University	14
47	Strelniker Yakov	strelniker@gmail.com	Department of Physics, Bar-Ilan University, Ramat Gan 52900, Israel	61-62
47	F.H. Tukhvatullin		Samarkand State University, Uzbekistan	34-35
48	Vinogradov Alexey Petrovich	a-vinogr@yandex.ru	Institution of the Russian Academy of Sciences Institute for theoretical and applied electromagnetics (ITAE RAS), Izhorskaya, 13, 125412, Russia, Moscow	15-18
49	Zayats Anatoly	a.zayats@kcl.ac.uk	King's College London	21
50	Zouhdi Said	said.zouhdi@supelec.fr	Paris-Sud University, Plateau de Moulon, 91192 Gif-sur-Yvette CEDEX, France	
51	Zhukov Arcady	arkadi.joukov@ehu.es	IKERBASQUE, Basque Foundation for Science, 48011 Bilbao and Dpto. Fisica de Materiales, Fac. Quimicas, UPV/EHU, 20018 San Sebastian, Spain	41-42